WEATHERING AND MAGNESIUM ISOTOPE FRACTIONATION IN ARID HAWAIIAN SOILS

A Dissertation

Presented to the Faculty of the Graduate School

of Cornell University

in Partial Fulfillment of the Requirements for the Degree of

Doctor of Philosophy

by

Kyle Daniel Trostle

August 2014

WEATHERING AND MAGNESIUM ISOTOPE FRACTIONATION IN ARID HAWAIIAN SOILS

Kyle Daniel Trostle, Ph.D.

Cornell University 2014

With the development of multi-collector inductively coupled plasma mass spectrometry, the stable isotopes of Mg have become available as a tool to constrain Mg cycling within the weathering environment. This advance is important, as Mg isotopes will allow the study of Mg transport within ecosystems and soils directly and may also lead to insight into Mg weathering and CO_2 cycling on geological timescales. Studies investigating the stable isotopes of Mg in soils, waters, and plants show that significant Mg isotopic fractionations are associated with weathering, secondary mineral formation, and biotic uptake. However, studies identifying Mg isotopic fractionation have yet to divide soils into detailed fractions to locate those isotopic fractionations in specific soil phases, and studies have yet to utilize the soil chronosequence concept to determine if the Mg isotopic composition of soil changes through time. We address these issues by conducting bulk soil Mg isotopic analyses along with a detailed sequential extraction on an arid Hawaiian soil chronosequence to determine the distribution of Mg and Mg isotopic composition within soil phases.

We find that the overall Mg isotopic compositions of our soil systems are determined by the secondary phases that dominate the functioning of each particular soil system. Our younger chronosequence site is dominated by pedogenic carbonate, leading to the net export of isotopically heavy Mg from this soil and the retention of isotopically light Mg, while our older

chronosequence site is dominated by non-carbonate phases, leading to the export of Mg near the Mg isotopic composition of basalt. This evidence illustrates that as secondary mineral phase assemblages evolve over time in soils, the isotopic composition of the Mg exported from soil systems can also change. Further, by looking at the detailed sequential extraction fractions, we see that Mg in the adsorbed cations and carbonates is isotopically lighter than the Mg inputs to our soils, and the Mg associated with soil organic matter, short-range-order phases, sesquioxides, and residuum is near the Mg isotopic composition of basalt or isotopically heavier.

BIOGRAPHICAL SKETCH

Kyle Daniel Trostle was raised in Lebanon, Pa by his supportive and caring parents, Donald and Nancy Trostle. Kyle's interest in the earth sciences began when he attended Franklin and Marshall College, where he majored in Environmental Science with a minor in Geology. While at Franklin and Marshall, he worked with Dr. Christopher Williams on a variety of environmental science and geology projects. He was able to travel to Alaska for a Keck Undergraduate Consortium project, where he identified fossil trees and determined patterns of diagenesis within the permineralized trees. This experience cemented his desire to continue work in the earth sciences. He graduated from Franklin and Marshall College in 2009 with a B.A. and transitioned to graduate school at Cornell University.

At Cornell, Kyle has worked toward a Ph.D. degree with Dr. Louis Derry. He spent a semester abroad in France, working with Dr. Nathalie Vigier, to learn how to properly prepare samples for Mg isotopic analysis and how MCICPMS instrumentation operates. Also while at Cornell, Kyle married his exceptional wife, Anne Rowand.

Kyle enjoyed his teaching duties as a TA for Introduction to Biogeochemistry, Mineralogy, and The Earth System, and he hopes to continue teaching in the future. He has also enjoyed the tea hour tradition in the Department of Earth and Atmospheric Sciences and hopes that this activity continues after his departure.

After Cornell, Kyle will be transitioning to a Postdoctoral Research Associate position at the University of Arizona, where he will be studying weathering in the deep critical zone.

ACKNOWLEDGMENTS

There are many people who deserve to be recognized for their positive influence on my intellectual development, this dissertation, and my time at Cornell. Thanks to my committee, Dr. Louis Derry, Dr. William White, and Dr. Joseph Yavitt, for providing me the opportunity to conduct research under their supervision. In particular, thank you to Lou for listening to my random ideas over the years, no matter how tangentially related to the topic at hand they may have been. In addition, thank you to everyone on my committee, and also Dr. Suzanne Kay, for having me as a teaching assistant in various courses. These experiences were important to me and helped me realize how enjoyable teaching can be.

Thanks to everyone who provided the technical support and know-how in order to create the robust results necessary to draw valuable conclusions from my work. Without the efforts of Gregg McElwee, Maura Weathers, and John Hunt, the data that forms the backbone of this dissertation would be a shadow of what it currently is. Thanks as well to George Hade, who made sure to fix most of the things that I ended up breaking (or finding broken, I swear!) in the lab.

In addition, the technical know-how and support of those at the Centre de Recherches Pétrographiques et Géochimiques (CRPG) in Nancy, France also deserves thanks. Aimeryc Schumacher ran multitudes of Mg isotope samples and Delphine Yeghicheyan provided the data necessary to calibrate my cation exchange columns while in France. Nathalie Vigier deserves special thanks, for her oversight of my work while I was in France and also for her continued efforts to help improve my manuscripts and interpret Mg isotope findings.

Thank you as well to Oliver Chadwick, whose encyclopedic knowledge of Hawaiian soils was greatly appreciated in choosing study sites for this work, and whose efforts in data interpretation and manuscript improvement are also much appreciated.

Undergraduate researchers Eva Golos and Mariela Garcia conducted research necessary for this dissertation, and both have helped teach me how to oversee others working in academic lab settings. Thanks for all of your hard work!

Thank you to my parents and extended family, who have always supported me in all my endeavors! Someday I will get a real job, I promise.

To my wife, Anne, thank you for all of your support and help. My dissertation would not exist without you, and my time at Cornell would have been much less enjoyable.

I have been fortunate to find a department with so many kind-hearted people. Thank you to all of the EAS staff who support the entire department, and thank you to all of the friends who have shared time in Snee with me. In particular, thank you to Gregg, Sander, Scott, Jennifer, Chen, Andres, Katie, Caitlin, and Ceren for all the times you have shared with me, and for making my stay in Ithaca so enjoyable.

Financially, my work has been supported by a variety of sources over the past 5 years. I am grateful for funding from National Science Foundation Grant 0922070, which provided the bulk of the funding necessary for this research. In addition, my stay in France was supported by a Chateaubriand Fellowship from the French government. My work also made use of the Cornell Center for Materials Research Shared Facilities, which are supported through the NSF MRSEC program (DMR-1120296).

TABLE OF CONTENTS

LIST OF FIGURES

LIST OF TABLES

CHAPTER 1

INTRODUCTION

1.1. THE IMPORTANCE OF MAGNESIUM

Magnesium is the fourth most abundant element on Earth and is a key constituent of olivines, pyroxenes, spinels, and mantle mineral phases. Mg is also a biologically necessary nutrient and is critical in organisms as a coordinating ion in chlorophyll and cofactor of many enzymes (Fraústo da Silva and Williams 1991). Mg also plays a key role in long-term climate regulation, along with Ca. These two elements, when weathered and transported to the oceans, can precipitate from seawater into carbonate phases, thereby tying the weathering of Ca and Mg silicates to CO_2 concentrations in the atmosphere over geological time periods (Urey 1952). On a smaller scale, Mg remaining in the weathering environment plays a role in the development of the secondary mineral phases that make up soils, and Mg also cycles through biota. As such the ability to trace the transport of Mg, whether it is through geological processes deep within the Earth, weathering processes on the surface of the Earth, or within an ecosystem, will allow geoscientists greater insight into how the Earth operates.

1.2. STABLE MAGNESIUM ISOTOPES

The use of stable Mg isotopes provides one way to constrain the transport of Mg and processes influencing Mg throughout the Earth. However, only recently have techniques been developed that can determine magnesium isotopic composition reliably, as magnesium isotopes have been difficult to measure due to instrumental mass fractionation effects (Young and Galy 2004). With the introduction of multiple collector inductively coupled plasma mass

spectrometry (MC-ICP-MS), these instrumental mass fractionation effects can be limited by rigorous sample preparation and careful standardization, providing a more precise measure of magnesium isotope ratios (usually expressed as $\delta^{26}Mg$). With this development, measurement of $\delta^{26}Mg$ has become a viable means to understand the transport of Mg, particularly in the weathering environment.

1.3. MAGNESIUM ISOTOPES AND PEDOGENESIS

The adoption of Mg isotopes as a tool to investigate the weathering environment can be seen in recently published studies that indicate there are significant variations in the isotopic composition of Mg produced during weathering, secondary mineral formation, and plant uptake (Brenot et al. 2008; Pogge von Strandmann et al. 2008; Black et al. 2008; Tipper et al. 2010). However, much work must still be conducted before Mg isotopes can be effectively used to understand the transport of Mg among soil reservoirs. The aforementioned studies have not endeavored to break soil into its constituent parts to determine Mg distribution among soil phases or Mg isotopic composition among soil phases, and they have not looked at weathering systems under arid climatic conditions. This dissertation addresses these gaps in the knowledge.

1.4. THE ROLE OF THIS DISSERTATION

Mg isotopic composition in soils is influenced by mixing between Mg sources, as well as isotopic fractionation during weathering processes. This study seeks to understand this mixing and fractionation of Mg isotopes in an arid soil chronosequence developed on the Island of Hawaii in order to better understand how Mg isotopes can be used as a tool for investigating pedogenesis and Mg cycling in ecosystems. This work ultimately has ramifications for

understanding the Mg isotopic composition of seawater through time, as riverine Mg fluxes and Mg isotopic compositions are the result of the interaction of weathering processes and precipitation.

Some of the processes during pedogenesis that influence Mg and Mg isotopes are secondary mineral formation, leaching, and biocycling. By understanding in detail the Mg distributions and Mg isotopic compositions of the soil phases making up our arid soil chronosequence, we can develop Mg isotopes as tracers for the production and fate of particular soil weathering products or organic matter, and we can model the fluxes of magnesium between soil, water, and biota. We do this by breaking down the soils into their constituent phases and analyzing the distribution of Mg in them (Chapter 2), looking at the soils as a whole to determine their bulk Mg isotopic compositions (Chapter 3), and by analyzing the Mg isotopic compositions of the constituent phases that make up our soils (Chapter 4).

1.5. CONCLUSIONS

Our research illustrates six main findings relating to Mg isotopic fractionation in the weathering environment and the distribution of Mg in soils.

1. In the arid volcanic soils used in our study, Mg is primarily sequestered into either short-range-order phases or carbonates. These phases are common throughout soils of the world and may dominate the Mg budgets of soils in many locations.

2. Our work shows that pedogenic carbonates preferentially incorporate isotopically light Mg and that the Mg isotopic compositions of individual generations of these carbonates are most likely controlled by a complicated Rayleigh fractionation process. This Rayleigh fractionation

process results from the slow evaporation of soil porewater over time in these arid systems and the removal of Mg by the formation of a variety of secondary soil phases.

3. At our study sites, all uncontaminated soil organic matter (SOM), short-range-order, sesquioxide, and residuum soil fractions appear to sequester isotopically heavy Mg or display little fractionation with respect to the Mg isotopic compositions of our soil Mg mixing estimates. These mixing estimates are based on the relative amount of Mg input from rainfall and basalt weathering to the soil, along with the Mg isotopic composition of each input.

4. The Mg isotopic composition of our bulk soils ultimately depends upon the secondary phases that are dominating the functioning of the soil system. In our younger study site carbonate is a large influence on Mg budgets, leading to the net export of isotopically heavy Mg from this soil. In our older study site short-range-order and residuum phases take on a larger role than carbonates in the Mg budget, and the net export of Mg from this soil is near the Mg isotopic composition of basalt. As secondary mineral phases change in importance over time, the isotopic composition of Mg exported from our soil systems also changes.

5. Mg isotopic compositions of adsorbed cation soil fractions are lighter than Mg mixing estimates in both soils, suggesting the export of isotopically light Mg from each soil currently, if no Mg isotopic fractionation occurs during adsorption/desorption. It is important to differentiate this finding from the previous conclusion, as the adsorbed cations represent a much shorter timescale than the net development of the bulk soil. This observation may suggest that the younger soil has begun to shift from carbonate dominance of its Mg budget and export of isotopically heavy Mg, to short-range-order and residuum phase dominance of its Mg budget and export of light Mg.

6. The residuum fractions of our soils are complex and vary isotopically with depth and between soils. The cause of this variation is not completely understood, but it is likely dependent on differences in the abundances of phases making up the residuum fractions.

WORKS CITED

Black, J.R., Epstein, E., Rains, W.D., Yin, Q.Z. and Casey, W.H., 2008. Magnesium-isotope Fractionation During Plant Growth. Environmental Science & Technology, 42(21): 7831-7836.

Brenot, A., Cloquet, C., Vigier, N., Carignan, J. and France-Lanord, C., 2008. Magnesium isotope systematics of the lithologically varied Moselle river basin, France. Geochimica et Cosmochimica Acta, 72(20): 5070-5089.

Fraústo da Silva, J. J. R., and Williams R. J. P., 1991. The biological chemistry of the elements: The inorganic chemistry of life. Clarendon Press, Oxford. 1991.

Pogge von Strandmann, P.A.E. et al., 2008. The influence of weathering processes on riverine magnesium isotopes in a basaltic terrain. Earth and Planetary Science Letters, 276: 187–197.

Tipper, E.T., Gaillardet, J., Louvat, P., Capmas, F., White, A.F., 2010. Mg isotope constraints on soil pore-fluid chemistry: Evidence from Santa Cruz, California. Geochimica et Cosmochimica Acta, 74: 3883-3896.

Urey, H.C., 1952. The planets, their origin and development: New Haven, Yale University Press.

Young, E.D. and Galy, A., 2004. The isotope geochemistry and cosmochemistry of magnesium. In: C.M. Johnson, B.L. Beard and F. Albarede (Editors), Geochemistry of Non-Traditional Stable Isotopes. Reviews in Mineralogy & Geochemistry: 197-230.

CHAPTER 2

THE CHARACTERIZATION OF TWO ARID HAWAIIAN SOILS AND THE DISTRIBUTION OF MAGNESIUM WITHIN SOIL PHASES

Abstract

In order to understand the fractionation of Mg isotopes in the weathering environment, we must first understand the processes occurring during weathering, and how this may influence the distribution and export of Mg. This chapter uses characterization data generated from the study of two arid chronosequence soil sites from Kohala Volcano, Hawaii to understand the functioning of these soils, the distribution of Mg, and the pedologic processes influencing that Mg distribution. In these study sites, the major process driving the changes between the older and younger soil is the leaching of soluble cations through time. Other soil forming processes also play a role in the development of these soils, but leaching is key in determining the relative abundance of non-carbonate and carbonate phases in a particular soil. In the Hawi soil, which has undergone less intensive leaching, carbonate is the largest reservoir of Mg (69±11%). In the Pololu soil, carbonate is important in individual soil horizons as a reservoir of Mg, but when looking at the soil as a whole is a smaller reservoir of Mg (16±2%). Therefore in the Pololu soil other secondary mineral pools take on larger roles in determining Mg distribution. In particular, short-range-order phases (allophane, imogolite, ferrihydrite) and residuum (primary basalt phases, gibbsite, spinel phases and associated weathering products) are the largest reservoirs of Mg in the <2-mm portions of our soils. Short-range-order phases are of particular interest, because these phases are metastable through time and will recrystallize into soil mineral pools with relatively little Mg (sesquioxides and kaolin group minerals).

2.1. INTRODUCTION

This chapter characterizes two arid Hawaiian soil sites that are part of an established soil chronosequence, with particular emphasis on Mg distribution between soil phases. This background information is necessary to understand the pedogenic processes at work at these two study sites and to construct valid models of how Mg is transported and how Mg isotopes are fractionated in these environments, topics discussed in later chapters.

2.1.1. Geochemical Consideration of Hawaii

As described in Vitousek (2004), geochemical homogeneity of the Hawaiian Islands simplifies two soil-forming factors: parent material and time. This homogeneity of the Hawaiian Islands is due to the nature of the intraplate oceanic island volcanism that has produced the islands. The volcanism is largely basaltic, and study sites can be found that have very similar parent material over the entire age range of the Hawaiian Islands. This basaltic parent material is also Mg-rich compared to more silicic rocks, making the islands perfect for a study of Mg from an analytical perspective, as this increases the amount of Mg within the soil during the initial stages of weathering and allows for the creation of more Mg-rich secondary soil minerals. There are subtle chemical and textural differences among lava flows, but these differences are relatively minor compared to the variation found in continental parent materials in both composition and crystallinity. Time is also well constrained by the Hawaiian lava flows, since one can use radiogenic isotope techniques to date many of the lava flows or use C-14 techniques to date charcoal associated with incinerated organic material.

2.1.2. Isolation of Hawaii

Vitousek (2004) also describes how the isolation of the Hawaiian Islands helps to simplify the soil forming factors of parent material and biota. Their location in the middle of the Pacific Ocean, away from continental landmasses, limits the influx of continental dust, which has a different chemical composition than the basaltic parent material and acts as an addition to surface soil horizons. In addition to directly altering the composition of the soil, the mica present in the dust can incongruently weather, forming a series of clay minerals that otherwise would not develop within the soils, thereby further confounding attempts to understand the formation of secondary soil minerals and their influence on the Mg isotopic system. On the older islands, and especially on the windward coasts that receive heavy rainfall, this dust may play an important role in the maintenance of the ecosystems that develop (Chadwick et al. 1999). Younger arid soils developing on the leeward coasts of Hawaiian volcanoes are less influenced by this input (Jackson et al. 1971; Kurtz et al. 2001).

The isolation of the Hawaiian Islands has also prevented many species from reaching them, allowing the few species that have arrived to diversify and fill multiple ecological niches. This paucity of species and the closely related nature of extant species reduces variability within the biota soil-forming factor. Isolation has also prevented humans from reaching and altering the soil development of Hawaii until relatively recently; the first Polynesians arrived on Hawaii around 500 AD.

2.1.3. Soil Sites

We chose two study sites on the arid leeward coast of Kohala Volcano with comparable parent material, present-day climatic conditions, biotic factors and topography, but which varied in age to allow us to investigate the evolution of the Mg isotopic systematics of basaltic soils

through time (Figure 2.1). These sites have been studied by a number of previous researchers, providing a rich set of data on which to develop the current study (Goodfellow et al. 2013).

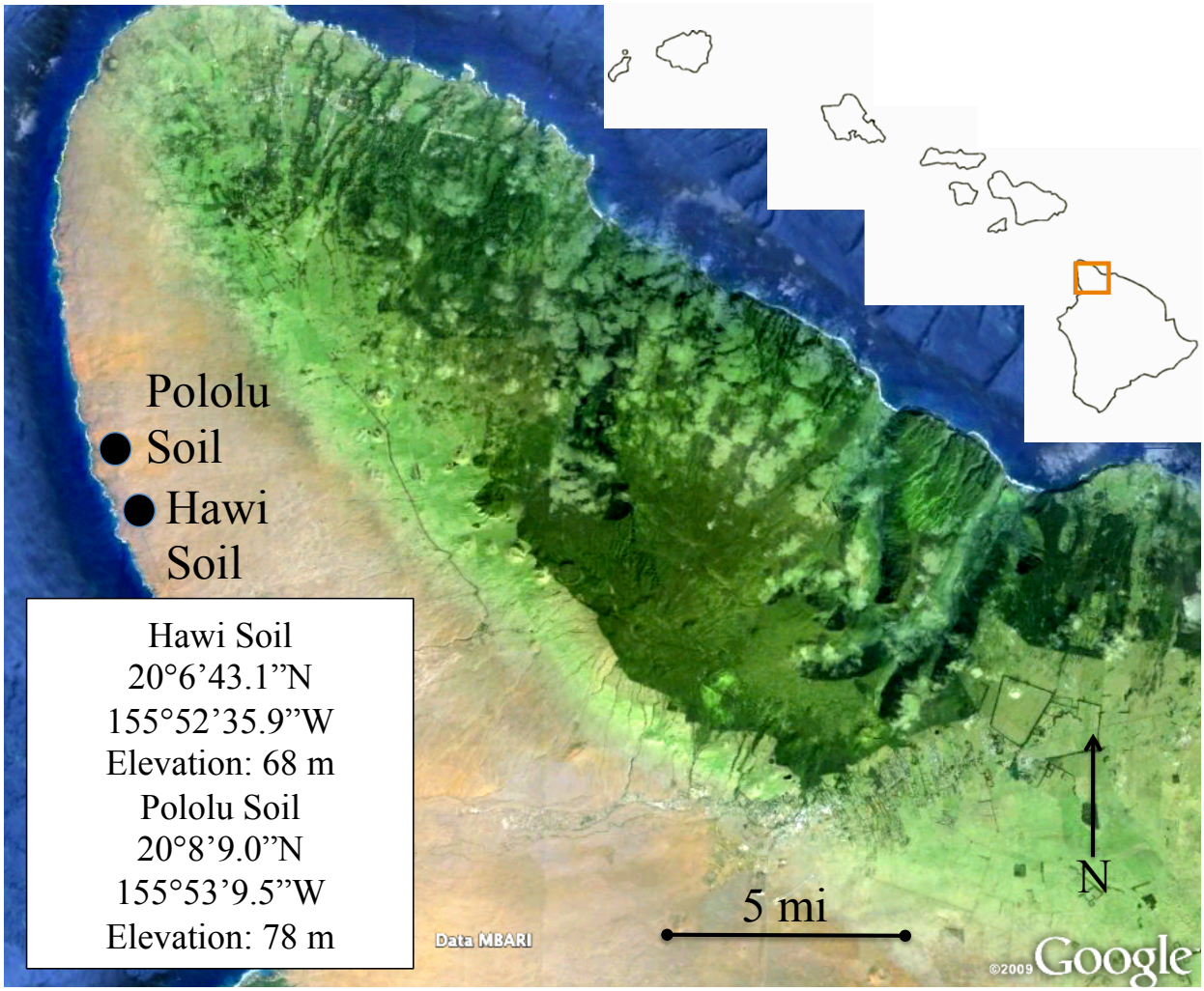

Figure 2.1: Map of study sites from a modified Google Earth image. Tradewinds from the northeast interact with the topography of the Kohala Volcano to create a rain shadow effect.

The soil-forming factors are nearly identical for the two sites. Both are at similar elevation and aspect with a mean annual precipitation of 35.0±0.5 cm for the Pololu site and 28.0±0.5 cm for the Hawi site, usually delivered by sporadic cyclonic storms (Giambelluca and Schroeder 1998; Giambelluca et al. 2013). Vegetation is dominated by non-native buffel grass (*Chenchrus ciliaris*) and kiawe trees (*Prosopis pallida*) with no current land use at both sites. Variations in soil properties between the two sites are primarily due to the age difference between sites, but slight differences in the parent materials may play a role as well (Porder et al. 2007).

The local climate has varied over the period of soil development for both sites. Ziegler et al. (2003) reconstructed the paleoenvironment of this area taking into account glacial-interglacial cycles and long-term subsidence. With these variables they arrive at a higher rainfall value of 63 cm/yr for these soils 170 ka ago during glacial intervals, and a soil temperature 3.7°C degrees cooler than the modern mean annual soil temperature of 28°C. This implies that both the Hawi and Pololu sites have experienced these wetter and cooler conditions during their history. Other studies have advanced our understanding of the paleoconditions at these sites, concluding that the sites were never closer to sea level than they are at present (Whipkey et al. 2002), and also that the water table at these sites has remained well below the pedogenic zone (Stearns and MacDonald 1946; Takasaki 1978).

The Hawi study site (Figure 2.2) is a soil developed on an alkalic a`a flow that caps Kohala Volcano and has been K-Ar dated at 0.23 to 0.12 Ma, hereafter referred to as 170 ka for simplicity (Wolf and Morris 1996; Chadwick et al. 2003). These lava flows are aphyric, contain higher percentages of trace elements than tholeiitic flows, and also lack phenocrystic clinopyroxene (McDougall 1969; McDougall and Swanson 1972; Macdonald et al. 1983;

Spengler and Garcia 1988). MgO weight percent throughout the Hawi flows averages ~3% (Spengler and Garcia 1988). The soil found at this site is classified as an isohyperthermic Typic Haplotorrands (Soil Survey Staff 1999).

The Pololu study site (Figure 2.3) has been K-Ar dated at 0.46 to 0.26 Ma, hereafter referred to as 350 ka for simplicity, and is composed of soil developed on a tholeiitic pahoehoe lava (Wolf and Morris 1996; Chadwick et al. 2003). The Pololu lavas are recognized by larger and more abundant phenocrysts and lack the trace mineral apatite, as found in the Hawi flows (McDougall 1969; McDougall and Swanson 1972; Macdonald et al. 1983; Spengler and Garcia 1988). MgO weight percent throughout the Pololu flows averages ~8% (Spengler and Garcia 1988). The soil found at this site is classified as an isohyperthermic Sodic Haplocambid (Ziegler et al. 2003).

Both soils contain a variety of secondary minerals including calcite, dolomite, allophane, imogolite, halloysite, gibbsite, ferrihydrite, hematite, and other trace phases (Chadwick et al. 2003; Zeigler et al. 2003). These soils have been utilized as the arid endmember of the Kohala climosequence and were also utilized in studies documenting the development of magnesian carbonates and the stability of halloysite (Capo et al. 2000; Whipkey et al. 2002; Ziegler et al. 2003; Chadwick et al. 2003), and so a significant amount of literature exists on their pedogenesis. Table 2.1 shows mineralogy from the Hawi and Pololu soils as determined by XRD (Ziegler et al. 2003; National Cooperative Soil Survey 2014).

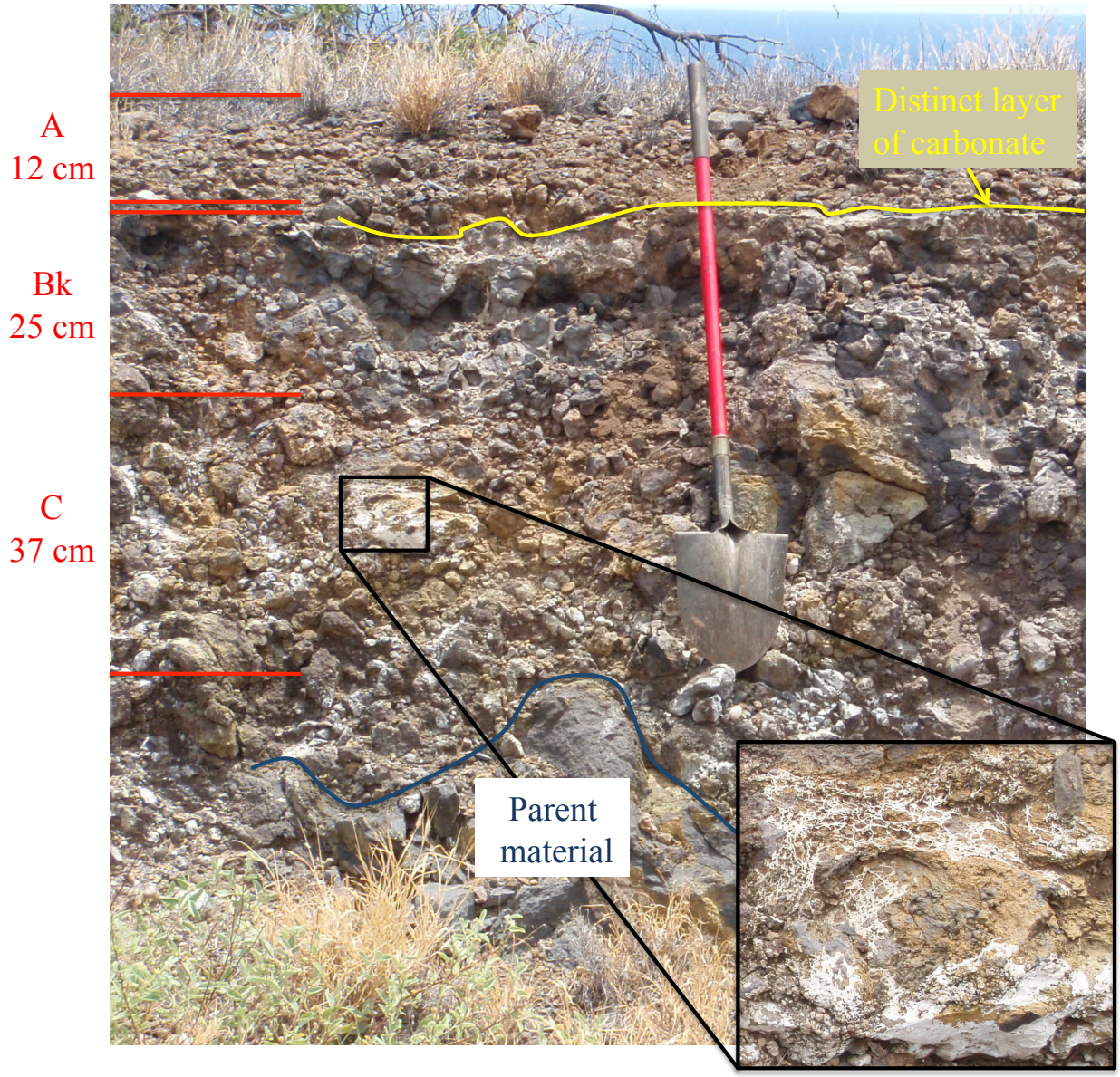

Figure 2.2: Soil development atop the Hawi (170 ka) lava flow. Inset image magnifies a region of carbonate accumulation.

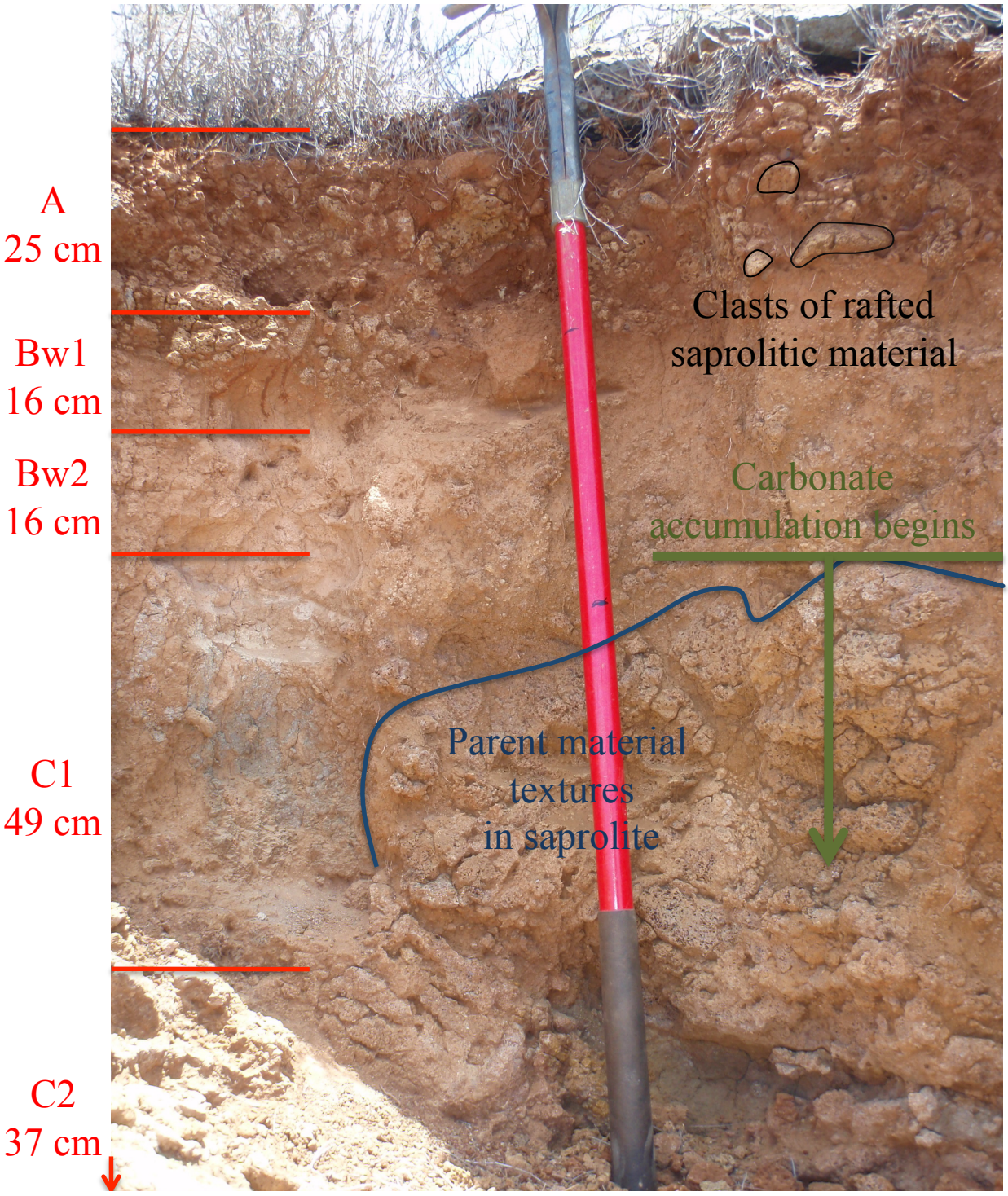

Figure 2.3: Soil development atop the Pololu (350 ka) lava flow. Horizon C2 continues down from this image until reaching unweathered parent material at 143 cm depth.

Table 2.1: Mineralogy by XRD for the Hawi and Pololu sites. Hawi data from Ziegler et al. (2003). Pololu data from the National Cooperative Soil Survey, Cooperative Soil Characterization Database (2014).

Soil Horizon	Depth to Horizon (cm)	Kaolin	Mica	Gibbsite	Hematite	Goethite
Pololu (350 ka)		0= not detected; 1= trace; 2= small quantity; 3= medium quantity; 3+= large quantity				
A	0--5	2	1	1	0	0
Bw1	5--26	--	--	--	--	--
Bw2	26--43	1	0	3	1	0
Bw3	43--60	--	--	--	--	--
Bw4	60--90	1	0	1	1	2
Bw5	90--102	--	--	--	--	--
Bw6	102--115	2	0	1	1	2
Hawi (170 ka)						
A	0--10	3+	1	1	1	0
Bw1	10--37	3+	1	1+	1+	0
Bw2	37--65	3	0	0	0	0
2Cr	65--100	3	0	1	1	0

2.2. REVIEW OF SOIL MINERALOGY

Understanding the mineralogy of these soils is key to understanding pedogenesis at the Kohala chronosequence sites and the distribution of Mg among soil phases. As such a brief review of important soil mineral phases at our study sites is included below.

2.2.1. Allophane and Imogolite

Allophane and imogolite are two hydrous, short-range-order, aluminosilicate clay minerals with variable chemical compositions that often form during the initial weathering of volcanic material (Parfitt 2009). Imogolite has a chemical formula of $(OH)_3Al_2O_3SiOH$ and "consists of an outer gibbsite-like curved sheet, while the inner surface consists of O_3SiOH, with oxygen replacing the inner hydroxyls of the gibbsite sheet"(Cradwick et al. 1972; Farmer and Fraser 1979). Allophane is chemically similar to imogolite but has a variable Al:Si ratio, anywhere from around 2:1 to 1:1 (Parfitt 2009). Some Fe^{3+} may also substitute into the octahedral site for Al^{3+}, but at higher Fe:Al ratios the iron-rich compositions can form their own phase of ferrihydrite (McBride et al. 1984). Structural Mg present in allophane would most likely be incorporated in the gibbsite-like sheet, substituting for Al; however, work conducted by Gerrard et al. (2007) shows that magnesium values fall below detectable limits for their microprobe energy dispersive X-ray spectroscopy (EDS) in all of their altered allophanitic phases.

The specific surface area of the aggregates formed by allophane and imogolite is high, with a value of around 600 m^2/g (Hall et al. 1985). This high surface area, along with regions of positive and negative charge, strong binding with organic material that stabilizes soil carbon, and strong interactions with anions (Parfitt 1990), makes the presence of these phases significant in

the biogeochemical functioning of soil. The stabilization of soil carbon can also lead to the development of greater water holding capacity of the soil (Dahlgren et al. 2004), which further influences secondary mineral formation. The large surface area and high variable surface charge of allophane and imogolite also make them excellent candidates for adsorbing Mg from soil solution.

2.2.2. Halloysite

Halloysite is composed of a tetrahedral sheet of silica and a gibbsite-like sheet, as in a 1:1 clay, with a single layer of water between separate structural 1:1 units (King 2009). It has an ideal chemical formula of $Si_2Al_2O_5(OH)_4*2H_2O$ and tends to form tubules with a diameter of 50 nm (Moore and Reynolds 1997). Halloysite can either form from allophane and imogolite at high silicic acid activity, or directly precipitate from soil solution (Parfitt et al. 1984; Parfitt and Wilson 1985). The length of the dry season in the soil-forming environment influences the transition from allophane to halloysite, as halloysite only forms in regions with a dry season; in particular only the 0.7 nm halloysite forms in regions with a long dry season, whereas those regions with shorter dry seasons form both 0.7 nm halloysite and 1 nm halloysite (Siefferman and Millot 1969). Much like allophane and imogolite, it is not known how much Mg can substitute into the structure of halloysite, but if present, Mg probably occurs in octahedral coordination substituting for Al in the gibbsite-like sheet. Halloysite also has a lower surface area (65 m^2/g) and lower variable surface charge than either allophane or imogolite (Theng et al. 1982).

2.2.3. Gibbsite

Gibbsite, with a chemical formula of $Al(OH)_3$, can be thought of as stacked sheets of closely packed hydroxide anions, with Al^{3+} ions between in 2/3 of the available octahedral positions, forming hexagonal rings. In gibbsite these layers are stacked atop one another with OH units directly above one another (Megaw 1934). Other polymorphs of $Al(OH)_3$ also exist, simply by altering the stacking of the layers, but the dominant polymorph in nature is gibbsite (Hsu 1989). $Al(OH)_3$ tends to form in highly weathered acidic soils where slow crystallization occurs, thereby favoring gibbsite over other polymorphs (Hsu 1989). It can be formed from the desilication of intermediary mineral weathering products, such as allophane, imogolite, and halloysite, but may also form directly from the chemical breakdown of primary minerals, if the leaching intensity is high enough (Hsu 1989). The solubility product (K_{sp}) for gibbsite is $10^{-33.96}$, so after formation it is relatively insoluble (Singh 1974). While the surface area of gibbsite can be high, the charge of gibbsite is determined by variable charge dependent on pH, as structural charge due to isomorphic substitution into gibbsite is limited (Hsu 1989). Gibbsite formation is associated with intense leaching; as such the amount of Mg available to be incorporated into the gibbsite structure is probably low.

2.2.4. Ferrihydrite

Ferrihydrite is a poorly ordered Fe^{3+} oxide, with a chemical composition often given as $5Fe_2O_3*9H_2O$ (Schwertmann and Taylor 1989). The structure of ferrihydrite is similar to hematite, which is composed of hexagonally closest packed oxygen and contains iron in 2/3 of the octahedral interstitial sites (Schwertmann and Taylor 1989). Ferrihydrite, however, has vacant iron sites, as well as water substituting for O, and variable crystallinity, all of which distort the crystal lattice (Schwertmann and Taylor 1989). It is associated with young Fe-oxide

accumulations and has a high surface area of 200 – 500 m^2/g (Schwertmann and Taylor 1989). As seen with allophane and imogolite, this large surface area contributes to its importance in biogeochemical cycling in soils (Schwertmann and Taylor 1989). Ferrihydrite has pH-dependent charge due to its hydroxylated surface, and its large surface area and poorly crystalline nature can result in charge from unsatisfied surface bonds (Schwertmann and Taylor 1989). It is known for its ability to adsorb cations, anions and organics, but this is dependent on pH and ionic strength (Schwertmann and Taylor 1989). Ferrihydrite itself is found in environments rich in organic matter and/or silicate in which Fe^{2+} is rapidly oxidized (Schwertmann and Taylor 1989). It is believed to form in these environments due to the inhibition of goethite phase formation by silica and/or organic anions (Schwertmann and Taylor 1989). Increases in temperature or decreases in moisture may result in the transformation of ferrihydrite to hematite (Williams and Coventry 1979; Coventry et al. 1983; Curi and Franzmeier 1984; Pena and Torrent 1984).

Mg is not commonly substituted into oxide structures (Schwertmann and Taylor 1989), and it is unknown if Mg can be a significant structural element in ferrihydrite. Ferrihydrite is a phase with a large surface area and high variable charge due to its poorly crystalline nature and could potentially play a large role in the adsorption of Mg.

2.2.5. Hematite

Hematite has the chemical formula Fe_2O_3. The structure of hematite consists of hexagonally closest packed oxygen and contains iron in 2/3 of the octahedral interstitial sites (Schwertmann and Taylor 1989). These layers are stacked atop of one another, but distorted in such a way as to produce waves within the iron layer in hematite (Schwertmann and Taylor 1989). In most aerobic soils goethite (FeOOH) is the stable iron oxide phase, but high temperature, well-drained, high pH soils favor the formation of hematite over goethite

(Schwertmann and Taylor 1989). Hematite formation may further require ferrihydrite as a precursor and then form from ferrihydrite by aggregation, dehydration and internal structural rearrangement (Schwertmann and Taylor 1989). Hematite has a surface area of around 50 to 120 m^2/g, which is less than that of ferrihydrite (Schwertmann and Taylor 1989). As with ferrihydrite, pH in the system is important in determining surface charge (Schwertmann and Taylor 1989). In addition, Al substitution can also occur in hematite, and Ti substitution can produce permanent structural charge (Tessens and Zauyah 1982). Mg substitution into hematite is unknown.

2.2.6. Calcite and Dolomite

Calcite, chemical formula $CaCO_3$, is a common pedogenic carbonate. Dolomite, chemical formula $CaMg(CO_3)_2$, is less common as a pedogenic phase (Whipkey et al. 2002). The structure of calcite has a rhombohedral unit cell as illustrated in Figure 2.4 (Doner and Lynn, 1989). This normal calcite structure can accommodate Mg into its crystal lattice, until around 10 mole percent $MgCO_3$ is reached (Reeder 1983). After this transition, the unit cell collapses along the a- and c-axes with additional Mg substitution, causing changes in crystal structure amenable to the smaller ionic size of Mg (Bischoff et al. 1983). These distortions are found in high-Mg calcite, which has anywhere from 5 mole percent to around 25 mole percent of $MgCO_3$ substituted into the calcite structure. Above this 25 mole percent $MgCO_3$, another transition occurs, owing again to the difference in size between the Ca^{2+} and Mg^{2+} ions. For higher percentages of Mg, a dolomite structure is formed. Stoichiometric dolomite has an ideal chemical formula of $CaMg(CO_3)_2$, but non-stoichiometric, less crystalline dolomite may have a lower mole percentage of $MgCO_3$ (Prothero and Schwab 2004). The structure of dolomite is similar to calcite, but its rhombohedral unit cell is distorted from calcite due to evenly distributed

layers of Ca and Mg (Prothero and Schwab 2004). The close similarity in ionic size between Fe^{2+} and Mg^{2+} (74 pm and 66 pm) leads to extensive solid solution between dolomite and ankerite, an iron-rich carbonate with an ideal chemical formula of $CaFe(CO_3)_2$ (Doner and Lynn 1989). The calcite structure can also accommodate a few mole percent $FeCO_3$ as well, and other divalent cation impurities can occur (Mn^{2+}, Zn^{2+}, Sr^{2+}, Ba^{2+}, Pb^{2+}, Cu^{2+}).

Both calcite and dolomite are found in arid environments due to the inability of weathering products to drain from soils completely. Upon subsequent evaporation and concentration of the soil solution, carbonates precipitate due to supersaturation (McFadden et al. 1991). After precipitation, the carbonates are still moderately soluble in water and may be redissolved and reprecipitated during following rainfall events. This can also lead to their advection in soil porefluids (Doner and Lynn 1989). Soil carbonates usually initially form as fine particles or coatings within certain horizons of the soil profile, and over time they may be concentrated into calcic or petrocalcic horizons at depth, as percolation transfers carbonates to lower soil horizons (Doner and Lynn 1989).

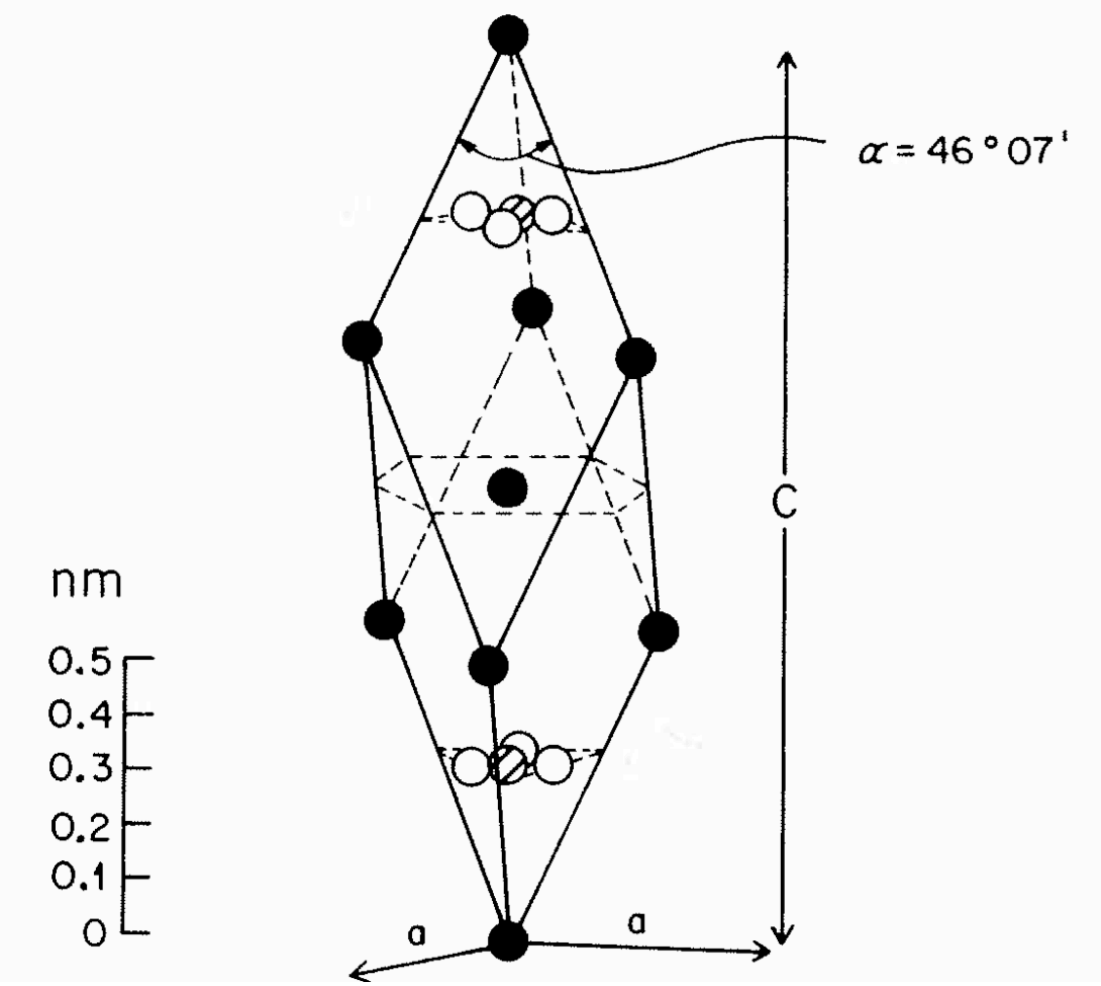

Figure 2.4: Calcite structure from Lippmann (1973). Black spheres indicate calcium, white spheres indicate oxygen, and striped spheres are carbon.

Figure 2.5 recaps the genetic pathways for the silicate and oxide mineral phases reviewed above and provides a generalized review of their properties. Note that the metastable short-range-order phases initially precipitated from soil solution (allophane, imogolite, ferrihydrite) usually have high surface areas and high surface charge, but gradually recrystallize to more stable phases (halloysite, gibbsite, hematite) with lower surface areas and charges.

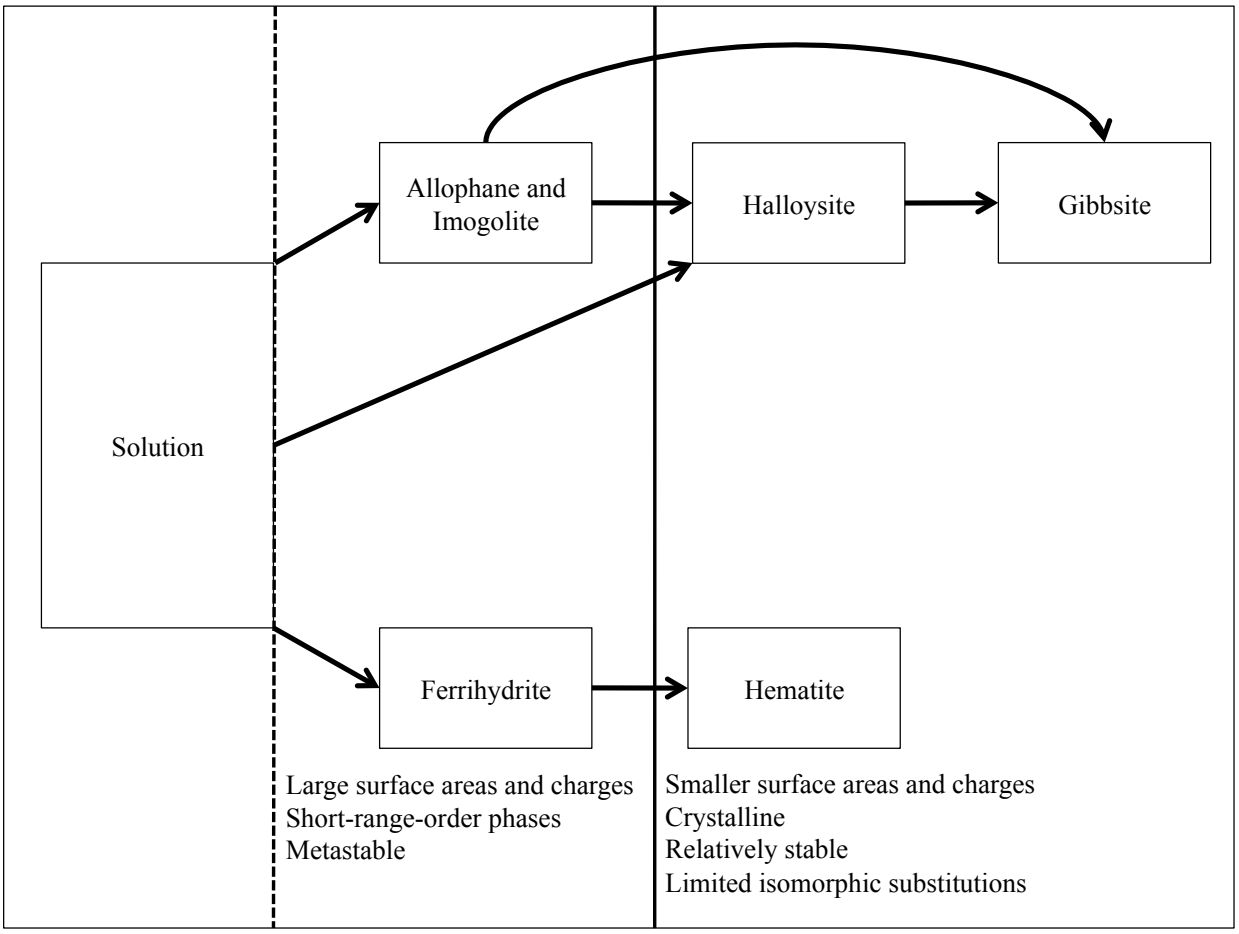

Figure 2.5: Genetic pathways for silicate and oxide minerals found at our Hawaiian study sites.

2.3. METHODS

2.3.1. Soil and Rock Sampling

Soils were described in the field and sampled by horizon to unweathered rock. For the two sites extensive chemical and physical characterization of the soils and basalts is available (Capo et al. 2000; Whipkey et al. 2002; Chadwick et al. 2003; Zeigler et al. 2003; Goodfellow et al. 2013).

2.3.2. Mineralogical Examination

Soils were analyzed by powder XRD to determine mineralogy. These XRD scans were conducted on bulk unoriented soils, as well as oriented <2-μm soil clay fractions in unglycolated and glycolated states. Indurated soil horizons and basalts were analyzed by optical microscopy to determine mineralogical compositions and replacement textures. The indurated soil horizons were also stained utilizing the technique of Dickson et al. (1966) in order to differentiate carbonates from one another. Some cathodoluminescent microscopy was attempted to distinguish trace element distributions in carbonate in indurated horizons. A semiquantitative EMPA (Electron Microprobe Analysis) was also conducted, in order to provide information on the chemistry of secondary phases too fine-grained to be identified by optical microscopy.

2.3.3. Bulk Soil and Rock Dissolutions

Soil samples were sieved on a 2-mm mesh screen. For each horizon, the <2-mm fraction was kept as a separate sample and dissolved. By contrast, the >2-mm fraction was combined with that of all the horizons in the soil profile. These >2-mm fractions were composed of rafted chunks of similar coherent saprolite material found throughout the soil profile. This combined

sample was then ground and dissolved. Using the relative proportions of the <2-mm and >2-mm fractions for each horizon, the bulk composition of each horizon was calculated.

Bulk soils and rock samples underwent the same treatment for dissolution. They were ground to a powder in a ceramic shatterbox, weighed (~0.05 g), and dissolved in 3 ml of HNO_3 and 1 ml of HF overnight in sealed Teflon beakers. The samples were evaporated to dryness in the presence of $HClO_4$. They were then redissolved in HNO_3. This solution was split into two fractions. One aliquot underwent the ion exchange column chemistry procedure described in Chapter 3 to isolate Mg for isotope work, and the other was analyzed by inductively coupled plasma optical emission spectrometry (ICPOES) to determine bulk composition. To provide a sense of soil heterogeneity on a decimeter scale, a subset of one of the soil horizons with a more competent texture different from the bulk horizon was also processed and designated C1 (57-106 subset) in the tables and figures of the results section.

2.3.4. Individual Carbonate Extraction

An individual extraction was conducted to remove carbonates from those soil horizons that contained them. Carbonates were dissolved from bulk samples (<2-mm and >2-mm fractions) of each soil horizon. A solution (either sodium acetate or ammonium acetate mixed with glacial acetic acid) buffered to a pH of 5 was added to each sample. The pH of these samples was monitored, along with effervescence. Additional glacial acetic acid was gradually added to each of these samples over the course of days until effervescence was no longer observed and pH dropped. Samples were then centrifuged, and the supernatant was removed. Samples were washed with an additional 10 ml of 0.5 M ammonium acetate and centrifuged again. This supernatant was added to the other and saved for chemical analysis.

2.3.5. Vegetation Dissolutions

Vegetation samples (0.75g) consisting of roots and shoots of Hawaiian grasses were dissolved in a microwave digester using a mixture of 9 ml of 5 N HNO_3 and 1 ml of H_2O_2. After this digestion the samples were treated with HF to remove silica phytoliths. Samples were centrifuged to ensure complete dissolution and the resulting solution used for analysis on ICPOES.

2.3.6. Soil Sequential Extractions

Samples of the <2-mm fraction of each soil horizon were subjected to a series of sequential extractions. These extraction methods are based on previous soil studies (McKeague and Day 1966; Holmgren et al. 1967; Jackson et al. 1986; Blakemore et al. 1987; Chadwick et al. 2003) that have been modified, and they are operationally-defined. The modified sequential mineral extraction consisted of seven steps, removing the following; adsorbed cations, soil organic matter (SOM), carbonates (in sequence), short-range-order (SRO) phases, sesquioxides, kaolin group minerals, and residual material (primary basalt phases, gibbsite, spinels and their weathering products). These fractions and the chemical operation to remove them can be seen in Figure 2.6. The supernatant from each of these steps was analyzed via ICPOES for chemistry and underwent ion exchange procedures to isolate Mg for isotopic analysis, described in Chapter 4.

A portion of each sample was oven-dried at 105 °C, so that all soils could be compared on an oven dry basis; however, sequential extractions were only performed on air-dried samples to prevent mineralogical changes due to heating. As the amount of water removed by oven drying was small for all samples (2-8 % by weight), and samples were not oven-dried between sequential extraction steps due to concerns over mineralogic alteration, all sequential extraction

data are presented relative to air-dried material. Extractions were initially carried out on 10 g of material to ensure adequate Mg for analysis in each extraction, but following the extraction of short-range-order phases by ammonium oxalate in the dark, a subset of material was used for the last three extractions.

The first extraction consisted of the removal of adsorbed cations by exchange with an ammonium acetate solution. This step is based on the Soil Survey Method Manual 5A8c. Adsorbed cations were removed from the soil using two rounds of 50 ml of 1 M ammonium acetate solution buffered to a pH of 7. The samples were centrifuged and filtered (0.45 μm), and the supernatant was saved for analysis.

The second extraction consisted of the removal of SOM by oxidation with hydrogen peroxide. A 30% hydrogen peroxide solution was added 20 ml at a time to the soils until reaction ceased and the soils were bleached. To these samples 20 ml of a 6.8 M ammonium acetate solution was added as a flocculant and to remove any adsorbed cations. Samples were centrifuged, and the filtered supernatant was removed. The samples were then washed with 10 ml of 0.5 M ammonium acetate, centrifuged and filtered. This supernatant was added to the other and saved for analysis.

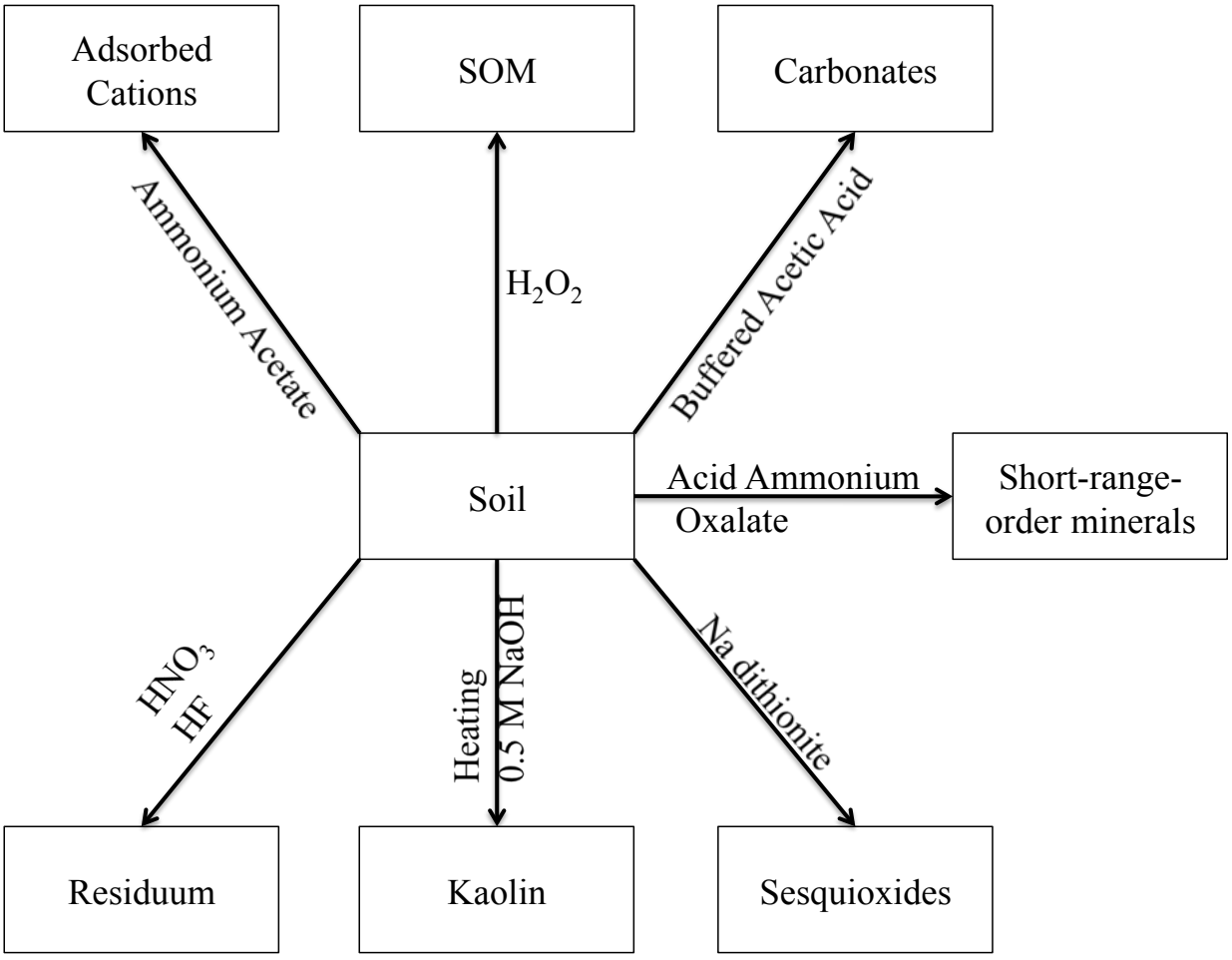

Figure 2.6: Overview of sequential extraction technique. Extractions were performed clockwise from "Adsorbed Cations".

The third extraction removed carbonates via the same procedure used for the individual carbonate extraction mentioned above, using a buffered ammonium acetate and glacial acetic acid solution. This process was done both in the sequential extraction and also independently to bulk soil samples for two reasons. First, the carbonate horizons were often cemented, and therefore the <2-mm fraction did not accurately reflect the carbonate in the soil system. Second, the carbonate extraction would also remove any adsorbed cations, so it needed to be conducted after the adsorbed cations were removed in the sequential extraction. However, as the sequential extractions for the adsorbed cations and SOM potentially removed reactive carbonate, a true estimate of overall carbonate is better presented by the individual carbonate extraction conducted on bulk soils.

The fourth extraction removed short-range-order phases through the acid oxalate in the dark (AOD) extraction (McKeague and Day 1966; Jackson et al. 1986; Chadwick et al. 2003). Following this extraction procedure an oxalate base solution (0.2 M) and an oxalate acid solution (0.2 M) were created and mixed together in a 4:3 ratio and adjusted to a pH of 3. This solution (600 ml) was added to each sample and the samples were shaken for four hours in the dark. Samples were centrifuged and the supernatant filtered. The samples were then washed twice with 10 ml of 0.5 M ammonium acetate, centrifuged and filtered. These supernatants were added to the other and saved for analysis.

The fifth extraction removed iron sesquioxides and goethite through the Na-dithionite reduction method (Holmgren et al. 1967; Blakemore et al. 1987; Chadwick et al. 2003). Following this method, 180 ml of a 0.68 M Na-citrate solution along with 3g of Na-dithionite were added to 2 g of the AOD processed sample. The samples were shaken overnight and then centrifuged and filtered to isolate the supernatant. Samples were washed once with 10 ml of 0.68

M Na-citrate solution and twice with 10 ml of 0.5 M ammonium acetate, centrifuged and filtered. These supernatants were added to the other and saved for analysis.

The sixth extraction removed kaolin group minerals and poorly crystalline components and is a simplification of other sequential extractions in the literature (Jackson et al. 1986; Chadwick et al. 2003). A 200 mg subset of sample following the removal of iron sesquioxides was weighed into porcelain crucibles and heated in a muffle furnace for 4 hours at 500ºC. This material was weighed again after heating and then placed into 170 ml of a boiling 0.5 M NaOH solution for 2.5 minutes, after which the beakers were cooled in a water bath. Samples were centrifuged and supernatants removed and filtered. Samples were washed twice with 20 ml of 0.5 M ammonium acetate, centrifuged and filtered. These supernatants were added to the other and saved for analysis.

The final extraction consisted of the dissolution of the residuum left over after the other extractions, which should have been predominantly gibbsite and spinel phases. This material was dissolved by the same HNO_3:HF dissolution as used for bulk soil and rock dissolutions.

2.4. RESULTS

2.4.1. Mineralogical Examination

The XRD analyses and thin sections support the mineralogical findings of the previous studies (Capo et al. 2000; Whipkey et al. 2002; Chadwick et al. 2003; Zeigler et al. 2003; Goodfellow et al. 2013). As such the detailed mineralogical data from previous studies are used as a source of mineralogic data for our sites, supplemented by our own analyses. XRD data from our analyses can be found in Table 2.2.

Table 2.2: Results from XRD analyses conducted on bulk samples and oriented clay-sized (<2-μm) grain mounts in glycolated and unglycolated states.

Soil Horizon	Depth to Horizon (cm)	Calcite	Dolomite	Kaolin	Gibbsite	Hematite	Plagioclase
Pololu (350 ka)		**Mineral detected**					
A	**0-25**			yes	yes	yes	
Bw1	**25-41**			yes	yes	yes	
Bw2	**41-57**			yes	yes	yes	
	57 (transition)	yes				yes	
C1	**57-106**	yes					
	57-106 (subset)	yes		yes			
C2	**106-143**	yes					
Hawi (170 ka)							
A	**0-12**						
	12-13	yes					
Bk	**13-38**	yes	yes				
C1	**38-75**					yes	yes

Optical microscopy of basalts shows that samples used as parent material are composed predominantly of primary phases (plagioclase, clinopyroxene, olivine, oxides), but that some slight alteration had occurred to these samples due to weathering. This alteration is visible in the rims and fractures of olivine or clinopyroxene phenocrysts. Basaltic glass in sample matrices also appears to have undergone alteration and may currently be palagonite (a hydrated basaltic glass).

Optical microscopy of the indurated soil horizons shows that they are cemented by a variety of phases, some of which are unidentifiable using optical microscopy due to small grain size or lack of distinguishing optical characteristics. Many of these horizons maintain the textural relationships of the parent basalts, but the primary minerals are often completely replaced by weathering products, except for the opaques. Images of one of the indurated carbonate horizons from the Hawi soil, along with semiquantitative EMPA analyses, illustrate the replacement of almost all primary basalt phases with secondary phases, without disturbing textural relationships of the parent rock (Figure 2.7). A significant and easily identifiable phase in these horizons is calcite, which replaces plagioclase or fills voids within in the original basalt. A light-colored isotropic phase or mixture of phases also replaces plagioclase in addition to calcite and is easily distinguished from carbonate in cross-polarized light (Figure 2.7). Other secondary phases or mixtures of phases include a yellow anisotropic fine-grained material that appears to replace clinopyroxene or basaltic glass, an orange or red anisotropic material replacing olivine, and a dark brown material of which it is difficult to discern the optical properties (Figure 2.7). A qualitative element map from EMPA of a similar thin section from the Pololu soil also allows insight into the chemical composition of these weathering phases. This map shows that the light-colored isotropic phase or mixture of phases replacing plagioclase is

associated with Si and Al, void spaces in the original parent basalt are associated with Ca and Mg, and phases replacing olivine and CPX are associated with Fe and to a lesser extent Mg (Figure 2.8).

Some indurated horizons do not maintain the original textures of parent materials. These horizons contain many similar phases to the indurated horizons described before, but the aluminosilicate and oxide secondary phases are contained in spheroidal aggregates cemented together by calcite (Figure 2.9).

Our carbonate staining technique allowed us to determine that most of the carbonate filling voids is a ferroan calcite phase (Figure 2.10). CL microscopy focused on carbonates only produced weak luminescence and was unable to assist in discerning different generations of carbonate. This may be due to the presence of Fe in the carbonate, which often acts as a quenching agent to luminescence (Machel 1985).

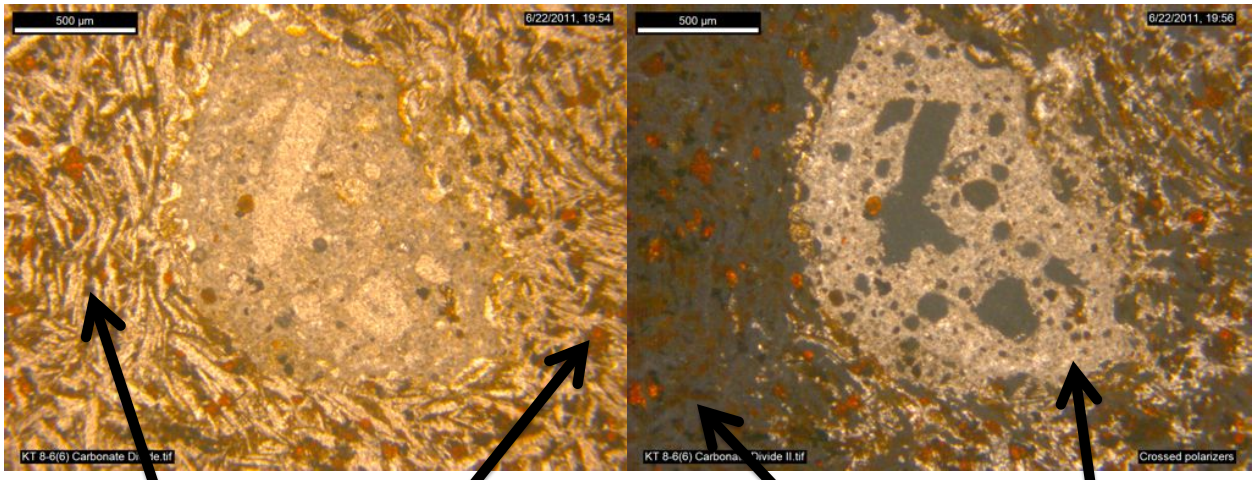

Oxide	Weight Percent
MgO	1.44
Al_2O_3	1.57
TiO_2	27.12
MnO	0.87
Fe_2O_3	68.96

Oxide	Weight Percent
MgO	3.42
Al_2O_3	14.11
SiO_2	7.28
CaO	0.91
TiO_2	0.57
MnO	3.99
Fe_2O_3	67.85

Oxide	Weight Percent
MgO	0.38
Na_2O	0.42
Al_2O_3	42.96
SiO_2	51.80
Fe_2O_3	3.05

Oxide	Weight Percent
MgO	6.5
CaO	93.47

Figure 2.7: Image of an indurated Hawi soil horizon in plane polarized light (left) and cross polarized light (right), along with semiquantitative EMPA analyses for weathering products in these horizons. Note replacement of all primary phases except for opaque oxides.

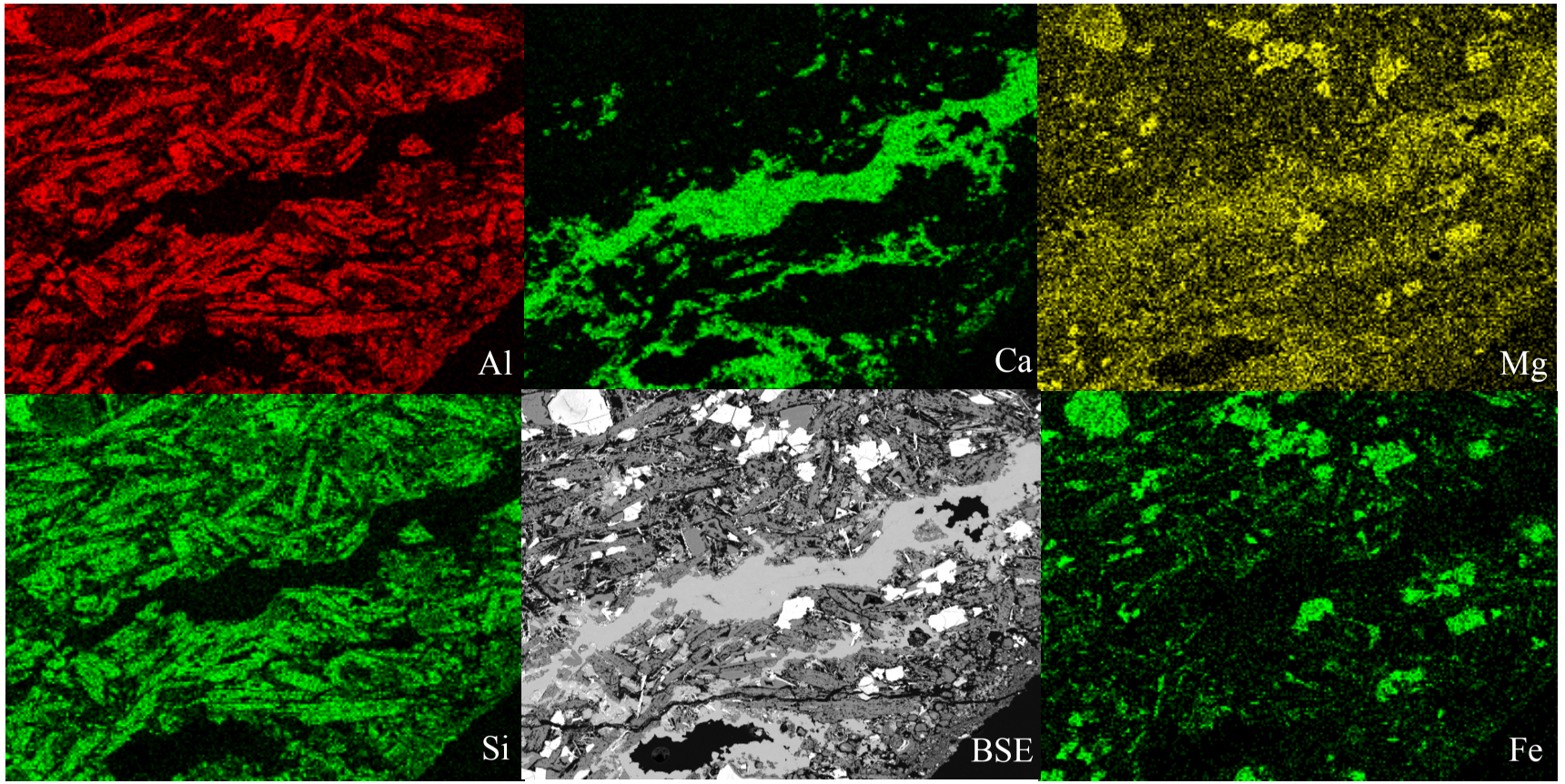

Figure 2.8: Qualitative element map of one of the indurated horizons of the Pololu soils. Back scatter electron (BSE) image is at center.

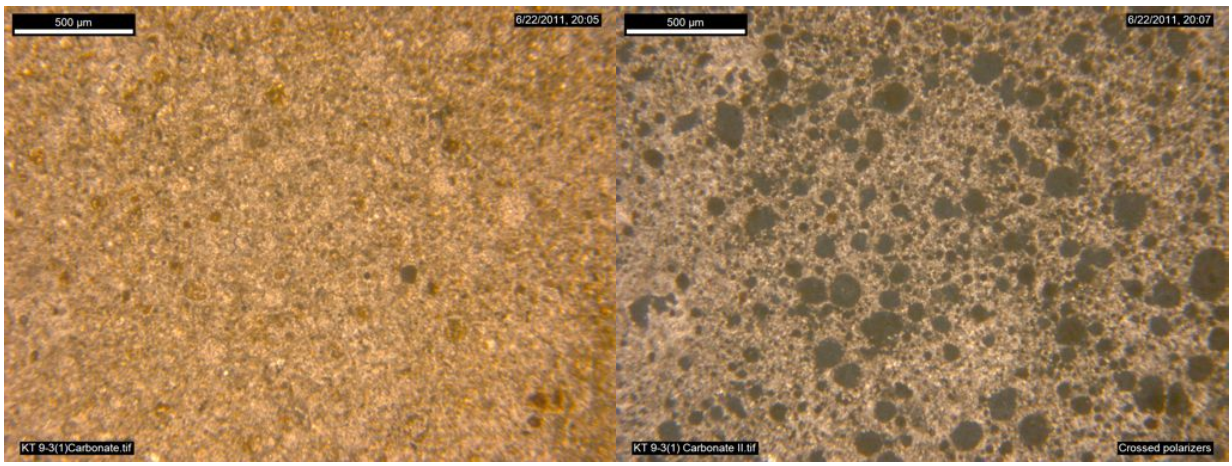

Figure 2.9: Image of an indurated Hawi soil horizon in plane polarized light (left) and cross polarized light (right). Carbonate matrix surrounds spheroidal aggregates of other secondary phases.

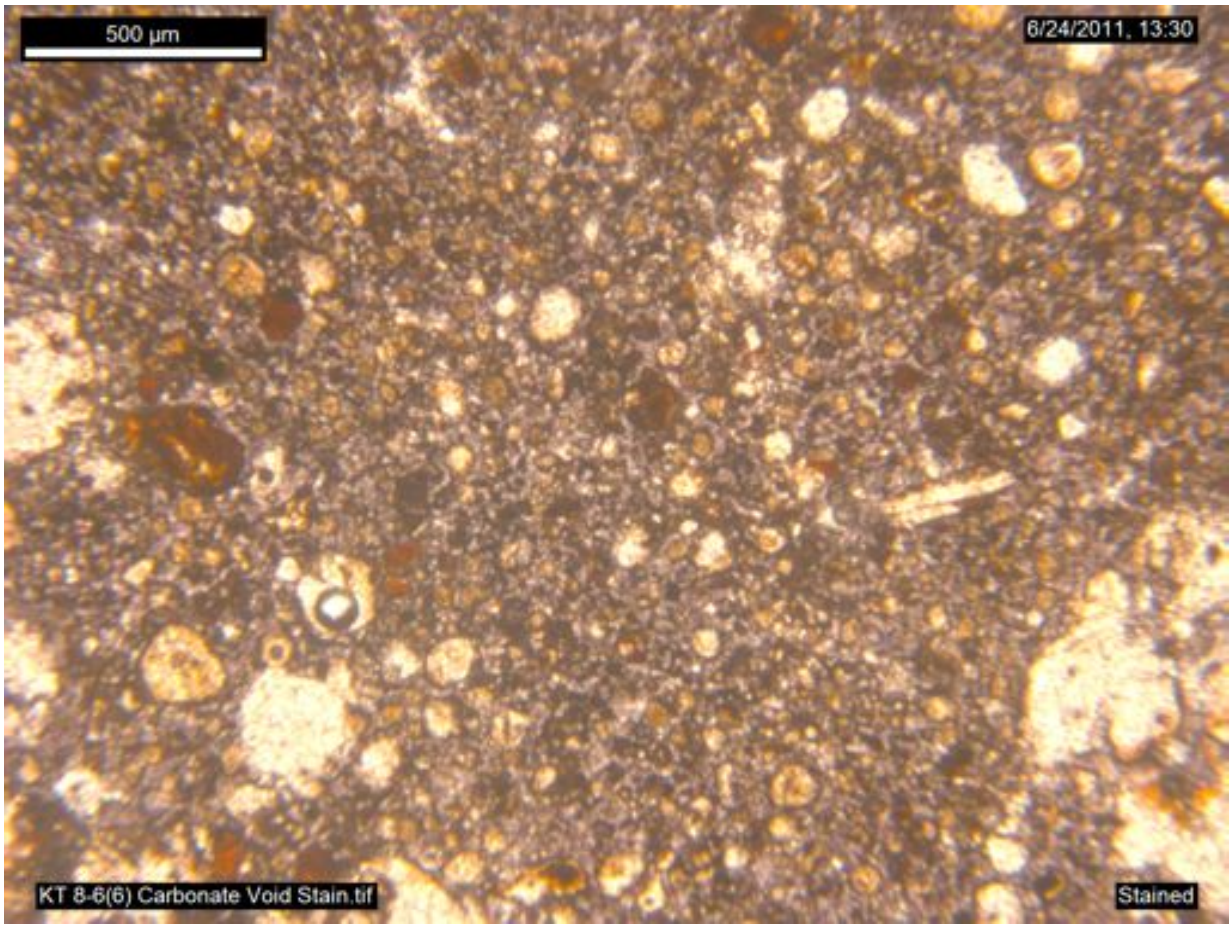

Figure 2.10: Image of an indurated Hawi soil horizon in plane polarized light after the staining technique of Dickson et al. 1966. The carbonate has taken the stain and turned blue, suggesting a ferroan calcite phase. This procedure also enhances the contrast between the carbonate cementing matrix and the spheroidal aggregates of other secondary phases.

2.4.2. Parent Material and Precipitation

Data for the bulk chemistry of basalt dissolutions are presented in Table 2.3 and elemental ratios in Table 2.4. Chemistry values of the Pololu tholeiitic basalts are more consistent than the Hawi alkalic basalts. Mg/Zr ratios can vary significantly in these parent materials from different locations, due to the partitioning of Mg into major phases, and the partitioning of Zr into trace phases. By using chemistry values from basalts sampled directly beneath the soil profiles, the uncertainty should be limited to basalt heterogeneity at the meter scale.

Average precipitation chemistry values for the island of Hawaii from Carrillo et al. (2002) are 1600 µg/l Na, 60 µg/l Mg, 200 µg/l K, and 50 µg/l Ca, but these values are highly variable. Basalt weathering and precipitation are the two main Mg inputs to our soil system. Basalts have Mg/Ca molar ratios ~1, and rainfall Mg/Ca molar ratios are ~2.

Table 2.3: Basalt bulk dissolution chemistry by ICPOES. Errors are 1σ analytical errors.

Soil Profile	Depth to Horizon (cm)	Na	Mg	Al	K	Ca	Sr	Fe	Mn	Ti	Zr
Pololu (350 ka)		**mg/g rock**									
1	143 +	24.0±0.3	38±1	81±1	9.0±0.4	64±1	0.73±0.01	99±2	1.39±0.02	18.7±0.3	0.26±0.03
1	143 +	22.3±0.3	36.1±0.9	77±1	8.7±0.1	63.9±0.9	0.68±0.02	93±1	1.29±0.02	17.7±0.4	0.26±0.01
Hawi (170 ka)											
2	107 +	18.5±0.3	53.6±0.9	69±1	5.7±0.3	72±2	0.494±0.008	91±2	1.27±0.03	15.8±0.3	0.159±0.006
3	75 +	36±1	27.2±0.7	81±1	12.6±0.3	53±1	1.78±0.02	91±1	1.69±0.03	17.6±0.3	0.30±0.01

Table 2.4: Basalt bulk dissolution elemental ratios. Errors are 1σ analytical errors.

Soil Profile	Depth to Horizon (cm)	K/Na	Mg/Ca	Fe/Al	Ti/Al	Mg/Zr
Pololu (350 ka)		**moles/moles**				
1	143 +	0.22±0.01	0.98±0.04	0.60±0.02	0.130±0.003	550±60
1	143 +	0.232±0.005	0.93±0.03	0.59±0.01	0.130±0.004	520±20
Hawi (170 ka)						
2	107 +	0.18±0.01	1.23±0.04	0.63±0.02	0.129±0.003	1270±50
3	75 +	0.202±0.008	0.85±0.03	0.55±0.01	0.123±0.003	340±20

2.4.3. Bulk Soil Samples

Data for the chemistry of the <2-mm portion of each soil horizon are shown in Tables 2.5 and 2.6. Table 2.7 and 2.8 show the arithmetically weighted average chemistry values for each entire bulk soil horizon, given the proportions of the <2-mm and >2-mm fractions of each. Values from Table 2.5 and 2.7 are used to create soil depletion index plots ($\tau_{element}$) with Zr as an immobile index element in Figures 2.11 and 2.12 (Anderson et al. 2002). These plots are calculated by the equation:

$$\tau_{element} = \left[\frac{(element/Zr)_{sample}}{(element/Zr)_{parent}}\right] - 1$$

These plots illustrate the diminished concentrations of alkali and alkaline earth elements in the soils compared to parent materials, and they also show the overall greater extent of weathering in the Pololu soil compared to the Hawi, especially for Na, Mg, K and Ca. When looking at the combined <2-mm and >2-mm tau plots (Figure 2.12), we see that much of the Na, K, Ca and Sr leached from the upper Hawi soil horizon has been translocated to depth. In the Pololu soil, however, these elements have been exported from all soil horizons.

Table 2.5: Soil bulk dissolution chemistry by ICPOES. Data for each horizon are for the bulk chemistry of the <2-mm soil fraction. Errors are 1σ analytical errors.

Soil Horizon	Depth to Horizon (cm)	Na	Mg	Al	K	Ca	Sr	Fe	Mn	Ti	Zr
Pololu (350 ka)		**(mg/g dry soil)**									
A	0-25	2.39±0.03	14.2±0.3	122±3	3.5±0.1	4.4±0.2	0.252±0.007	149±3	1.92±0.06	26.2±0.6	0.49±0.01
Bw1	25-41	1.11±0.02	11.4±0.2	151±5	1.56±0.02	2.58±0.03	0.132±0.003	141±3	1.50±0.02	26.3±0.6	0.64±0.01
Bw2	41-57	2.42±0.03	12.8±0.3	138±3	2.02±0.04	3.21±0.05	0.184±0.004	140±2	1.70±0.04	27.6±0.6	0.541±0.008
C1	57-106	3.66±0.05	14.4±0.5	104±1	1.5±0.1	25.8±0.6	0.183±0.004	126±3	1.01±0.02	23.8±0.8	0.43±0.02
C1	57-106 (subset)	3.84±0.07	14.1±0.4	113±2	3.2±0.1	21.2±0.8	0.182±0.004	119±3	1.35±0.02	24.3±0.3	0.40±0.01
Hawi (170 ka)											
A	0-12	3.08±0.04	20.54±0.3	119±2	3.4±0.2	20.7±0.6	0.49±0.01	140±2	2.60±0.04	24.7±0.6	0.488±0.009
	12-13	2.15±0.03	34±1	48±1	1.46±0.04	233±4	2.40±0.04	43±1	1.10±0.02	7.7±0.1	0.158±0.005

Table 2.6: Elemental ratios from the <2-mm bulk soil dissolutions. Errors are 1σ analytical errors.

Soil Horizon	Depth to Horizon (cm)	K/Na	Mg/Ca	Fe/Al	Ti/Al	Mg/Zr
Pololu (350 ka)		**moles/moles**				
A	0-25	0.87±0.04	5.3±0.3	0.59±0.02	0.121±0.004	109±3
Bw1	25-41	0.83±0.02	7.3±0.2	0.45±0.02	0.098±0.004	67±2
Bw2	41-57	0.49±0.02	6.6±0.2	0.49±0.02	0.113±0.004	89±2
C1	57-106	0.24±0.02	0.92±0.04	0.59±0.02	0.129±0.005	126±6
C1	57-106 (subset)	0.48±0.03	1.09±0.05	0.51±0.02	0.121±0.002	132±5
Hawi (170 ka)						
A	0-12	0.66±0.04	1.64±0.06	0.57±0.02	0.117±0.004	158±4
	12-13	0.40±0.01	0.238±0.009	0.43±0.02	0.090±0.003	810±40

Table 2.7: Soil bulk dissolution chemistry by ICPOES. Data for each horizon are a weighted average of the <2-mm bulk chemistry sample for that horizon and the >2-mm soil fraction bulk chemistry saprolite sample for that soil. Errors are 1σ analytical errors.

Soil Horizon	Depth to Horizon (cm)	Na	Mg	Al	K	Ca	Sr	Fe	Mn	Ti	Zr
Pololu (350 ka)		mg/g dry soil									
A	0-25	3.32±0.09	14.8±0.5	119±3	3.7±0.2	5.7±0.2	0.223±0.008	153±4	1.83±0.07	26.9±0.7	0.48±0.02
Bw1	25-41	1.58±0.09	12.0±0.4	146±5	1.9±0.1	3.2±0.2	0.139±0.005	144±4	1.53±0.03	26.5±0.7	0.62±0.02
Bw2	41-57	3.85±0.09	14.7±0.4	123±3	3.2±0.2	6.0±0.2	0.183±0.006	151±4	1.69±0.05	27.8±0.8	0.49±0.02
	57 (transition)	4.58±0.06	20.8±0.4	97±1	2.1±0.2	68.1±1	0.262±0.005	122±2	1.34±0.02	21.9±0.5	0.392±0.006
C1	57-106	4.4±0.1	15.3±0.6	112±2	3.1±0.2	13.1±0.6	0.183±0.006	148±5	1.48±0.04	26.6±0.9	0.45±0.02
	57-106 (subset)	4.4±0.1	15.2±0.5	115±2	3.7±0.2	11.8±0.8	0.183±0.006	146±4	1.58±0.04	26.8±0.6	0.44±0.02
C2	106-143	15.2±0.3	19.2±0.3	95±2	8.1±0.2	28.0±0.4	0.346±0.006	122±2	1.45±0.03	22.2±0.4	0.359±0.008
Hawi (170 ka)											
A	0-12	6.2±0.2	23.4±0.5	111±3	4.7±0.3	26.2±0.8	0.55±0.02	133±3	2.38±0.06	23.9±0.7	0.46±0.01
	12-13	8.9±0.2	28±1	95±2	5.6±0.2	56±4	0.83±0.04	116±2	2.01±0.04	21.3±0.4	0.390±0.009
Bk	13-38	9.9±0.2	44±1	64±1	5.1±0.2	132±2	1.61±0.03	56±1	1.37±0.03	9.7±0.2	0.25±0.01
C1	38-75	25.3±0.4	34.8±0.5	60±1	10.5±0.3	114±3	2.03±0.04	68±1	1.17±0.03	12.5±0.3	0.22±0.02

Table 2.8: Elemental ratios from the <2-mm and >2-mm combined bulk soil chemistry. Errors are 1σ analytical errors.

Soil Horizon	Depth to Horizon (cm)	K/Na	Mg/Ca	Fe/Al	Ti/Al	Mg/Zr
Pololu (350 ka)		**moles/moles**				
A	0-25	0.65±0.04	4.23±0.2	0.62±0.03	0.127±0.005	116±6
Bw1	25-41	0.69±0.07	6.1±0.4	0.48±0.02	0.102±0.005	73±4
Bw2	41-57	0.49±0.03	4.0±0.2	0.59±0.02	0.127±0.005	113±6
	57 (transition)	0.27±0.02	0.50±0.02	0.61±0.02	0.128±0.003	199±5
C1	57-106	0.42±0.03	1.9±0.1	0.64±0.02	0.134±0.005	128±8
	57-106 (subset)	0.49±0.03	2.1±0.2	0.62±0.02	0.132±0.004	130±7
C2	106-143	0.31±0.01	1.13±0.03	0.62±0.02	0.132±0.004	201±6
Hawi (170 ka)						
A	0-12	0.56±0.05	2.1±0.2	0.61±0.02	0.126±0.005	191±7
	12-13	0.48±0.04	0.9±0.1	0.65±0.02	0.134±0.004	270±20
Bk	13-38	0.30±0.02	0.55±0.02	0.42±0.01	0.085±0.003	660±50
C1	38-75	0.24±0.01	0.50±0.02	0.55±0.02	0.118±0.004	600±50

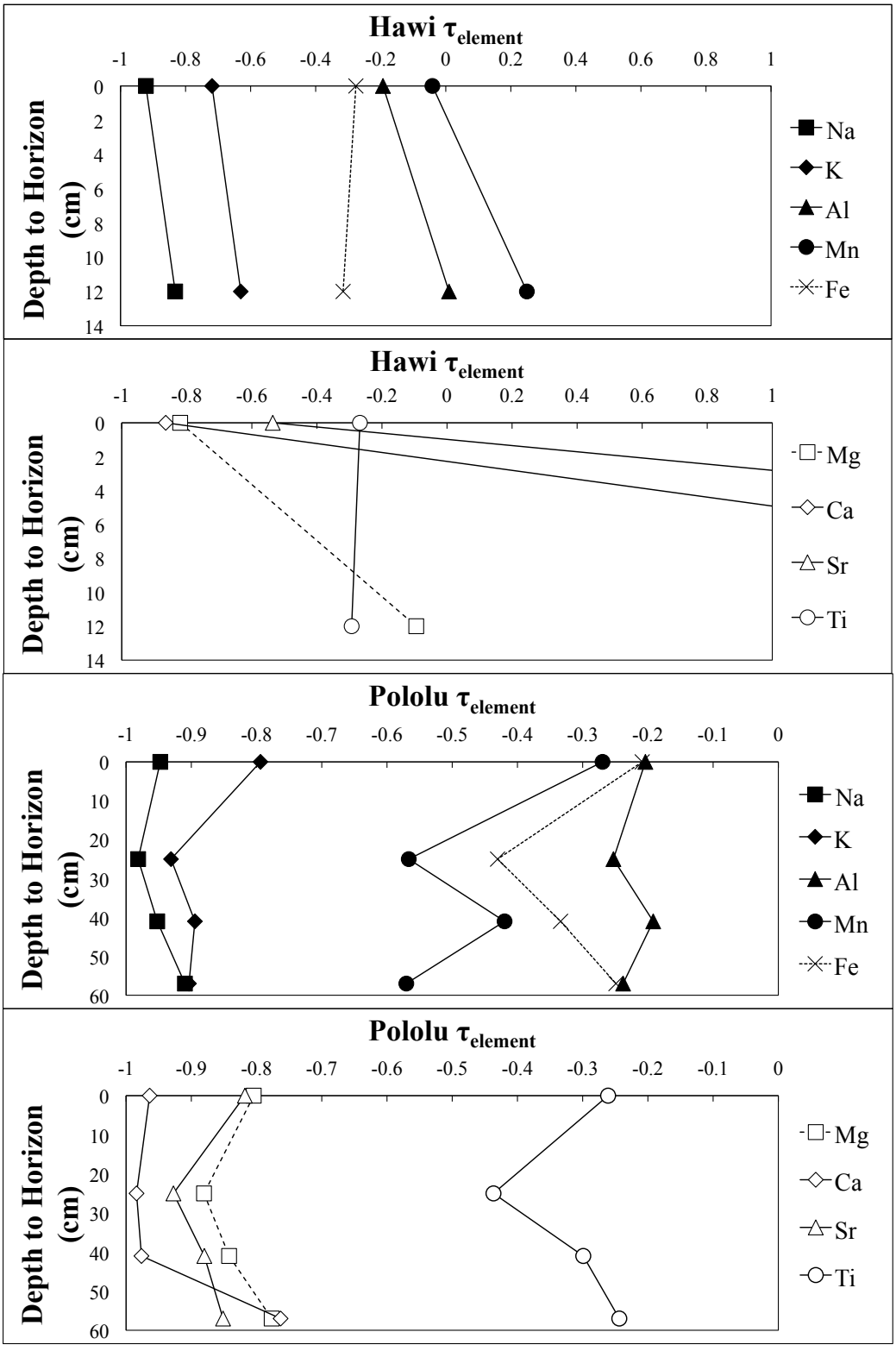

Figure 2.11: Soil depletion index plots for the Hawi and Pololu soils, using Zr as an immobile index element for the <2-mm fractions of our soils.

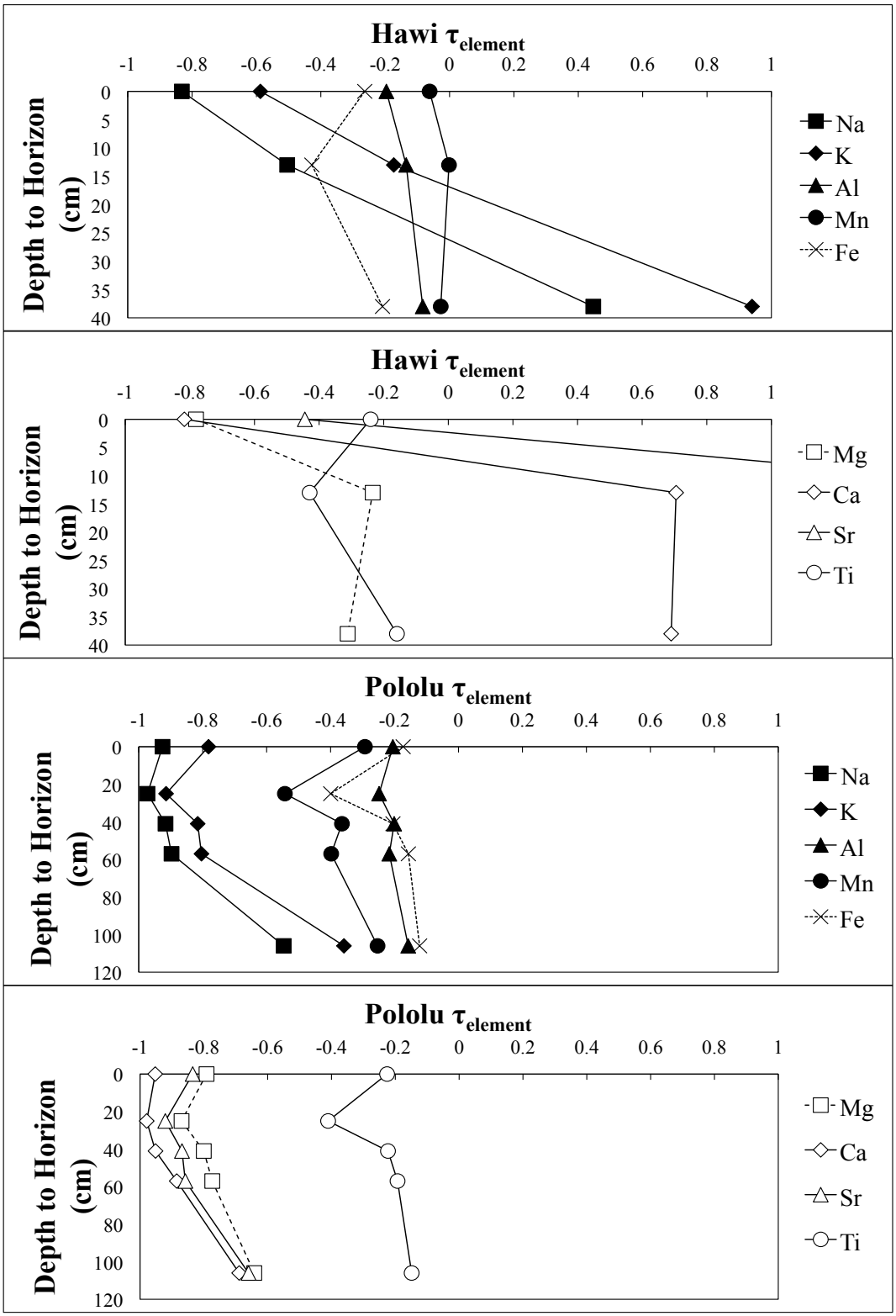

Figure 2.12: Soil depletion index plots for the Hawi and Pololu soils, using Zr as an immobile index element for the combined <2-mm and >2-mm fractions of our soils.

2.4.4. Individual Carbonate Extraction

Data for the individual carbonate dissolutions are presented in Tables 2.9 and 2.10. The chemical makeup of the extracted solutions suggests that the method designed to target carbonates was successful. Ca and Mg dominate the makeup of these fractions. Mg/Ca ratios for these carbonates increase with depth from 0.139±0.005 to 1.192±0.004 in the Pololu soil, suggesting the presence of a dolomitic phase. Pedogenic dolomite has previously been identified in these soils (Whipkey et al. 2002).

2.4.5. Vegetation

Chemistry and elemental ratios for the vegetation dissolutions are presented in Tables 2.11 and 2.12. The samples all have enriched K/Na ratios, suggesting that the dissolution was successful as plant samples should be enriched in K. Included in this dataset are two additional samples from a nearby study site "Mauna Kea" for comparison.

Table 2.9: Bulk chemistry results from the individual carbonate extraction as determined through ICPOES. No data indicate values are lower in concentration than our calibration curves or our limit of quantification (LOQ). For Na, Mg, Ca, Fe, Al, Ti and Si this limit is 100ppb; the limit is 1ppm for K and 10 ppb for Sr and Mn. Errors are 1σ analytical errors.

Soil Horizon	Depth to Horizon (cm)	Na	Mg	Al	K	Ca	Sr	Fe	Mn	Ti	Si
Pololu (350 ka)		**mg/g dry soil**									
C1	57-106	1.72±0.03	5.5±0.1	3.4±0.1	--	65±1	0.0158±0.0002	1.12±0.02	0.0263±0.0005	--	0.80±0.01
	57-106 (subset)	--	19.4±0.5	6.2±0.2	--	182±3	0.0464±0.0009	1.24±0.02	0.106±0.002	--	1.58±0.03
C2	106-143	1.44±0.04	2.69±0.05	2.28±0.05	--	3.71±0.06	--	2.52±0.05	0.236±0.003	--	1.52±0.03
Hawi (170 ka)											
	12-13	1.10±0.05	25.0±0.4	11.7±0.2	--	243±4	0.255±0.004	2.33±0.03	0.076±0.003	--	2.43±0.05
Bk	13-38	4.79±0.08	36.7±0.7	6.6±0.1	--	137±2	0.163±0.003	1.71±0.03	0.111±0.002	--	1.67±0.04
C1	38-75	--	23.9±0.5	0.85±0.01	--	87±1	0.084±0.001	0.71±0.01	0.152±0.002	--	1.61±0.03

Table 2.10: Molar ratios among divalent cations from the individual carbonate extraction. Errors are 1σ analytical errors.

Soil Horizon	Depth to Horizon (cm)	Mg/Ca	Sr/Ca	Sr/Mg
Pololu (350 ka)		**molar ratio**		
C1	57-106	0.139±0.005	0.000111±0.000004	0.000798±0.00003
	57-106 (subset)	0.176±0.007	0.000117±0.000004	0.000663±0.00003
C2	106-143	1.192±0.004	--	--
Hawi (170 ka)				
	12-13	0.170±0.005	0.000480±0.00002	0.00283±0.00009
Bk	13-38	0.44±0.02	0.000546±0.00002	0.00123±0.00004
C1	38-75	0.45±0.02	0.000441±0.00001	0.000971±0.00004

Table 2.11: Vegetation dissolution chemistry by ICPOES. Errors are 1σ analytical errors.

Vegetation Sample	Na	Mg	Al	K	Ca	Sr	Fe	Mn	Ti
	mg/g oven dried vegetation								
Pololu (350 ka)	0.219±0.003	2.12±0.03	0.348±0.006	11.0±0.2	2.58±0.03	0.00424±0.00005	0.79±0.01	0.148±0.002	0.084±0.002
Hawi (170 ka)	0.174±0.003	1.72±0.02	0.468±0.006	10.9±0.2	2.41±0.03	0.0110±0.0002	0.467±0.006	0.0600±0.0007	0.0597±0.0008
Mauna Kea	0.121±0.003	0.93±0.01	0.567±0.007	2.09±0.03	1.93±0.02	0.00296±0.00004	0.578±0.006	0.0178±0.0002	0.085±0.001
Mauna Kea	0.175±0.004	1.03±0.02	0.522±0.007	2.86±0.04	2.53±0.03	0.00375±0.00005	0.679±0.008	0.0159±0.0002	0.0710±0.0008

Table 2.12: Vegetation elemental ratios. Errors are 1σ analytical errors.

Vegetation Sample	K/Na	Mg/Ca	Sr/Ca
	moles/moles		
Pololu (350 ka)	29.7±0.6	1.35±0.02	0.00075±0.00001
Hawi (170 ka)	36.9±0.9	1.18±0.02	0.00208±0.00004
Mauna Kea	10.2±0.2	0.80±0.01	0.00070±0.00001
Mauna Kea	9.6±0.3	0.67±0.01	0.00068±0.00001

2.4.6. Sequential Extractions

2.4.6.1. Adsorbed Cations

Data for the chemistry of the adsorbed cations by soil horizon for the <2-mm soil fractions can be found in Tables 2.13 and 2.14. The chemical composition of the adsorbed cation extraction suggests that this extraction was not confounded, with the exception of the lowest soil horizons in both the Hawi and Pololu soils. Elements not usually found adsorbed onto surfaces (Al, Fe, Mn, Ti) are below our analytical abilities to quantify. Other elements show well-documented trends due to biological uptake, such as the concentration of Ca and K in surface horizons. Mg and Ca concentrations increase in the lowest horizons of both the Pololu and Hawi soils in this fraction. This increase is a result of the inadvertent dissolution of reactive calcite. The dissolution of calcite is inferred from the decrease in both Mg/Ca and Sr/Ca ratios for these horizons, as calcite has low Mg and Sr partition coefficients (Rimstidt et al. 1998).

2.4.6.2. SOM

The chemistry of SOM fractions is presented in Tables 2.15 and 2.16. The chemistry of the SOM extraction shows similar trends to the adsorbed cation extraction, with Al, Fe, Mn, and Ti at low concentrations or below our analytical capabilities. This suggests that the extraction successfully targeted the SOM, with the exception of the lower soil horizons that contain carbonates. Mg/Ca and Sr/Ca ratios decrease in the lower soil horizons. These trends indicate the dissolution of calcite, which is expected for this extraction, as the pH of these solutions was not buffered, and the addition of H_2O_2 to these soils would produce acidity (Mikutta et al. 2005).

Table 2.13: Chemistry data from the adsorbed cation sequential extraction. Errors are 1σ analytical errors.

Soil Horizon	Depth to Horizon (cm)	Na	Mg	Al	K	Ca	Sr	Fe	Mn	Ti	Si
Pololu (350 ka)		**mg/g dry soil**									
A	0-25	0.55±0.02	1.75±0.02	--	2.13±0.03	6.19±0.08	0.408±0.006	--	--	--	0.062±0.006
Bw1	25-41	0.56±0.01	1.19±0.02	--	--	3.43±0.05	0.167±0.002	--	--	--	0.041±0.001
Bw2	41-57	1.53±0.03	2.12±0.04	--	1.17±0.02	4.89±0.06	0.279±0.005	--	--	--	0.047±0.002
C1	57-106	6.0±0.2	4.73±0.06	--	1.59±0.03	15.9±0.2	0.175±0.003	--	--	--	0.023±0.002
C1	57-106 (subset)	1.12±0.01	3.45±0.04	--	1.28±0.02	14.6±0.2	0.173±0.003	--	--	--	0.032±0.001
Hawi (170 ka)											
A	0-12	1.04±0.01	2.49±0.03	--	1.92±0.02	8.7±0.1	0.615±0.009	--	--	--	0.046±0.001
	12-13	3.81±0.05	4.26±0.05	--	2.45±0.03	28.4±0.4	0.604±0.007	--	--	--	0.022±0.002

Table 2.14: Elemental ratios from the adsorbed cation sequential extraction. Errors are 1σ analytical errors.

Soil Horizon	Depth to Horizon (cm)	K/Na	Mg/Ca	Sr/Ca
Pololu (350 ka)		**moles/moles**		
A	0-25	2.26±0.08	0.466±0.008	0.0301±0.0006
Bw1	25-41	--	0.57±0.01	0.0223±0.0004
Bw2	41-57	0.45±0.01	0.71±0.02	0.0260±0.0006
C1	57-106	0.156±0.005	0.492±0.008	0.0050±0.0001
C1	57-106 (subset)	0.67±0.01	0.388±0.007	0.0054±0.0001
Hawi (170 ka)				
A	0-12	1.08±0.02	0.471±0.008	0.0322±0.0006
	12-13	0.379±0.006	0.247±0.004	0.0097±0.0002

Table 2.15: Chemistry data from the SOM sequential extraction. Errors are 1σ analytical errors.

Soil Horizon	Depth to Horizon (cm)	Na	Mg	Al	K	Ca	Sr	Fe	Mn	Ti	Si
Pololu (350 ka)		**mg/g dry soil**									
A	0-25	0.423±0.006	0.231±0.003	--	0.069±0.005	0.291±0.007	0.0294±0.0009	--	0.0176±0.0002	--	0.046±0.002
Bw1	25-41	0.224±0.003	0.139±0.002	0.97±0.01	0.035±0.004	0.532±0.006	0.0252±0.0003	0.0120±0.0002	0.219±0.003	--	0.183±0.003
Bw2	41-57	0.298±0.004	0.277±0.006	--	--	0.320±0.006	0.0214±0.0004	--	0.0352±0.0005	--	0.067±0.001
C1	57-106	0.473±0.006	0.73±0.02	--	0.05±0.01	4.667±0.05	0.0307±0.0003	--	--	--	0.0256±0.0003
C1	57-106 (subset)	0.409±0.007	0.71±0.03	--	--	3.44±0.04	0.0223±0.0003	--	--	--	0.0266±0.0004
Hawi (170 ka)											
A	0-12	0.51±0.01	0.42±0.01	0.026±0.001	0.050±0.004	0.084±0.003	0.0444±0.0002	--	0.0217±0.0003	--	0.083±0.001
	12-13	0.565±0.007	2.37±0.09	--	0.067±0.009	19.3±0.6	0.230±0.0003	--	--	--	0.037±0.002

Table 2.16: Elemental ratios from the SOM sequential extraction. Errors are 1σ analytical errors.

Soil Horizon	Depth to Horizon (cm)	Mg/Ca	Sr/Ca
Pololu (350 ka)		**moles/moles**	
A	0-25	1.31±0.04	0.046±0.002
Bw1	25-41	0.432±0.008	0.0217±0.0003
Bw2	41-57	1.43±0.04	0.0305±0.0008
C1	57-106	0.257±0.006	0.00301±0.00005
C1	57-106 (subset)	0.34±0.01	0.00297±0.00005
Hawi (170 ka)			
A	0-12	8.3±0.4	0.24±0.01
	12-13	0.20±0.01	0.0055±0.0002

2.4.6.3. Sequential Carbonates

The chemical analyses of the sequential carbonate dissolution are presented in Tables 2.17 and 2.18. These extractions are dominated by Ca and Mg as expected for an extraction targeting carbonates, but evidence of significant quantities of Al suggests other phases may have dissolved. The petrologic work illustrating the intermingling of carbonate and aluminum silicate phases in indurated horizons may explain the release of some Al during the dissolution of carbonate (Figure 2.7). High molar ratios of Mg/Ca in the carbonates suggest that the carbonate phase is predominantly high-Mg calcite or mixtures of calcite and dolomite. As carbonate contamination of the adsorbed cation and SOM sequential extractions has been illustrated, it should be noted that this extraction does not accurately portray the chemistry of all the carbonate in the <2-mm soil fraction of each horizon. Preferential dissolution of certain carbonate generations during the earlier extractions could lead to skewed results. Comparing elemental ratios between the individual carbonate extraction and the sequential carbonate extraction supports this view, as Mg/Ca ratios and Sr/Ca ratios are consistently higher in the sequential extraction.

Table 2.17: Chemistry data from the carbonate sequential extraction. Errors are 1σ analytical errors.

Soil Horizon	Depth to Horizon (cm)	Na	Mg	Al	K	Ca	Sr	Fe	Mn	Ti	Si
Pololu (350 ka)		**mg/g dry soil**									
A	0-25	--	--	--	--	--	--	--	--	--	--
Bw1	25-41	--	--	--	--	--	--	--	--	--	--
Bw2	41-57	--	--	--	--	--	--	--	--	--	--
C1	57-106	0.0710±0.0008	3.03±0.07	6.44±0.08	--	21.6±0.3	0.075±0.002	2.41±0.04	0.106±0.002	--	1.12±0.01
C1	57-106 (subset)	0.072±0.001	2.40±0.06	3.96±0.04	--	13.6±0.2	0.050±0.001	0.653±0.008	0.106±0.002	--	0.88±0.01
Hawi (170 ka)											
A	0-12	--	--	--	--	--	--	--	--	--	--
	12-13	0.108±0.002	6.01±0.06	11.8±0.2	--	38.4±0.6	0.397±0.007	2.46±0.03	0.110±0.002	--	1.85±0.03

Table 2.18: Elemental ratios from the carbonate sequential extraction. Errors are 1σ analytical errors.

Soil Horizon	Depth to Horizon (cm)	Mg/Ca	Sr/Ca
Pololu (350 ka)		**moles/moles**	
C1	57-106	0.231±0.006	0.00158±0.00004
C1	57-106 (subset)	0.292±0.008	0.00169±0.00004
Hawi (170 ka)			
	12-13	0.258±0.005	0.0047±0.0001

2.4.6.4. SRO phases

The chemistry data for the SRO extraction are in Tables 2.19 and 2.20. In these soils the dominant SRO materials should be allophane [$Al_2O_3(SiO_2)_{1.3\text{-}2}$•2.5-3$H_2O$], imogolite [$(OH)_3Al_2O_3SiOH$], and ferrihydrite [$5Fe_2O_3$•$9H_2O$]. These phases are dominated by Al, Si, and Fe, as are the results from our chemical analyses, suggesting that the sequential extraction was successful in targeting SRO materials. Si:Al ratios vary between 0.366±0.008 and 0.95±0.02 in our results and are indicative of the dissolution of allophane and imogolite, which have Si:Al ratios that range from 0.5 to 1 (Parfitt 2009). The chemistry results also suggest that a significant amount of Mg, Mn, and Ti can be sequestered in these phases. Ti concentrations correlate with Fe concentrations in the Pololu soil horizons, suggesting Ti is predominantly sequestered in ferrihydrite (Figure 2.13). Mg follows a similar trend but is less strongly correlated with Fe concentrations, suggesting that allophane and imogolite play a role as well. High Mg/Ca ratios show that Mg is preferentially retained in these SRO phases compared to Ca.

Table 2.19: Chemistry data from the SRO sequential extraction. Errors are 1σ analytical errors.

Soil Horizon	Depth to Horizon (cm)	Na	Mg	Al	K	Ca	Sr	Fe	Mn	Ti	Si
Pololu (350 ka)		**mg/gram dry soil**									
A	0-25	--	6.0±0.2	18.8±0.3	--	0.42±0.01	--	57±2	1.04±0.02	4.9±0.1	11.4±0.2
Bw1	25-41	--	4.31±0.09	29.1±0.5	--	0.51±0.03	--	49±1	0.67±0.01	4.39±0.08	11.1±0.2
Bw2	41-57	--	8.1±0.2	22.9±0.4	--	0.36±0.02	--	63±1	1.01±0.02	5.7±0.1	15.8±0.3
C1	57-106	--	6.9±0.2	20.1±0.3	--	0.230±0.009	--	69±1	0.437±0.007	6.5±0.2	14.7±0.2
C1	57-106 (subset)	--	6.4±0.2	11.7±0.2	--	0.249±0.005	--	50±1	0.59±0.01	5.03±0.08	11.6±0.2
Hawi (170 ka)											
A	0-12	--	6.8±0.2	33.3±0.6	--	0.24±0.01	--	37±2	0.88±0.02	3.16±0.05	14.2±0.4
	12-13	--	4.9±0.1	28.0±0.5	--	0.49±0.02	--	23.5±0.5	0.73±0.01	2.62±0.06	16.1±0.3

Table 2.20: Elemental ratios from the SRO sequential extraction. Errors are 1σ analytical errors.

Soil Horizon	Depth to Horizon (cm)	Mg/Ca	Si/Al	Fe/Al	Ti/Al
Pololu (350 ka)		**moles/moles**			
A	0-25	24±1	0.58±0.01	1.46±0.04	0.146±0.004
Bw1	25-41	14.0±0.7	0.366±0.008	0.81±0.03	0.085±0.002
Bw2	41-57	38±2	0.66±0.02	1.34±0.03	0.141±0.004
C1	57-106	50±2	0.70±0.01	1.67±0.04	0.183±0.005
C1	57-106 (subset)	43±2	0.95±0.02	2.08±0.05	0.242±0.005
Hawi (170 ka)					
A	0-12	47±2	0.41±0.01	0.54±0.03	0.0535±0.001
		16.7±0.7	0.55±0.02	0.40±0.01	0.0527±0.002

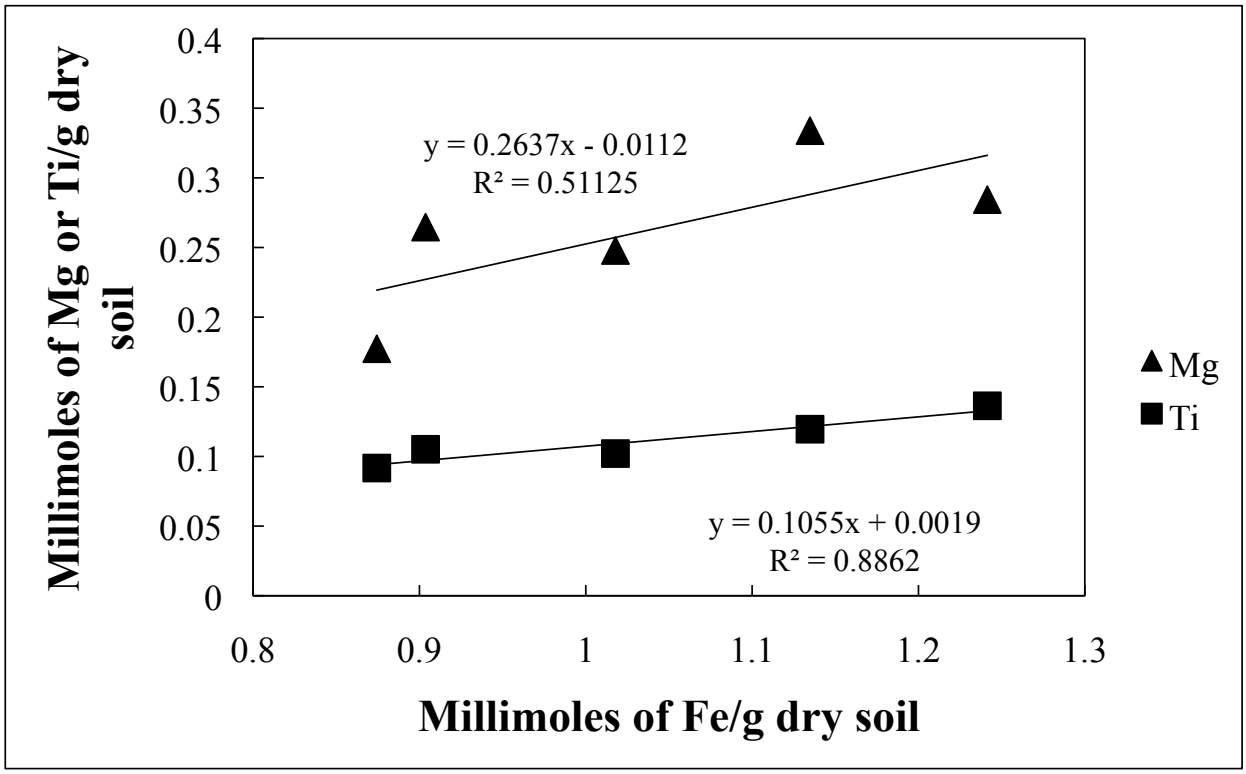

Figure 2.13: Mg and Ti trends with Fe for the SRO extraction. One σ analytical errors are smaller than symbol size.

2.4.6.5. Sesquioxides

Sesquioxide fraction chemistry data are presented in Tables 2.21 and 2.22. The sesquioxide extraction is designed to remove the crystalline iron phases hematite (Fe_2O_3) and goethite (FeOOH) from the soil. Chemical analyses support the efficacy of the extraction, as iron is the predominant cation liberated to solution. Significant amounts of Si and Al are also liberated, which may suggest dissolution of other phases, although Al is known to substitute into hematite and goethite (Schwertmann and Taylor 1989). Ti and Mg concentrations correlate with Fe concentrations in the Pololu soil horizons, suggesting that Mg and Ti are derived from hematite or goethite, rather than from the dissolution of Si- and Al-based phases (Figure 2.14). Mg and Ca are relatively minor in this extraction, and Mg/Ca ratios vary significantly between the Pololu soil and Hawi soil, with Mg/Ca ratios higher in the older Pololu soil.

2.4.6.6. Kaolin Group Minerals

Tables 2.23 and 2.24 show the chemical analysis of the kaolin group minerals sequential extraction. This extraction is designed to remove kaolinite ($Al_2Si_2O_5(OH)_4$) and its polymorphs, as well as poorly crystallized clays of similar chemistry. This extraction has large amounts of Si and Al in an approximately 1:1 elemental ratio with relatively little else at analyzable concentrations, as expected for the dissolution of kaolin phases and poorly crystalline clays. In addition to the large quantities of Si and Al, there is a small amount of Fe and Mg. When concentrations of Fe and Mg are plotted against Al concentrations, Fe and Mg individually do not correlate with Al concentration, but Fe + Mg does (Figure 2.15). This trend may illustrate competition of Fe and Mg over defects in the structure of kaolin group minerals and poorly crystalline clays.

Table 2.21: Chemistry data from the sesquioxide sequential extraction. Errors are 1σ analytical errors.

Soil Horizon	Depth to Horizon (cm)	Na	Mg	Al	K	Ca	Sr	Fe	Mn	Ti	Si
Pololu (350 ka)		**mg/gram dry soil**									
A	0-25	--	1.36±0.03	4.76±0.06	--	1.15±0.02	--	35.5±0.6	0.315±0.004	2.91±0.03	3.84±0.05
Bw1	25-41	--	1.57±0.03	5.73±0.07	0.45±0.03	0.90±0.01	--	40.7±0.5	0.125±0.004	2.58±0.03	4.3±0.1
Bw2	41-57	--	0.92±0.01	5.55±0.07	--	1.59±0.06	--	25.9±0.3	0.206±0.002	2.27±0.03	4.01±0.05
C1	57-106	--	1.45±0.03	5.39±0.07	--	2.07±0.05	--	29.9±0.5	0.153±0.003	1.75±0.02	4.26±0.09
C1	57-106	--	0.581±0.009	3.31±0.04	--	3.3±0.1	--	19.4±0.3	0.169±0.002	0.97±0.01	3.02±0.03
Hawi (170 ka)											
A	0-12	--	3.73±0.05	3.57±0.04	--	17.4±0.2	--	19.7±0.3	0.581±0.007	1.96±0.02	5.51±0.06
	12-13	--	0.532±0.006	1.20±0.02	--	10.8±0.2	--	6.23±0.07	0.105±0.001	0.275±0.004	2.59±0.03

Table 2.22: Elemental ratios from the sesquioxide sequential extraction. Errors are 1σ analytical errors.

Soil Horizon	Depth to Horizon (cm)	Mg/Ca	Si/Al	Fe/Al	Ti/Al	Mn/Al
Pololu (350 ka)		**moles/moles**				
A	0-25	1.95±0.05	0.77±0.02	3.60±0.07	0.345±0.006	0.0325±0.0006
Bw1	25-41	2.86±0.07	0.72±0.02	3.43±0.06	0.254±0.004	0.0107±0.0003
Bw2	41-57	0.95±0.04	0.70±0.01	2.26±0.04	0.230±0.004	0.0182±0.0003
C1	57-106	1.16±0.03	0.76±0.02	2.68±0.06	0.183±0.003	0.0140±0.0004
C1	57-106 (subset)	0.29±0.01	0.88±0.02	2.82±0.05	0.164±0.003	0.0251±0.0004
Hawi (170 ka)						
A	0-12	0.354±0.007	1.48±0.02	2.67±0.05	0.3095±0.005	0.080±0.001
	12-13	0.082±0.002	2.08±0.04	2.51±0.05	0.1294±0.003	0.0430±0.0008

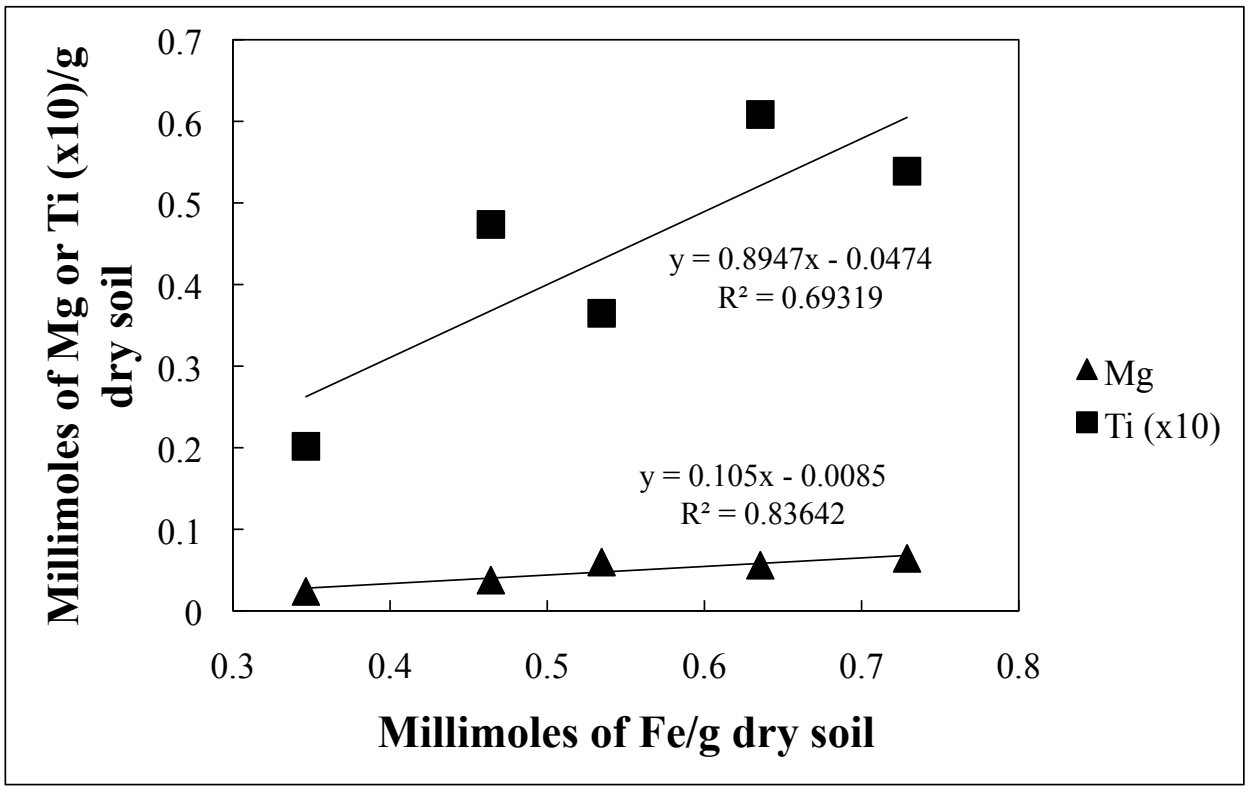

Figure 2.14: Mg and Ti (x10) trends with Fe for the sesquioxide extraction. One σ analytical errors are smaller than symbol size.

Table 2.23: Chemistry data from the kaolin group minerals sequential extraction. Errors are 1σ analytical errors.

Soil Horizon	Depth to Horizon (cm)	Na	Mg	Al	K	Ca	Sr	Fe	Mn	Ti	Si
Pololu (350 ka)		**mg/g dry soil**									
A	0-25	--	0.252±0.003	89±1	--	--	--	0.350±0.004	--	--	82±1
Bw1	25-41	--	0.326±0.004	62.9±0.9	--	--	--	--	--	--	37.2±0.4
Bw2	41-57	--	0.269±0.004	96±1	--	--	--	0.329±0.005	--	--	81±1
C1	57-106	--	0.183±0.002	82.6±0.9	--	--	--	0.377±0.005	--	--	91±2
C1	57-106 (subset)	--	0.104±0.003	87±1	--	--	--	0.74±0.01	--	--	89±1
Hawi (170 ka)											
A	0-12	--	0.327±0.004	73±0.8	--	--	--	0.231±0.008	--	--	66±1
	12-13	--	0.328±0.004	55.7±0.6	--	--	--	--	--	--	62.9±0.8

Table 2.24: Elemental ratios from the kaolin group minerals sequential extraction. Errors are 1σ analytical errors.

Soil Horizon	Depth to Horizon (cm)	Mg/Al	Fe/Al	Si/Al
Pololu (350 ka)		**moles/moles**		
A	0-25	0.00313±0.00005	0.00189±0.00003	0.88±0.02
Bw1	25-41	0.0057±0.0001	--	0.57±0.01
Bw2	41-57	0.00312±0.00006	0.00165±0.00003	0.81±0.02
C1	57-106	0.00246±0.00004	0.00221±0.00004	1.05±0.02
C1	57-106 (subset)	0.00133±0.00004	0.00410±0.00008	0.98±0.02
Hawi (170 ka)				
A	0-12	0.00497±0.00008	0.00152±0.00006	0.86±0.02
	12-13	0.0066±0.0001	--	1.09±0.02

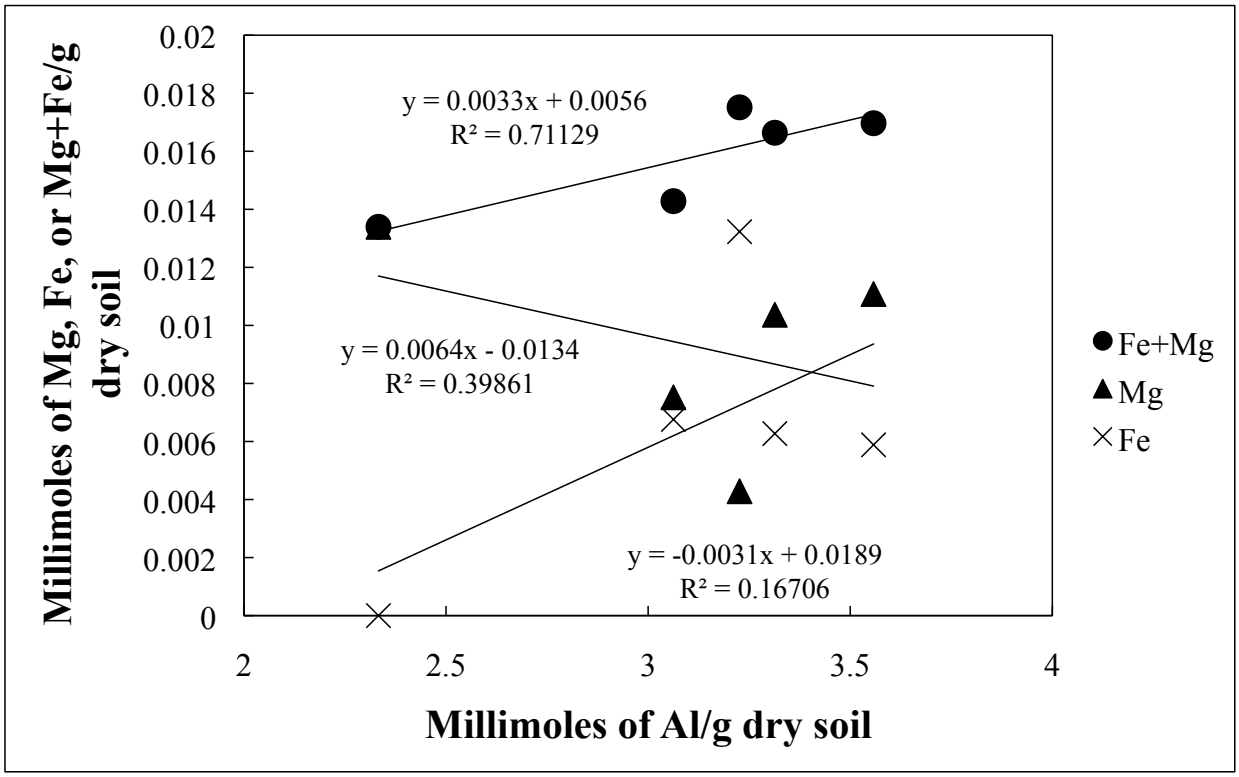

Figure 2.15: Mg, Fe, and Mg+Fe trends with Al for the kaolin sequential extraction. One σ analytical errors are smaller than symbol size.

2.4.6.7. Residuum

The chemistry of the residuum fractions is presented in Tables 2.25 and 2.26. Potential mineral phases remaining after the previous six sequential extractions include primary basalt phases, gibbsite [$Al(OH)_3$], and members of various spinel solid solution series and their weathering products (ulvospinel [Fe_2TiO_4], ilmenite [$FeTiO_3$], magnetite [Fe_3O_4], maghemite [Fe_2O_3], etc.). These phases are predominantly composed of Al, Fe, and Ti, as is the chemical composition of the extraction. Si concentrations for this extraction do not exist, as HF was used during the dissolution, ultimately removing Si from our samples as $SiF_{4(g)}$. Unfortunately the complicated nature of this extraction convolutes the sources of elements of interest. One of the few distinct trends involves the concentration of Mn, which is correlated with Fe in the Pololu soil horizons (Figure 2.16). This trend can be explained if Fe and Mn are both derived from the same source phase, as Mn often substitutes for Fe.

Table 2.25: Chemistry data from the residuum sequential extraction. Errors are 1σ analytical errors.

Soil Horizon	Depth to Horizon (cm)	Na	Mg	Al	K	Ca	Sr	Fe	Mn	Ti	Si
Pololu (350 ka)		**mg/g dry soil**									
A	0-25	1.66±0.02	3.51±0.04	29.4±0.3	2.14±0.08	1.09±0.02	--	40.0±0.5	0.385±0.005	16.3±0.2	--
Bw1	25-41	0.633±0.009	3.98±0.05	73.2±0.8	0.78±0.03	0.287±0.004	--	60.3±0.8	0.473±0.007	22.3±0.3	--
Bw2	41-57	0.95±0.01	1.23±0.02	47.2±0.5	1.12±0.05	0.231±0.003	--	44.2±0.5	0.422±0.005	20.3±0.2	--
C1	57-106	0.765±0.009	1.92±0.02	19.2±0.2	0.77±0.02	0.68±0.01	--	47.1±0.7	0.448±0.006	10.2±0.3	--
C1	57-106 (subset)	2.80±0.03	1.63±0.02	25.8±0.3	2.29±0.04	1.40±0.02	--	39.2±0.6	0.390±0.005	6.2±0.2	--
Hawi (170 ka)											
A	0-12	1.43±0.02	7.8±0.1	24.2±0.3	1.44±0.03	2.11±0.03	--	74±1	1.03±0.01	12.7±0.2	--
	12-13	2.68±0.03	7.67±0.08	28.3±0.4	1.66±0.09	5.79±0.08	--	72.1±0.8	0.99±0.02	19.6±0.3	--

Table 2.26: Elemental ratios from the residuum sequential extraction. Errors are 1σ analytical errors.

Soil Horizon	Depth to Horizon (cm)	K/Na	Mg/Ca	Fe/Al	Mn/Al	Ti/Al
Pololu (350 ka)		**moles/moles**				
A	0-25	0.760±0.03	5.3±0.1	0.66±0.01	0.0064±0.0001	0.313±0.005
Bw1	25-41	0.721±0.03	22.9±0.4	0.398±0.007	0.00317±0.00006	0.171±0.003
Bw2	41-57	0.692±0.04	8.8±0.2	0.452±0.007	0.00439±0.00007	0.242±0.004
C1	57-106	0.588±0.02	4.63±0.09	1.18±0.02	0.0115±0.0002	0.30±0.01
C1	57-106 (subset)	0.480±0.009	1.92±0.03	0.73±0.02	0.0074±0.0002	0.135±0.005
Hawi (170 ka)						
A	0-12	0.589±0.02	6.1±0.1	1.47±0.03	0.0209±0.0004	0.295±0.005
	12-13	0.363±0.02	2.19±0.04	1.23±0.02	0.0171±0.0004	0.390±0.008

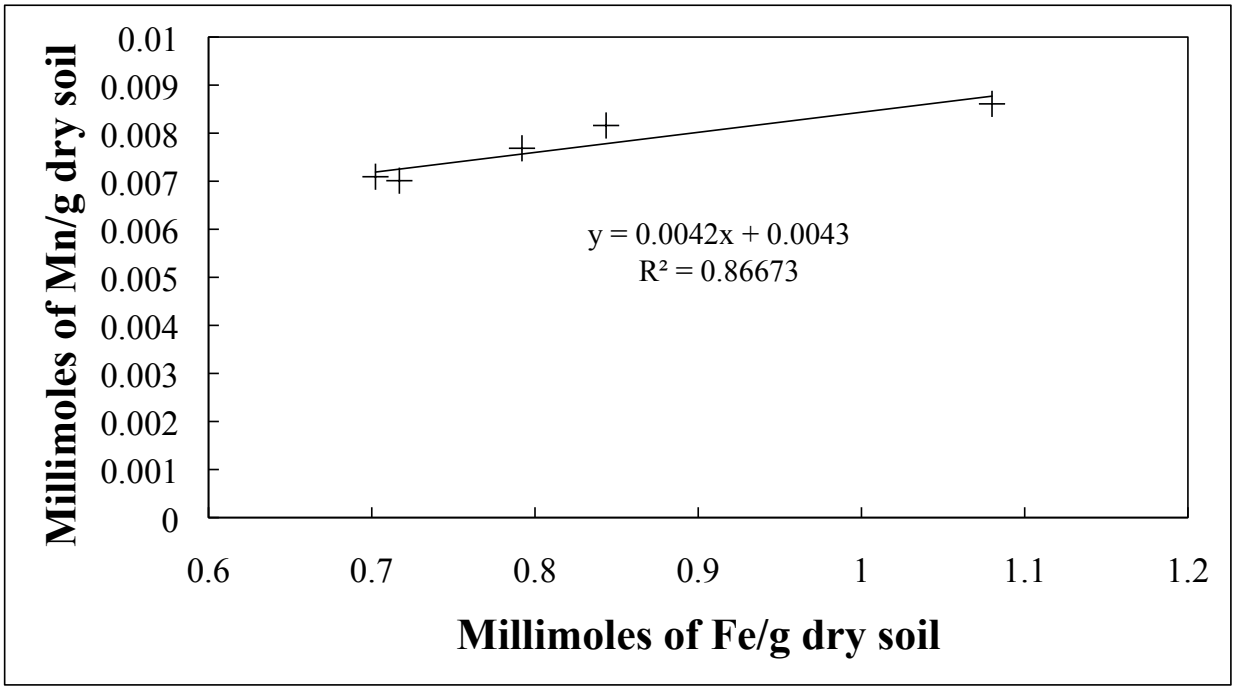

Figure 2.16: Mn trend with Fe for the residuum sequential extraction. One σ analytical errors are smaller than symbol size.

2.4.6.8. Sequential Extraction Totals

We can total the chemistry values from each of the sequential extractions to see if they approach the total chemistry values of our <2-mm bulk horizon dissolutions, as a check on the efficacy of the sequential extraction. Total elemental data from the sequential extractions are shown in Tables 2.27 and 2.28 and can be compared to Tables 2.5 and 2.6. Some caveats apply to this summation process that should be noted. As the sesquioxide extraction utilized Na citrate and Na dithionite, Na data for this extraction do not exist. The kaolin extraction required NaOH, therefore Na data do not exist for this extraction either. The residuum dissolution destroyed any Si by using HF in the dissolution process. Further, the sequential extraction and <2-mm bulk horizon dissolutions were not performed on exactly the same sample split, adding some additional uncertainty due to sample heterogeneity. Given those caveats, the results from the sequential extraction and <2-mm bulk horizon dissolutions agree well. Some significant differences exist between Al and Ca concentrations ascertained by the two methods, and this may be a result of contamination during our sequential extraction steps, as the sequential extraction data are consistently higher for both elements. This contamination could result from the reagents used in the sequential extraction, as reagent blanks were analyzed for Mg, but not for Ca and Al. Significant differences in the chemistry of the second horizon of the Hawi soil between methods are most likely the result of sample heterogeneity, due to the nature of this horizon as a thin, heterogeneous, indurated carbonate horizon.

The sequential extraction also provides us with mineralogic data for the <2-mm fractions of these soils, and the weight percentage of soil mass removed during each sequential extraction step by horizon is illustrated in Figure 2.17. Mineralogically, the upper horizons of the Pololu soil and upper horizon of the Hawi soil are quite similar. Looking at horizon C1 and the subset

of horizon C1 sampled from the Pololu soil provides an idea of intra-horizon heterogeneity amongst sequential extraction fractions.

Mg distribution by sequential extraction fraction and soil horizon is shown in Figure 2.18 for both soils. If Mg were uniformly distributed among sequential extraction fractions this diagram would mirror Figure 2.17. In both soils it becomes clear that SRO phases are an important reservoir of Mg, particularly in soil horizons without carbonate. Kaolin phases, on the other hand, are a negligible reservoir of Mg in any horizon, even though they play a large role in the mineralogy of the soil. Adsorbed cations are also important in Mg budgets, and in those horizons that contain carbonate, carbonate has a significant influence on the overall Mg budget. Note that in those horizons that contain carbonate, adsorbed cation and SOM Mg numbers have been inflated by contamination with carbonate, so the total amount of Mg in carbonate is probably greater than shown, at the expense of adsorbed cations and SOM. Mg in the residuum extraction is variable, but can be an important reservoir of Mg, particularly in upper soil horizons. SOM and sesquioxides contribute to the Mg budget roughly in accordance with their mineralogical abundances.

Weighing each soil horizon accordingly for the Hawi and Pololu soils based on soil density, thickness and proportion of horizon <2-mm, we create Figure 2.19, which shows the average sequential extraction mineralogy and Mg distribution within the <2-mm portion of each soil. We see that the trends described for Figures 2.17 and 2.18 are maintained after this averaging process. One caveat to note is that carbonates are very minor in this figure, but this is an artifact of using the <2-mm fraction of the soils for the sequential extractions.

Table 2.27: Chemistry totals for all of the sequential extraction fractions. Errors are 1σ analytical errors.

Soil Horizon	Depth to Horizon (cm)	Na	Mg	Al	K	Ca	Sr	Fe	Mn	Ti	Si
Pololu (350 ka)		**mg/g dry soil**									
A	0-25	2.64±0.03	13.1±0.2	142±1	4.34±0.08	9.14±0.09	0.437±0.006	133±2	1.76±0.03	24.1±0.2	98±1
Bw1	25-41	1.41±0.01	11.5±0.1	172±2	1.8±0.2	5.65±0.05	0.192±0.003	150±2	1.49±0.02	29.2±0.3	52.8±0.5
Bw2	41-57	2.78±0.03	12.9±0.2	172±2	2.29±0.06	7.38±0.08	0.300±0.005	134±1	1.67±0.02	28.3±0.3	101±1
C1	57-106	7.3±0.2	19.0±0.2	134±1	2.41±0.04	45.1±0.4	0.280±0.004	149±2	1.14±0.01	18.5±0.4	111±2
C1	57-106 (subset)	4.41±0.04	15.3±0.2	132±1	3.57±0.04	36.58±0.3	0.245±0.003	110±1	1.25±0.02	12.2±0.2	105±1
Hawi (170 ka)											
A	0-12	2.99±0.03	21.5±0.2	134±1	3.40±0.04	28.5±0.3	0.660±0.009	130±2	2.51±0.02	17.8±0.2	85±1
	12-13	7.16±0.06	26.1±0.2	125±1	4.2±0.1	103±1	1.23±0.01	104±1	1.93±0.02	22.5±0.3	83.5±0.8

Table 2.28: Elemental ratios from all the sequential extraction fractions. Errors are 1σ analytical errors.

Soil Horizon	Depth to Horizon (cm)	K/Na	Mg/Ca	Si/Al	Fe/Al	Ti/Al
Pololu (350 ka)		**moles/moles**				
A	0-25	0.97±0.02	2.37±0.05	0.658±0.009	0.450±0.006	0.095±0.001
Bw1	25-41	0.74±0.09	3.36±0.04	0.295±0.004	0.421±0.006	0.096±0.001
Bw2	41-57	0.48±0.02	2.89±0.06	0.565±0.008	0.377±0.005	0.093±0.001
C1	57-106	0.193±0.005	0.692±0.009	0.79±0.01	0.538±0.007	0.078±0.002
C1	57-106 (subset)	0.476±0.006	0.69±0.01	0.76±0.01	0.405±0.006	0.052±0.001
Hawi (170 ka)						
A	0-12	0.670±0.009	1.24±0.02	0.612±0.009	0.470±0.009	0.0747±0.0008
	12-13	0.343±0.009	0.417±0.005	0.642±0.008	0.403±0.005	0.101±0.002

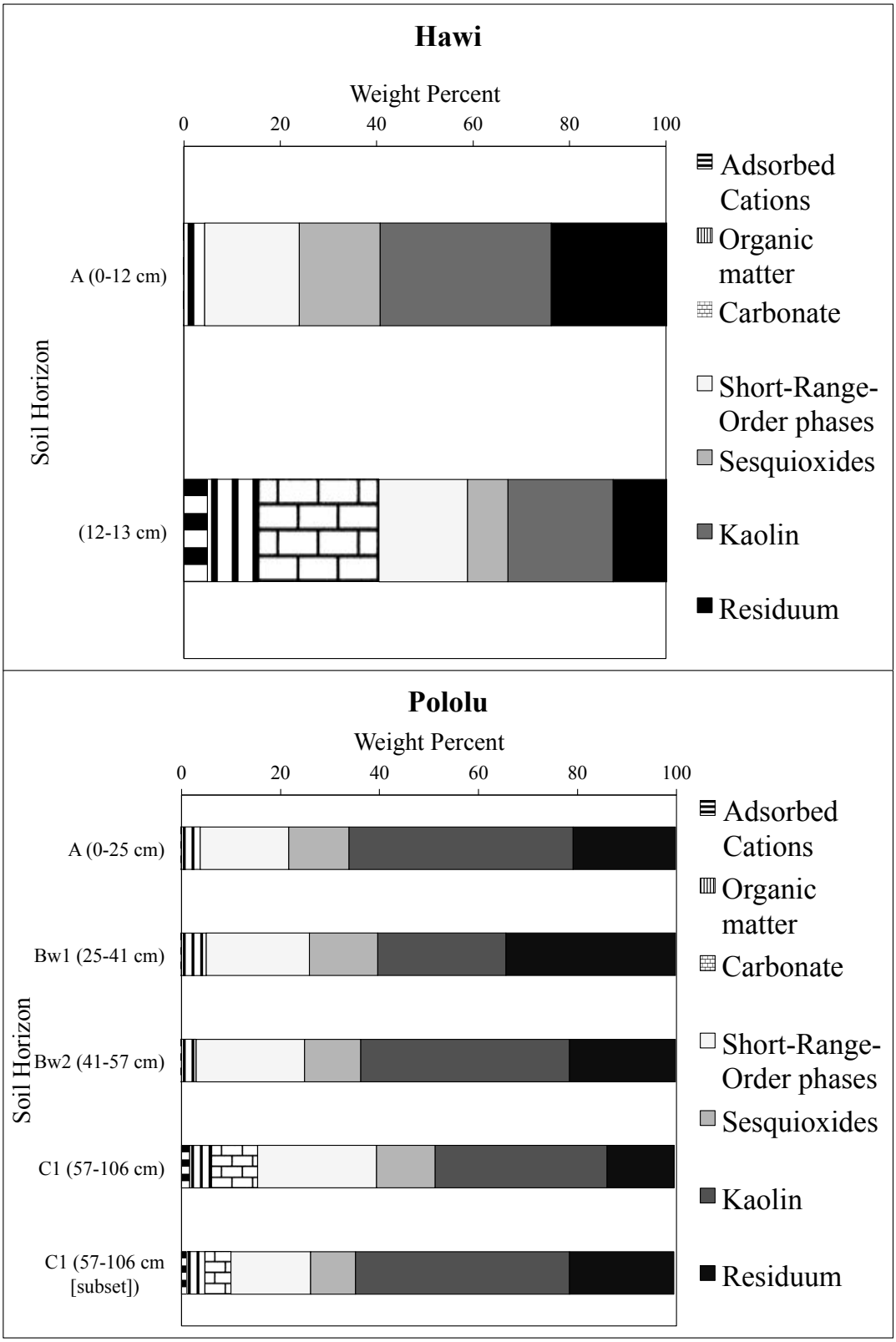

Figure 2.17: Sequential extraction fractions by weight percent of the <2-mm soil fractions by horizon for the Hawi (top) and Pololu (bottom) soils.

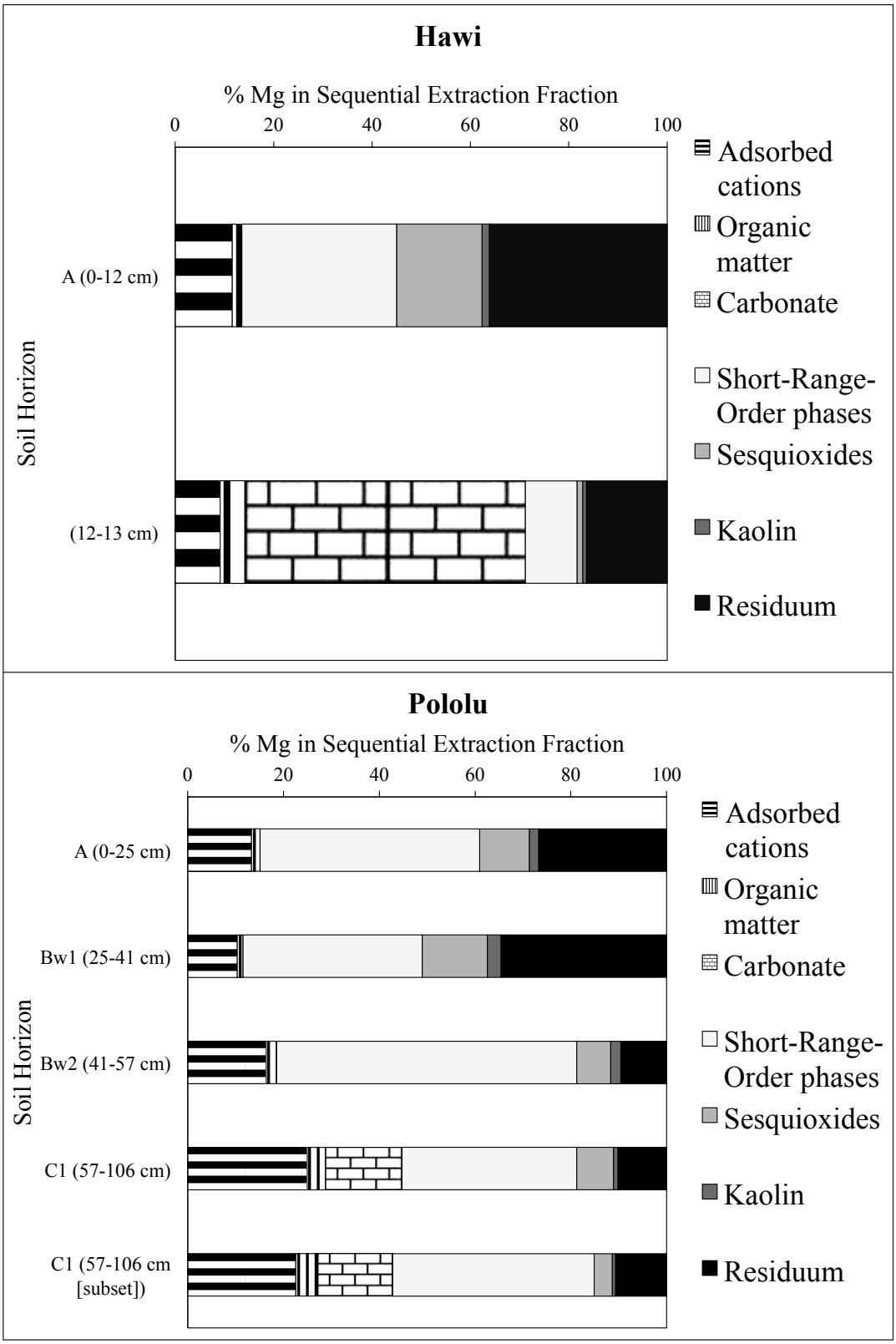

Figure 2.18: Percentage of Mg in each sequential extraction fraction of the <2-mm soil fractions by horizon for the Hawi (top) and Pololu (bottom) soils.

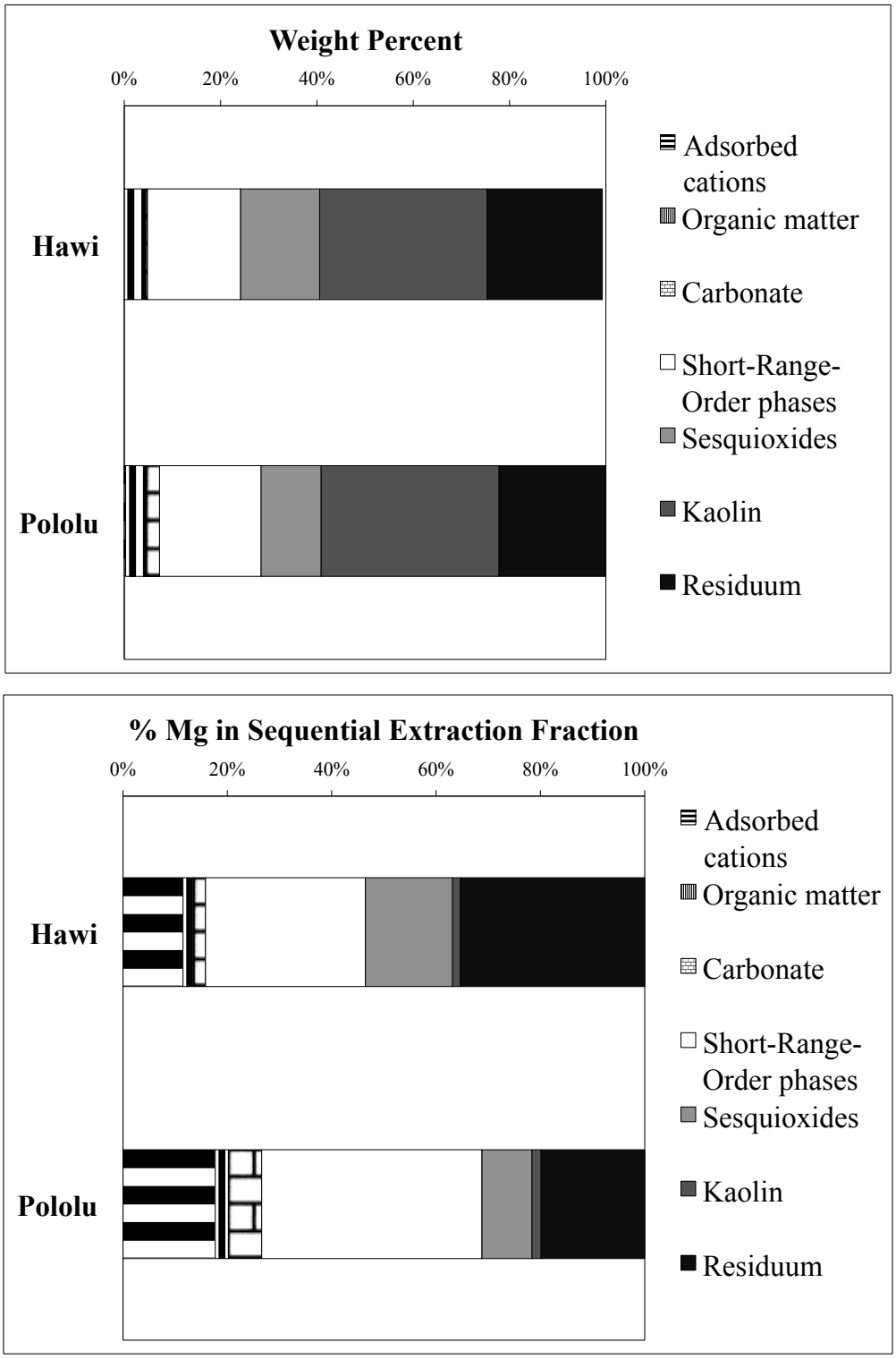

Figure 2.19: Sequential extraction fractions by weight percent of the <2-mm soil fractions averaged over all soil horizons for the Hawi and Pololu (top). Percentage of Mg in each sequential extraction fraction of the <2-mm soil fractions averaged over all soil horizons for the Hawi and Pololu (bottom).

2.5. DISCUSSION

The results of the mineralogical and chemical analyses of these soils must be put into a pedological framework in order to understand the processes that influence Mg and the distribution of Mg between soil phases. Soils are complex, with multiple weathering processes operating on different time-scales. Previous work has outlined the development of the morphology and mineralogy of these soils.

2.5.1. Kohala Pedogenesis: Morphology

As outlined in Ziegler et al. (2003) formation of all Hawaiian soils follows a predictable sequence after the emplacement of a lava flow. The sequence starts with the gradual trapping of dust by the lava flow. This dust can begin to hold water, as well as allow for the germination of plant life, leading to the beginnings of true soil genesis on the lava flow. The increased water-holding capacity, as well as plant productivity and the addition of organic compounds and acids increases weathering and soil formation rates.

In the arid Kohala study sites the gradual weathering and the capture of dust may lead to the formation of a desert pavement surface, due to the settling of fine-grained materials around larger basalt fragments, gradually rafting these pieces to the surface. This process may lead to relatively unweathered rock fragments sitting atop horizons of very fine-grained secondary weathering products, protecting the fine-grained secondary weathering products from wind erosion.

Other morphologic features may also develop in these young soils. The establishment of a community of grasses adds organic matter to the surface of the soil while preventing erosion of the underlying fine material. This leads to the development of an A horizon.

The fine material captured by the desert pavement, as well as the fine amorphous and crystalline phases produced by secondary mineral formation in situ, develop into cambic B horizons, which gradually increase in depth through time. These horizons no longer have any of the structure of the parent material. They may accumulate secondary clay minerals but are otherwise considered weakly developed, due to the lack of water available to translocate clays throughout the soil profile.

The lack of water in these weathering environments also influences the formation of salts and carbonates within the soil. High rates of evaporation prevent the leaching of soluble cations and anions completely from the soil profile. These cations and anions may precipitate at depth in the soil profile as evaporation concentrates soil porewater and translocation of soil porewater down profile brings solutes into an environment with lower carbon dioxide concentrations (Whipkey et al. 2002). Initially carbonates form as diffuse coatings within the fine material, but after dissolution and reprecipitation through time, carbonates may become concentrated in an indurated petrocalcic horizon (Whipkey et al. 2002). The first presence of carbonates in these arid Kohala soils is after 10 ka of soil development, and more indurated carbonates form by 170 ka of development (Whipkey et al. 2002). As weathering continues and the water-holding capacity in soil systems increases, carbonates form deeper within the soil profile (Whipkey et al. 2002).

2.5.2. Kohala Pedogenesis: Mineralogy

As the morphology of the soils on Kohala evolves through time, so does the mineralogy of the soils, and in some instances, the two are inextricably related. Basaltic glass and minerals are parent materials susceptible to weathering, and they weather rapidly under pedologic

conditions. Secondary soil minerals may then either form directly from solutes in solution, or replace existing primary minerals.

The first products of weathering are short-range-order materials such as allophane, imogolite, and ferrihydrite. These phases are metastable, and as the soil profile thickens these phases gradually recrystallize into more stable secondary phases. This recrystallization is due in part to the increased water-holding capacity of the soil generated by the formation of the metastable secondary soil minerals, as well as the strong wet-dry cycles within the Kohala soils (Hsieh et al. 1998; Zeigler et al. 2003). The recrystallization results in the replacement of allophane and imogolite by halloysite and gibbsite and the replacement of ferrihydrite by hematite over time. Halloysite and gibbsite may also precipitate directly from soil solution, but the dominant mechanism of their formation appears to be from the short-range-order aluminosilicate phases (Hsu, 1989). Gibbsite formation in this environment also tends to be limited to microenvironments of extreme desilication and areas of the most intense weathering. Carbonate formation may also begin in the soil profile after 10 ka, but the carbonate appears to become increasingly magnesian with age and development, even to the point where dolomite is an important carbonate phase (Whipkey et al. 2002).

2.5.3. Integrating Our Soil Characterization with the Pedological Model

We can interpret our findings using the pedological model outlined above to understand the soil-forming processes occurring in the Hawi (170 ka) and Pololu (350 ka) soils and the differences between them. We can also focus on Mg within this context and identify processes that may be important to the distribution of Mg within the soil and among phases. Biotic uplift of Mg to surface horizons, redistribution of Mg through the formation of a desert pavement, and leaching of Mg from the soil profile will all be important drivers in the ultimate fate of Mg. Also

important in the fate of Mg will be how Mg is released from primary phases during weathering, which secondary phases form and incorporate Mg, and the fate of Mg during the recrystallization of metastable secondary phases through time. We can look at how these processes affect our soils horizon by horizon, as well as how they differ between the Hawi and Pololu soils.

2.5.4. A Horizons

The A horizons of the Hawi and Pololu soils are dominated mineralogically by short-range-order phases, kaolin group minerals, gibbsite, and hematite, and their bulk chemistry data illustrate the leaching of alkali and alkaline earth cations from both soils in these uppermost horizons (Tables 2.1 and 2.2, Figures 2.12 and 2.17). These horizons are similar between both soils, illustrating many of the same mineralogical and chemical trends. However, as the upper horizon of the Pololu soil has experienced weathering and leaching over a longer time interval, it is more depleted in the alkali and alkaline earth elements than the Hawi (Figures 2.11 and 2.12). Neither the Hawi or Pololu soils have carbonates in the A horizons.

Both A horizons also show an enrichment of K relative to Na (Table 2.6) when compared to K:Na ratios of basalt (Table 2.4) and rainfall. This evidence suggests that vegetation is playing a role in the translocation of elements at these sites, as vegetation has highly enriched K:Na ratios (Table 2.12). This trend is more distinct in the Pololu soil than the Hawi soil, suggesting that this process of K enrichment via plant translocation operates continually through time. This trend is also apparent in the adsorbed cation sequential extraction (Table 2.14) suggesting that K is fairly mobile and not incorporated into mineral phases, another piece of evidence supporting plant translocation as an explanation.

These A horizons also have <2-mm bulk soil Mg:Ca ratios that are higher than those of basalts and of rainfall, suggesting that Mg is preferentially retained compared to Ca during the

formation of secondary phases in these horizons (Table 2.5). With our detailed sequential extraction results of the <2-mm soil fractions, we can clearly see that Mg:Ca ratios are largest in short-range-order phases and residuum phases (Tables 2.20 and 2.26), and the ratios may also be high for kaolin group minerals (Table 2.24), but Ca numbers do not exist for kaolin group minerals due to analytical limits. The formation of these secondary phases therefore drives the preferential enrichment of Mg with respect to Ca in these soils over time.

Based on the <2-mm soil fractions, the distributions of mineralogical phases in the A horizons of the Hawi and Pololu soils are similar (Figure 2.17). In order to maintain this distribution of phases over the course of an additional 180 ka of weathering to transition from the Hawi to Pololu soil, relatively fresh material must be supplied to the A horizon to maintain the production of short-range-order phases, as these phases would otherwise be depleted by recrystallization over time. This resupply of short-range-order phases may occur by weathering of material in the >2-mm soil fractions or by rafting of relatively unweathered material to the soil surface via the formation of a desert pavement. This process could maintain the formation of SRO phases through time and would move indurated clasts of >2-mm material upwards through the soil profile.

Mg distributions in the <2-mm soil fractions of the A horizons are dominated by short-range-order phases, along with residual materials (Figure 2.18). By looking in detail at the chemistry results of the sequential extractions for these two reservoirs of Mg, we can understand which phases within these sequential extraction fractions are important.

Analysis of the short-range-order phase chemistry from the sequential extraction shows that Mg concentrations correlate poorly with Fe concentrations (Figure 2.13). The same is true for the correlation of Mg concentrations with Si concentrations. These results suggest that Mg is

not only incorporated into ferrihydrite phases, but allophane and imogolite phases. Poor correlation with endmember chemistry is also a product of the highly variable chemical compositions of these phases. For instance, ferrihydrites often contain some Al in their structures and may have silica directly adsorbed onto their surfaces, as adsorbed silica is important in preventing the transformation of ferrihydrite into more stable iron oxide phases (Carlson and Schwertmann 1981; Campbell and Schwertmann 1984).

However, the short-range-order phases are not stable over the long term in these soils and will recrystallize over time. By studying the mineralogical prevalence of short-range-order phases, kaolin group minerals, and sesquioxides, along with the Mg content of each of these extractions (Figures 2.17 and 2.18), we can interpolate that the recrystallization process, from allophane, imogolite and ferrihydrite to halloysite, other kaolin group minerals, and hematite, results in the expulsion of Mg. Estimates of how important this process may be to the Mg budget of the soils are hampered by the limited knowledge of how much halloysite and kaolin group minerals form directly from solution rather than from recrystallization of SRO phases. It also appears that the transition from ferrihydrite to hematite results in less expulsion of Mg than the transitions of allophane and imogolite to hallosite and kaolin group minerals, but this trend is difficult to establish given the unknown distribution of Mg between allophane, imogolite, and ferrihydrite.

The phases comprising the residuum fraction consist potentially of gibbsite, remaining primary basaltic phases, spinels, and oxide weathering products of spinels. These stable and recalcitrant phases are enriched in the A horizons of the Hawi and Pololu soils (Figure 2.17). The variety of phases that are part of this sequential extraction fraction makes it difficult to discern exactly from which phase Mg is derived. The extreme desilication usually associated

with the formation of gibbsite either directly from soil solution or following alteration of halloysite probably prevents much Mg from being incorporated into this phase. As such, Mg is most likely derived from phases other than gibbsite in this extraction.

2.5.5. B Horizons

As the Pololu soil has been subjected to weathering over a longer time period it has developed deeper and more weathered B horizons (Bw1 and Bw2) than the Hawi soil B horizon (Bk). The process of leaching has removed much of the alkali and alkaline earth cations from the Pololu B horizons, and these horizons are dominated by the same mineral phases as in the A horizons (Table 2.2, Figure 2.12). The B horizon of the Hawi soil is different. This horizon is a Bk horizon with calcite and dolomite in addition to other secondary phases. In Figure 2.12 we see that the presence of these carbonates leads to the enrichment of Ca and Sr at depth in this soil horizon, and we see that the horizon overall is less depleted in alkali and alkaline earth elements. In the Hawi soil the B horizon carbonate is a store of soluble elements leached from the A horizon above including Mg, Ca, and Sr.

The Pololu soil B horizons are quite similar to the Pololu and Hawi A horizons. We see that the <2-mm fractions of these horizons have high Mg:Ca ratios (Table 2.6), and that Mg distribution is dominated by short-range-order phases and residuum in the <2-mm soil fractions (Figure 2.18). Much of the discussion for the A horizons applies to these two soil horizons as well. One interesting difference is that the Mg distribution in the <2-mm sequential extraction fractions of the Bw2 horizon is almost entirely dominated by short-range-order phases, further highlighting the importance of short-range-order phases in the Mg budgets of these soils (Figure 2.18).

The Hawi Bk horizon is indurated by carbonates and other secondary phases. As such there is no <2-mm fraction on which to perform a series of sequential extraction steps. By looking at data for the combined >2-mm and <2-mm bulk soil dissolution (Table 2.7) and the individual carbonate extraction (Table 2.9) we can see the importance of carbonate formation in this horizon. In particular, as soon as the Bk horizon is reached, the Mg and Ca concentrations in the soil increase sharply, and Al and Fe concentrations are diluted by this increase. Mg:Ca ratios for the Hawi B horizon shows the opposite trend from the B horizons of the Pololu (Table 2.7). These Hawi B horizon Mg:Ca ratios decrease significantly, suggesting preferential retention of Ca with respect to Mg. This makes sense for the precipitation of calcite in these horizons, as experimentally derived Mg distribution coefficients are usually < 0.05 for calcite (Rimstidt et al. 1998). Even with the relative exclusion of Mg from carbonates forming in this soil horizon, the carbonate is still the largest reservoir of Mg in this soil horizon (83±3%). Also, given the low distribution coefficients of Mg and Sr during the precipitation of calcite, the carbonates have high Mg:Ca and Sr:Ca ratios. These high Mg:Ca and Sr:Ca ratios can be resolved with fractional crystallization during the evaporative precipitation of carbonates and will be discussed in more detail in Chapter 3.

2.5.6. C Horizons

The C horizons, C1 and C2, are where carbonates first appear in the Pololu soil. The C1 horizon of the Pololu soil is not completely indurated and provides sequential extraction information for the <2-mm soil fraction. This sequential extraction data shows that the <2-mm fraction is similar mineralogically to the soil horizons above it, with the relatively minor addition of carbonates (Figure 2.17). However, these <2-mm values are biased against carbonates and do not reflect the total influence of carbonate when looking at the combined <2-mm and >2-mm

bulk soil (Table 2.9). The C2 horizon of the Pololu soil is sufficiently indurated such that no <2-mm fraction exists for this soil horizon. The Hawi C horizon also contains carbonates like the Hawi Bk horizon above it, and the induration of the Hawi C horizon means that this horizon lacks a <2-mm soil fraction as well.

In the Pololu soil we see increases in soil depletion index values for Na, K, Ca, Mg, and Sr in the C horizons compared to the B and A horizons, but these increases are small compared to those of the Hawi soil C horizon, which has positive soil depletion index values for Na, K, Ca, and Sr (Figure 2.12). Ca and Mg values in Table 2.9 show that carbonate concentrations in the Pololu C horizons are on average lower than in the Hawi Bk and C horizons. These values suggest that in the Hawi soil many of the cations leached from the A horizon are transferred to the lower soil horizons and sequestered within carbonate phases, causing soil depletion index plots to be positive. In the Pololu soil, cations leached from upper soil horizons are also transferred to lower soil horizons and sequestered within carbonate phases, but over time much of this flux of cations has been leached away completely from the soil, leading to negative soil depletion index values overall in these horizons. Ultimately, the relative abundance of carbonate is less in the Pololu C horizons and the carbonates that exist are playing a smaller role in the functioning of the Pololu C horizons, when compared to the Hawi C horizon. For the C2 horizon of the Pololu soil, the Mg:Ca ratios of the carbonate extraction provide clear chemical evidence of the existence of dolomite. This evidence supports the scheme for the evolution of the Mg content of carbonates described by Whipkey et al. (2002).

Mg distribution in the Pololu C horizons for the combined <2-mm and >2-mm bulk soil fractions shows that most Mg is in non-carbonate phases when looking at the C1 and C2 horizons (64±5% and 86±3%, respectively). The Hawi soil C horizon is quite different in that

most Mg is within carbonate phases (69±3%). The lower importance of carbonates as a store of Mg in the Pololu C horizons is tied to the lower relative abundance of carbonates.

As a check on intra-horizon heterogeneity, the C1 horizon of the Pololu soil was sampled twice, once in a region representative of the overall bulk horizon, and again in a portion of the horizon that had a distinctly different texture. This allows us an estimate of the intra-horizon variability in these soils. For any analysis, C1 (57-106) represents the bulk horizon, whereas C1 (57-106 subset) represents the subset of the horizon with a different texture. The primary difference between these two samples is the amount of carbonate, as represented by the much higher Ca concentration for the subset sample of the horizon (Table 2.9). This evidence shows that the distribution of carbonate in these soil horizons can be a source of heterogeneity, which conceptually makes sense given the movement of precipitating solutions along preferential flow paths through soils.

The optical microscopy on thin sections of these horizons clearly shows that the secondary phases can replace the textures of parent materials and that the distribution of these secondary phases relates to the original chemistry of the basaltic phases being replaced (Figures 2.7 and 2.8). This observation suggests that there are complicated noncongruent dissolution processes leading to the formation of secondary soil phases. Also, indurated horizons are indurated not only by carbonates, but by a complex mixture of carbonates and non-carbonate isotropic secondary mineral phases based on optical properties and chemical data (Figure 2.7). Indurated horizons that lack parent material textures are composed of similar phases to indurated horizons that replace parent material textures, with carbonate acting as a matrix surrounding spherules of other secondary phases (Figures 2.9 and 2.10). This evidence also explains why Al and Si are released into solution during carbonate dissolutions, as spherules of reactive secondary

minerals are liberated by the dissolution of their encapsulating carbonate matrix. We also note that Mg in these indurated horizons seems to be preferentially distributed between carbonates and the secondary phases replacing olivine phenocrysts (Figure 2.8).

2.5.7. The Hawi and Pololu Soils as a Whole

The dominant pedologic process influencing these soils and controlling the differences between them appears to be the removal of soluble cations via leaching. Overall the Pololu soil is more weathered than the Hawi soil, having existed under similar or potentially wetter climatic conditions for an additional 180 ka of soil development. This additional development resulted in the leaching of more soluble cations from the Pololu soil system and a greater overall depth of weathering when compared to the Hawi soil. As such the Pololu soil has thicker surficial soil horizons without carbonates, and in those soil horizons with carbonates, the carbonates are of less significance. This difference in the importance of carbonate is reflected in the Mg budgets of both soils. The carbonates in the Hawi and Pololu soils, account for 69±11% and 16±2% of the total magnesium averaged over the <2-mm and >2-mm bulk soil profiles, respectively.

2.5.8. The Fate of Mg

The fate of Mg in these soils depends primarily on which secondary phases are formed during weathering and the residence time of these phases within the soils. Although none of these phases have sites specifically for Mg (except dolomite), Mg is incorporated in almost all secondary phases. In soil horizons without carbonate phases, short-range-order phases and residuum phases are the largest reservoirs of Mg when looking at the <2-mm soil fractions (Figure 2.19). Residuum phases are more significant in surface horizons than at depth, both in terms of Mg budget and overall abundance (Figure 2.18). This trend could be explained if Mg in

the residuum fraction is primarily in a recalcitrant phase that gradually accumulates in soil surface horizons over time. Unfortunately, detailed analysis of the chemical compositions of residuum sequential extraction fractions does not allow us to pinpoint exactly which phases within the residuum fraction contain Mg. One of the few trends observed for this extraction shows that Mn correlates with Fe, suggesting these are both derived from the same phase (Figure 2.16).

The short-range-order phases contain a significant amount of Mg in all <2-mm soil horizons (Figure 2.18). This observation seems reasonable, given that these phases are some of the first phases to form during weathering, when initial soil solutions should be rich in Mg. Our detailed analysis of the chemical composition of these sequential extraction fractions fails to distinguish if Mg is primarily derived from ferrihydrite, allophane, or imogolite. These phases, however, will recrystallize over time to more stable mineral phases, and so their continued presence in soil horizons requires continuous production from relatively unweathered saprolite or parent material. The phases that the short-range-order phases recrystallize to, which are in the sesquioxide and kaolin group mineral sequential extraction fractions, contain relatively little Mg, suggesting that Mg is expelled during this recrystallization process. The phases in the sesquioxide and kaolin group mineral sequential extraction fractions are stable over long time periods in the soils and may maintain minimal Mg concentrations within soil profiles over extended periods of time.

Translocation of Mg by vegetation is undoubtedly occurring as shown by K:Na ratios, but the amount of organic matter and vegetation at these sites is relatively low. Even though these reservoirs are small at any given time, the translocation of Mg via plants over the lifetime of a soil can be significant, a point that will be explored further in Chapter 3. SOM can also stabilize

short-range-order phases, increasing the residence time of both of these reservoirs in the soil system (Parfitt et al. 2009).

The adsorbed cation sequential extraction reservoir can also be a moderate source of Mg in our soils. This reservoir is the shortest-lived, and probably reflects more instantaneous processes as Mg is shuffled between longer-lived reservoirs. The abundance of this reservoir will also be altered over time by the transition of short-range-order phases to more stable phases, as this is accompanied by a decrease in surface area and surface charge.

Soil horizons with carbonate have an additional reservoir of Mg that can dominate the Mg budget or play a relatively minor role based on abundance. Although the abundance of calcite and dolomite enriched in Mg is supposed to increase with time in these soils, the importance of carbonate overall in the functioning of the soil decreases with time. So even though the carbonates may become more Mg-rich over time, overall they play a smaller role in the Mg budget of the older Pololu soil. This transition implies that carbonates are gradually removed from these soil profiles over time through leaching.

2.6. CONCLUSIONS

This chapter characterizes the Hawaiian soil study sites and provides important background information for the development of the rest of the dissertation. This arid chronosequence on the Kohala Volcano of the Island of Hawaii can be interpreted in a pedological framework, and our data illustrate processes that can influence the distribution of Mg during soil formation. We see clear evidence of pedological processes, such as the translocation of cations by vegetation, the rafting of clasts of saprolite, the leaching of soluble cations, the formation of secondary mineral phases, and the recrystallization of metastable secondary phases.

Major differences between our study sites are controlled by the amount of leaching of soluble cations from each. We can also look at the distribution of Mg in soil phases to understand which processes play major roles in the fate of Mg in these systems. In soil horizons without carbonate, Mg appears to be predominantly sequestered in short-range-order phases and residuum phases. The short-range-order phases recrystallize through time to more stable weathering products that have relatively low Mg contents, resulting in the expulsion of Mg, whereas the residuum phases are most likely a more stable reservoir of Mg. In soil horizons with carbonate, a large portion of Mg is often sequestered in carbonate, but non-carbonate phases can also play an important role depending on the abundance of carbonate. This difference in carbonate importance is seen when comparing the Hawi soil and the Pololu soil. Carbonates play a large role in the younger, less leached Hawi soil, but a minor role in the Pololu soil. Next we look at the bulk soil system in Chapter 3, utilizing Mg isotopes to better understand the trends of Mg distribution elucidated herein.

WORKS CITED

Anderson, S.P., Dietrich W.E., and Brimhall, G.H.J., 2002. Weathering profiles, mass-balance analysis, and rates of solute loss: Linkages between weathering and erosion in a small, steep catchment. Geol. Soc. American Bull. 114: 1143-1158.

Bischoff, W.D., Bishop, L.C., MacKenzie, L.G., 1983. Biogenically produced magnesian calcite: inhomogenetics in chemical and physical properties; comparison with synthetic phases. American Mineralogist, 68: 1183-1188.

Blakemore, L.C., Searle, R.L. and Daly, B.K., 1987. Methods for chemical analysis of soils. New Zealand Soil Bureau Science Report #80.

Campbell, A.S., and Schwertmann, U., 1984. Iron oxide mineralogy of placic horizons. J. Soil. Sci., 35: 569-582.

Capo, R.C., Whipkey, C.E., Blanchere, J. and Chadwick, O.A., 2000. Pedogenic origin of dolomite in a basaltic weathering profile, Kohala Peninsula, Hawaii. Geology, 28: 271-274.

Carlson, L., and Schwertmann, U., 1981. Natural ferrihydrites in surface deposits from Finland and their association with silica. Geochim. Cosmochim. Acta, 45: 421-429.

Carrillo, J.H., Hastings, M.G., Sigman, D.M. and Huebert, B.J., 2002. Atmospheric deposition of inorganic and organic nitrogen and base cations in Hawaii. Global Biogeochemical Cycles, 16(4): 1076 doi:10.1029/2002GB001892.

Chadwick, O.A., Derry, L.A., Vitousek, P.M., Huebert, B.J. and Hedin, L.O., 1999. Changing sources of nutrients during four million years of ecosystem development. Nature, 397: 491-497.

Chadwick, O.A., Gavenda, R.T., Kelly, E.F., Ziegler, K., Olson, C.G., Elliot, W.C., Hendricks, D.M., 2003. The impact of climate on the biogeochemical functioning of volcanic soils. Chemical Geology, 202(3-4): 195-223.

Coventry, R.J., Taylor, R.M., Fitzpatrick, R.W., 1983. Pedological significance of the gravels in some red and grey earth of Central North Queensland. Aust. J. Soil Res. 21: 219-240.

Cradwick P.D.G, Farmer V.C, Russell J.D., Masson C.R., Wada K. & Yoshinaga N. (1972) Imogolite –A hydrated aluminium silicate of tubular structure. Nature Physical Science, 240: 187-189.

Curi, N., and Franzmeier, D.P., 1984. Toposequence of oxisols from central plateau of Brazil. Soil Sci. Soc. Am. J. 48: 341-346.

Dahlgren, R.A., and Ugolini, F.C., 2004. The nature, properties and management of volcanic soils. Advances in Agronomy, 82: 113-182.

Dickson, J.A.D., 1966. Carbonate identification and genesis as revealed by staining. Journal of Sedimentary Petrology, 36(2): 491-505.

Doner, H. E., and Lynn, W.C., 1989, Carbonate, halide, sulfate, sulfide minerals, in Dixon, J.B., and Weed, S.B., eds., Minerals in Soil Environments: Madison, Wisconsin, Soil Science Society of America, p. 279-330.

Farmer V.C. & Fraser A.R. (1979) Syntheticimogolite, a tubular hydroxy-aluminium silicate. Pp. 547_553 in: International Clay Conference 1978 (M.M.Mortland & V.C. Farmer, editors). Elsevier, Amsterdam.

Gerard, M., Caquineau, S., Pinheiro, J., Stoops, G., 2007. Weathering and allophane neoformation in soils developed on volcanic ash in the Azores. European Journal of Soil Science 58: 496-515.

Giambelluca, T.W., Schroeder, T.A., 1998. Climate. In: Juvik S.P., Juvik, J.O. (Eds.), Atlas of Hawaii, 3rd ed. University of Hawaii Press, Honolulu: 49-59.

Giambelluca, T.W., Chen, Q., Frazier, A.G., Price, J.P., Chen, Y.-L., Chu, P.-S., Eischeid, J.K., Delparte, D.M., 2013: Online Rainfall Atlas of Hawai'i. *Bull. Amer. Meteor. Soc.* 94: 313-316, doi: 10.1175/BAMS-D-11-00228.1.

Goodfellow B.W., G.E. Hilley, and O.A. Chadwick. 2013. Depth and character of rock weathering across basalt-hosted climosequences on Hawaii and Kauai. *Earth Surface Processes and Landforms* DOI: 10.1002/esp.3505.

Hall, P.L., Churchman, G.J., Theng, B.K.G., 1985. Size distribution of allophane unit particles in aqueous suspensions. Clays and Clay Minerals, 33: 345-349.

Holmgren, G.C., 1967. A rapid citrate-dithionite extractable iron procedure. Proc. Soil Sci. Soc. Am., 31: 210-211.

Hsieh, J.C.C., Chadwick, O.A., Kelly, E.F. and Savin, S.M., 1998. Oxygen isotopic composition of soil water: Quantifying evaporation and transpiration. Geoderma, 82: 269-293.

Hsu, P.H., 1989. Aluminum Hydroxides and Oxyhydroxides. In: Dixon, J.B., and Weed, S.B., (Eds.) Minerals in Soil Environments. 2nd ed., Soil Science Society of America Book Series 1.

Jackson, M.L., Levelt, T.W.M., Syers, J.K., Rex, R.W., Clayton, R.N., Sherman, G.D., Uehara, G., 1971. Geomorphological relationships of tropospherically derived quartz in the soils of the Hawaiian Islands. Soil Science Society of America Proceedings 35: 515-525.

Jackson, M.L., Lim, C.H., Zelazny, L.W. and . In: (Ed.), A., vol. 9. ,, pp. . 1986. Oxides, hydroxides and aluminosilicates. In: A. Klute (Editor), Methods of Soil Analysis: Part 1. Physical and Mineralogical Methods. Soil Science Society of America, Madison, WI: 102–149.

King, R.J., 2009. Kaolinite. Geology Today, 25(2): 75-78.

Kurtz, A.C., Derry, L.A. and Chadwick, O.A., 2001. Accretion of Asian dust to Hawaiian soils: Isotopic, elemental, and mineral mass balance. Geochimica et Cosmochica Acta, 65: 1971– 1983.

Lippmann, F., 1973. Sedimentary carbonate minerals. Springer-Verlag New York, Inc., Secaucus, NJ.

Macdonald, G.A., Abbott, A.T., Peterson, F.L., 1983. Volcanoes in the Sea, 2nd ed. University of Hawaii Press, Honolulu.

Machel, H.-G., 1985. Cathodoluminescence in calcite and dolomite and its chemical interpretation. Geoscience Canada, 12(4): 139-147.

McBride M.B., Farmer V.C., Russell J.D. Tait, J.M. & Goodman B.A. (1984) Iron substitution in aluminosilicate sols synthesized at low pH. Clay Minerals, 19: 1-8.

McDougall, I., 1969. Potassium-argon Ages of Lavas from the Hawi and Pololu Volcanic Series, Kohala Volcano, Hawaii. Geol. Soc. Amer. Bull., 80: 2597-2600.

McDougall, I., Swanson, D.A., 1972. Potassium-Argon ages of lavas from the Hawi and Pololu Volcanic Series, Kohala Volcano, Hawaii. Geo. Soc. Amer. Bull., 83: 3731-3738.

McFadden, L.D., Amundson, R.G., Chadwick, O.A., 1991. Numerical modeling, chemical, and isotopic studies of carbonate accumulation in soils of arid regions. In: Nettleton, W.D. (Ed.), Occurrence, Characteristics, and Genesis of Carbonate, Gypsum and Silica Accumulations in Soils: Soil Science Society of America, Special Publication 26: 17-35.

McKeague, J.A. and Day, D.H., 1966. Dithionite- and oxalate-extractable Fe and Al as aids in differentiating various classes of soils. Canadian Journal of Soil Science, 46: 13-22.

Megaw, H.D., 1934. The crystal structure of hydrargillite Al(OH)3. Z. Kristallogr., 87: 185-204.

Mikutta, R., Kleber, M., Kaiser, K., Jahn, R., 2005. Review: Organic matter removal from soils using hydrogen peroxide, sodium hypochlorite, and disodium peroxodisulfate. Soil Science Society of America Journal, 69(1): 120-135.

Moore, D.M. and Reynolds, R.C., 1997. X-Ray Diffraction and the Identification and Analysis of Clay Minerals. Oxford University Press, New York.

National Cooperative Soil Survey, National Cooperative Soil Characterization Database. Pedon 95P 0259. http://ncsslabdatamart.sc.egov.usda.gov Accessed: 6/16/2014.

Parfitt, R.L., 1990. Allophane in New Zealand – A Review. Australian Journal of Soil Research, 28: 343-360.

Parfitt, R.L., 2009. Allophane and imogolite: role in soil biogeochemical processes. Clay Minerals 44: 135-155.

Parfitt, R.L., Saguisa, M., Eden, D.N., 1984. Soil development processes in an Aqualf-Ochrept sequence from loess with admixtures of tephra, New Zealand. Journal of Soil Science, 35: 625-640.

Parfitt, R.L., and Wilson, A.D., 1985. Estimation on allophane and halloysite in three sequences of volcanic soils, New Zealand. Catena Supplement, 7: 1-8.

Pena, F., and Torrent, J., 1984. Relationships between phosphate sorption and iron oxides in alfisols from a river terrace sequence of Mediterranean Spain. Geoderma: 283-296.

Porder, S., Hilley, G.E. and Chadwick, O.A., 2007. Chemical weathering, mass loss, and dust Inputs across a climate by time matrix in the Hawaiian Islands. Earth and Planetary Science Letters, 258(3-4): 414-427.

Prothero, D.R., and Scwab, F., 2004. Sedimentary Geology, 2nd ed.. W.H. Freeman and Company, New York.

Reeder, R.J., 1983. Crystal Chemistry of the Rhombohedral Carbonates. In: Reeder, R.J. (ed.) Carbonates: Mineralogy and Chemistry, Volume 11, Reviews in Mineralogy. Mineralogic Society of America, Washington D.C.: 1-47.

Rimstidt, J.D., Balog, A., Webb, J., 1998. Distribution of trace elements between carbonate minerals and aqueous solutions. Geochimica et Cosmochimica Acta, 62(11): 1851-1863.

Schwertmann, U., and Taylor, R.M., 1989. Iron oxides. In: Dixon, J.B., and Weed, S.B., (Eds.) Minerals in Soil Environments. 2nd ed., Soil Science Society of America Book Series 1.

Seifferman, G., Millot, G., 1969. Equatorial and tropical weathering of recent basalts from Cameroon: allophane, halloysite, metahalloysite and gibbsite. In: Heller, L. (Ed.), Proceedings of the International Clay Conference, Tokyo. Israel Universities Press, Jerusalem, pp. 417-430.

Singh, S.S., 1974. The solubility product of gibbsite at 15, 25, and 35 °C. Soil. Sci. Am. Proc., 38: 415-417.

Soil Survey Staff, 1999. Soil Taxonomy: A Basic System of Soil Classification for Making and Interpreting Soil Survey, 2nd ed. U.S. Government Printing Office, Washington, DC.

Spengler, S.R., Garcia, M.O., 1988. Geochemistry of the Hawi Lavas, Kohala Volcano, Hawaii, Contrib. Mineral. Petrol., 99: 90-104.

Stearns, H.T. and Macdonald, G.A., 1946. Geology and Ground-water Resources of the Island of Hawaii. Bulletin of the Division of Hydrography 9.

Takasaki, K.J., 1978. Summary appraisals of the nation's groundwater resources – Hawaii Region. Geological Survey Professional Paper, 813-M.

Tessens, E., and Zauyah, S., 1982. Positive permanent charge in oxisols. Soil Sci. Soc. Am. J., 46:1103-1106.

Theng, B.K.G., Russell, M., Churchman, G.J., Parfitt, R.L., 1982. Surface properties of allophane, halloysite, and imogolite. Clays and Clay Minerals 30, 143-149.

Vitousek, P.M. et al., 2004. Soils, agriculture, and society in precontact Hawai. Science, 304(5677): 1665-1669.

Whipkey, C.E., Capo, R.C., Hsieh, J.C.C. and Chadwick, O.A., 2002. Development of magnesian carbonates in Quaternary soils on the island of Hawaii. Journal of Sedimentary Research, 72(1): 158-165.

Williams, J., and Coventry, R.J. 1979. The constrasting hydrology of red and yellow earths in a landscape of low relief. In: The hydrology of areas of low precipitation. (Proc. Symp. Canberra) Int. Assoc. Sci. Hydrol. Publ. 128: 385-395.

Wolfe, E.W., Morris, J., 1996. Geologic map of the Island of Hawaii. US Geological Survey Map I-2524-A.

Ziegler, K., Hsieh J.C.C., Chadwick, O.A., Kelly E.F., Hendricks, D.M., Savin, S.M., 2003. Halloysite as a kinetically controlled end product of arid-zone basalt weathering. Chemical Geology, 202: 461-478.

CHAPTER 3

FRACTIONATION OF MAGNESIUM ISOTOPES DURING THE WEATHERING OF HAWAIIAN BASALTS UNDER ARID CLIMATIC CONDITIONS

Abstract

Our study combines Mg isotopic analyses with soil characterization methods to determine Mg isotopic compositions of bulk soils and basalts, carbonate fractions, non-carbonate fractions and vegetation at an arid (~30 cm mean annual precipitation) soil chronosequence on the Island of Hawaii. The chronosequence is developed on Pololu (350 ka) and Hawi (170 ka) lava flows. Bulk soil horizons at these sites range in δ^{26}Mg from -0.21±0.31‰ to -1.75±0.22‰ for the Hawi site and -0.01±0.31‰ to -0.21±0.31‰ for the Pololu site. Basalts underlying the soil profiles have average δ^{26}Mg values of -0.25±0.06‰. Carbonate δ^{26}Mg values at these sites vary from -1.05±0.22‰ to -2.31±0.22‰ and can be used to calculate the isotopic compositions of non-carbonate fractions when combined with bulk soil values for each soil horizon. The best-constrained calculated non-carbonate fraction is isotopically heavier than basalt, with a value of -0.07±0.28‰. Vegetation at these sites has an average δ^{26}Mg value of -0.07±0.26‰. Integrating the soils as a whole yields bulk soil isotopic compositions of -1.35±0.16‰ for the Hawi site and -0.12±0.12‰ for the Pololu site. This difference in overall δ^{26}Mg between total soils may be explained by the relative abundance of Mg in carbonate; in the Hawi soil 69±11% of Mg is within carbonate phases, while in the Pololu soil only 16±2% of Mg is within carbonate phases. Estimates of Mg input to the soils through time allow the calculation of the δ^{26}Mg of Mg exported from these systems. The export of Mg from the Hawi soil is poorly constrained but the exported Mg should be significantly isotopically heavier than basalt. The Pololu soil is much better constrained and should have exported Mg with a δ^{26}Mg of -0.36±0.26‰, near mixing

estimates for basalt and rainfall. These differences support that the evolution of the soil mineralogy and morphology through time results in changes in the isotopic composition of Mg exported.

3.1. INTRODUCTION

The stable isotopes of magnesium aid in understanding ecosystem-scale magnesium cycling. However, much work remains before the behavior of magnesium isotopes is completely understood in the weathering environment. Previous work shows that magnesium isotopes are fractionated in the weathering environment and that secondary mineral formation may play a role in this fractionation (Tipper et al. 2006; Brenot et al. 2008; Pogge von Strandmann et al. 2008; Tipper et al. 2010; Wimpenny et al. 2010; Bolou Bi et al. 2012; Opfergelt et al. 2012; Wimpenny et al. 2014). We investigate this mechanism of Mg isotope fractionation by analyzing the bulk soil and carbonate phase Mg isotopic values of the Hawi and Pololu soils dissected in Chapter 2. We then determine the overall direction of Mg isotopic fractionation during arid soil formation.

Development of multi-collector inductively coupled plasma mass spectrometry has enabled the use of Mg isotopes as a tool for investigating the weathering environment (Galy et al. 2001). Workers have surveyed Mg isotopic compositions in plants, waters, soils and parent materials, but analyses are still sparse. Figure 3.1 details the magnesium isotopic compositions of a variety of reservoirs according to literature reports compiled by White, in press. It seems that isotopically light Mg is released to streamwaters during weathering of parent materials, and the remaining pool of isotopically heavy Mg is stored in soils or plants (Tipper et al. 2006; Brenot et al. 2008). Although most studies indicate incorporation of isotopically heavy Mg into secondary silicate minerals (Tipper et al. 2006; Teng et al. 2010; Opfergelt et al. 2012; Huang et

al. 2012), other studies suggest the opposite (Pogge von Strandmann et al. 2008; Wimpenny et al. 2010), which may be a result of processes involving the adsorption/desorption of Mg (Huang et al. 2012; Opfergelt et al. 2014).

Magnesium isotopes are fractionated by plant uptake, with isotopically heavier magnesium incorporated into plant roots from solution (Black et al. 2008; Bolou Bi et al. 2010; Bolou Bi et al. 2012; Tipper et al. 2010). Thus it is possible that Mg in soil organic matter (SOM) forms a separate isotopically heavy reservoir in weathering systems. However, Mg assimilated into plants is subjected to further fractionation because isotopically light Mg may be preferentially transferred within the plant leading to progressive depletion of heavy Mg away from the roots (Black et al. 2008; Bolou Bi et al. 2010; Bolou Bi et al. 2012). Thus the source and fate of plant tissues that contribute Mg to SOM may be important to consider in an overall isotopic budget.

In contrast to pedogenic minerals and SOM, it is well documented that isotopically light magnesium is preferentially incorporated into marine carbonate (Figure 3.1). The magnitude of this fractionation is thought to be dependent upon vital effects and precipitation rate (Chang et al. 2003; Chang et al. 2004; Rose Koga et al. 2010; Saulnier et al. 2012; Mavromatis et al. 2013). Magnesium isotope variations in pedogenic carbonates have not been previously studied.

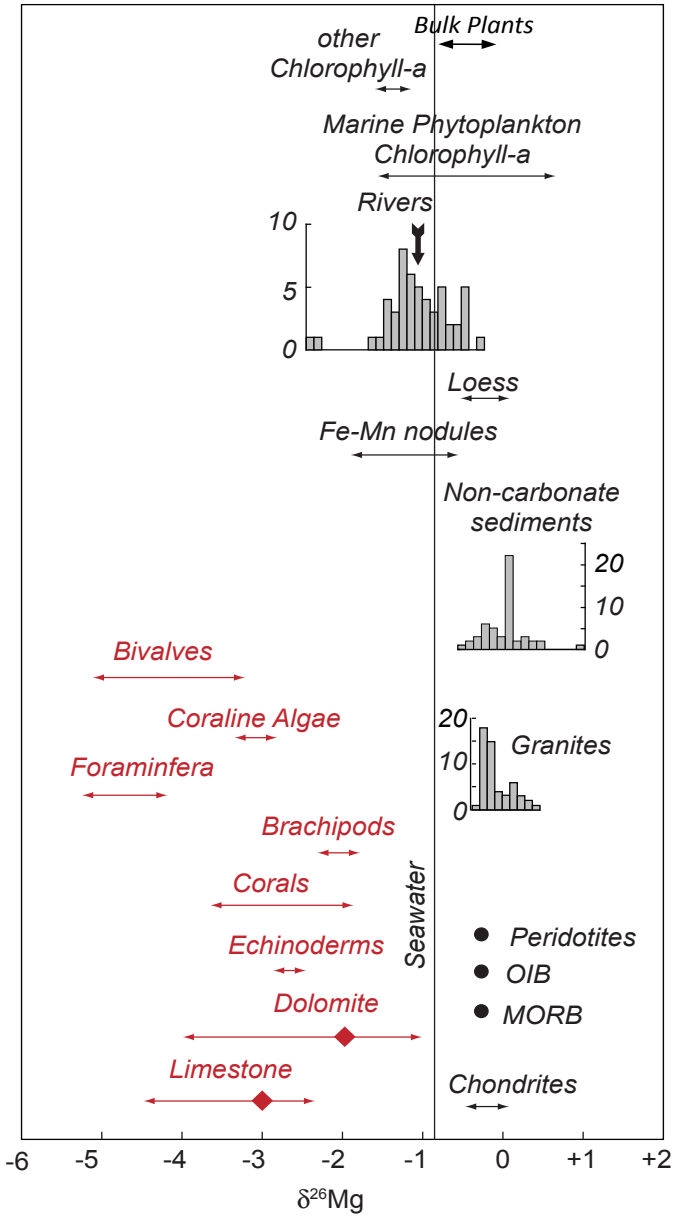

Figure 3.1: Magnesium isotopes in terrestrial materials. The 2σ variation in peridotites, seawater, OIB, and MORB are less than the size of the symbols. Data for peridotites, MORB, OIB, and chondrites are from Teng et al. 2010. Flux-weighted average riverine δ^{26}Mg is shown by the arrow and is from Tipper et al. 2006. Figure modified from White, in press. Bulk plant isotopic values are presented as the range expected if the growth solution had the isotopic composition of the flux-weighted average riverine flux, based on experimental plant-growth solution fractionations found in Bolou Bi et al. 2010.

3.1.1. Study Sites

The Kohala chronosequence (Hawi and Pololu) soil study sites are reviewed in Chapter 2 (2.1.3. Soil Sites).

3.2. METHODS

3.2.1. Soil Sampling

The methods behind soil and rock sampling, bulk soil and rock dissolutions, carbonate dissolutions, and vegetation dissolutions may all be found in Chapter 2 (2.3. Methods). An aliquot of each of these dissolved samples was prepared for isotopic analysis following the methodology below.

3.2.2. Isotopic Analysis

Mg samples for isotopic analysis were purified through a series of ion exchange columns. For dissolved soils, rock, vegetation, and carbonate, an amount of sample containing ~ 50 μg of magnesium was evaporated to dryness. The evaporated samples were dissolved in 2 ml of concentrated HNO_3 and heated at 80°C for five hours. This solution was evaporated to dryness and redissolved in 1 ml of 7 N HCl heated at 80°C overnight. This solution was evaporated to dryness, and then the sample was redissolved in 1 ml of 7 N HCl heated at 80°C for two hours. This solution was sonicated and centrifuged to ensure complete dissolution; if residue was observed following centrifugation we determined its identity and restarted the procedure from the beginning, after appropriate chemical treatment**.**

The ion exchange chemistry used a four-step process (modified from Bolou Bi et al. 2009): an anion exchange column step to remove transition metals, a cation exchange column

step to separate K from Mg, and a cation exchange column step, repeated twice, to purify Mg from traces of other elements.

Individual ion exchange columns were calibrated with BE-N rock standard to ensure adequate separation of magnesium from other elements. The products from this calibration were analyzed to determine yield and solution purity, as well as δ^{26}Mg. After finding both good yields (all yields >90%, average yield 97%) and appropriate δ^{26}Mg (-0.33±0.14‰) for our BE-N rock standards using our modified ion exchange chemistry procedure, the columns were used for sample preparation. A procedural blank and BHVO-2 rock standard or BE-N rock standard were run with each batch of eight samples, to ensure the consistency and accuracy of our results.

Prior to isotopic analysis, the samples were treated to remove organic matter leached from the ion exchange resin by dissolving them in 2 ml of concentrated HNO_3 for five hours on a hotplate at 80 °C. Samples were then evaporated down, dissolved in a small amount of concentrated nitric acid, and diluted to a concentration of ~ 100 ppb Mg and 0.05 N HNO_3 to run on a Thermo Fisher Neptune multi-collector inductively coupled plasma mass spectrometer (MCICPMS) at the Centre du Recherches Petrographiques et Geochimiques (CRPG) in Nancy, France. The samples were run using a standard-sample bracketing technique with either SRM-980 or DSM3 as the standard and check standard.

3.3. RESULTS

3.3.1. Isotope Overview, Standards, and Blanks

All magnesium isotope data are presented in Table 3.1 as δ^{26}Mg and δ^{25}Mg relative to DSM3. The "*n*" in this table refers to the total number of analyses for each sample, including replicates during a single instrument run as well as replicates over multiple instrumental runs. Figure 3.2 illustrates a three-isotope plot with all of our collected isotope data. All samples fall near the terrestrial equilibrium mass fractionation line (our slope=0.516; terrestrial equilibrium mass fractionation line slope=0.521 from Young and Galy (2004)). As such only δ^{26}Mg values are shown in subsequent figures. Although standard deviations were calculated for each magnesium isotopic value, one sample (HI-06-45) that underwent ion exchange column chemistry was run every time (n=21) isotopic analyses were conducted, to monitor long-term instrumental variability. The data in Figure 3.2 are all plotted with 2σ values for this sample, which are ±0.22‰ for δ^{26}Mg and ±0.12‰ for δ^{25}Mg. Basalt standards BHVO-2 and BE-N yielded mean δ^{26}Mg±2σ values of -0.21±0.14‰ (-0.19±0.05‰, Bizzaro et al. 2011) and -0.33±0.22‰ (-0.28±0.08‰, Bolou Bi et al. 2009), respectively, over this period of time. These standards were processed with each new batch of samples to ensure adequate ion exchange chemistry (full chemistry replicates). Procedural blanks were processed with each batch of ion exchange chemistry and varied from 3 ng to 52 ng, which is insignificant compared to the 50 µg of Mg passed through the ion exchange columns during purification.

Table 3.1: Overview of Mg isotope data. SE is the standard error of the mean.

Sample or Standard	$\delta^{26}Mg$	$\delta^{25}Mg$	n	SE on $\delta^{26}Mg$
Carbonates				
Hawi				
KT 8-6 C	-1.05	-0.56	4	0.08
KT 9-2 C	-1.50	-0.77	6	0.05
KT 9-3 C	-2.24	-1.17	5	0.05
KT 9-2 PCD	-2.06	-1.07	2	0.01
KT 9-3 PCD	-1.88	-0.97	2	0.01
KT 9-4 PCD	-1.97	-1.04	2	0.00
Pololu				
KT 7-5 C	-1.81	-0.95	5	0.03
KT 7-6 C	-2.31	-1.20	5	0.04
KT 7-7 C	-1.28	-0.68	5	0.04
KT 7-5 PCD	-1.89	-0.99	2	0.00
KT 7-6 PCD	-1.99	-1.05	3	0.02
KT 7-7 PCD	-1.08	-0.56	3	0.02
Soil Bulk Dissolutions				
Hawi				
KT 9 B	-0.27	-0.14	2	0.02
KT 9-1 B	-0.14	-0.07	2	0.01
KT 9-2 B	-1.35	-0.70	1	
KT 9-3 B	-1.75	-0.89	2	0.01
KT 9-4 B	-1.22	-0.61	1	
Pololu				
KT 7 B	-0.04	0.00	1	
KT 7-1 B	-0.33	-0.18	1	
KT 7-2 B	-0.12	-0.07	1	
KT 7-3 B	0.05	0.04	2	0.10
KT 7-4 B	-0.73	-0.40	2	0.05
KT 7-5 B	-0.35	-0.16	2	0.07
KT 7-6 B	-0.28	-0.14	3	0.08
KT 7-7 B	-0.09	-0.07	1	
Basalts				
Hawi				
KT 8-7 R	-0.18	-0.08	2	0.05
KT 9-5 R	-0.21	-0.11	2	0.02
Pololu				
KT 7-8 R	-0.30	-0.15	1	
KT 7-9 R	-0.31	-0.16	2	0.10
Other Hawaiian basalts				
KT 1 R	-0.23	-0.14	6	0.03
KT 4 R	-0.17	-0.11	2	0.05
KT 11-11 R	-0.16	-0.07	1	
Vegetation				
Hawi				
B1	0.10	0.05	8	0.06
Pololu				
P2	-0.22	-0.11	12	0.03
Other Hawaiian vegetation				
AUW1	-0.07	-0.04	12	0.04
AUW2	-0.09	-0.03	10	0.02

Table 3.1 (Continued)

Sample or Standard	$\delta^{26}Mg$	$\delta^{25}Mg$	n	SE on $\delta^{26}Mg$
Standards				
Instrumental Reproducibility Sample				
HI-06-45	-0.46	-0.24	21	0.02
Reference Materials				
CRPG SRM980	-4.00	-2.06	8	0.03
CRPG SRM980b	-4.08	-2.08	4	0.08
Column Processed Rock Standards				
BHVO-2	-0.21	-0.12	15	0.02
BEN	-0.33	-0.16	9	0.02
BEN	-0.31	-0.18	5	0.08

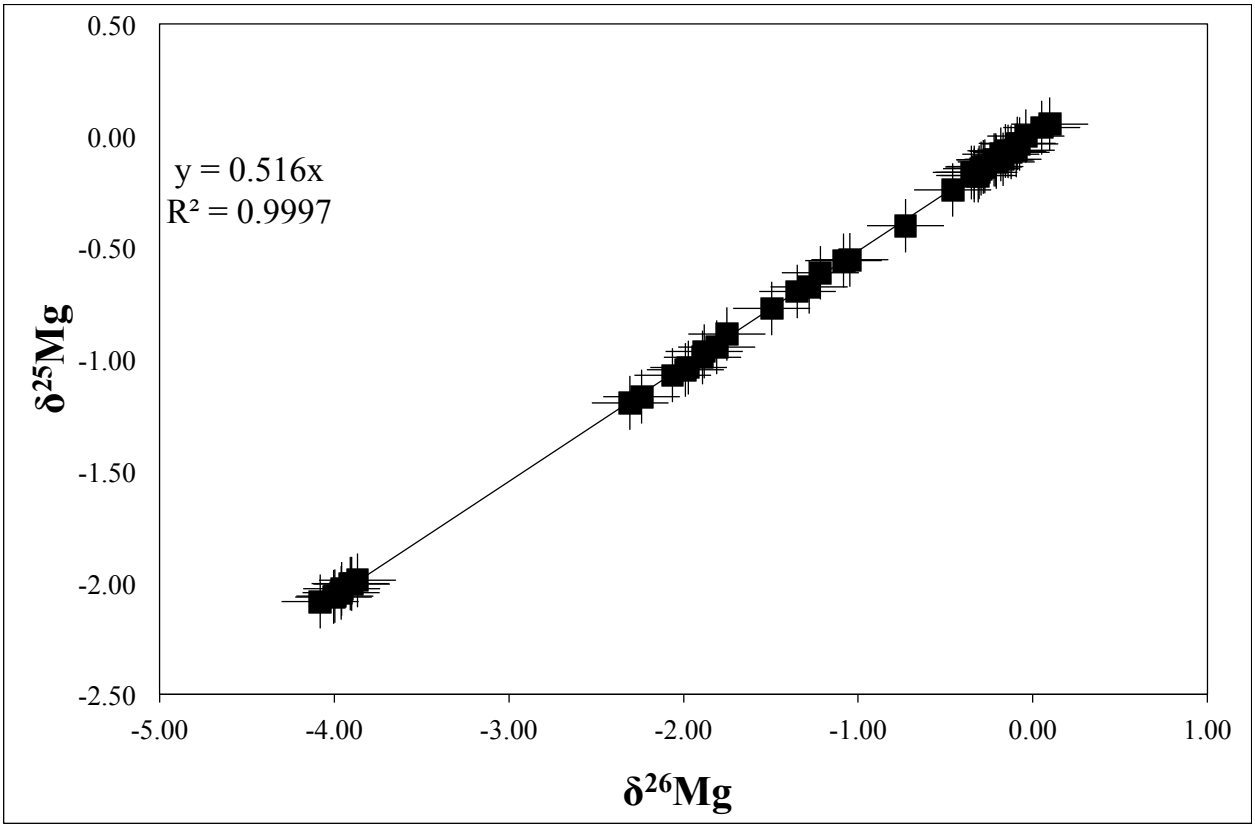

Figure 3.2: Three-isotope plot of all Mg data. All data fall on the terrestrial mass fractionation line.

3.3.2. Parent Material and Precipitation

Data for the bulk chemistry of basalt dissolutions are presented in Tables 2.3 and 2.4 from Chapter 2 (2.4.2. Parent Material and Precipitation). Average precipitation chemistry values for the Island of Hawaii from Carrillo et al. (2002) are 1600 µg/l Na, 60 µg/l Mg, 200 µg/l K, and 50 µg/l Ca, but these values are highly variable. Basalts and precipitation are the two main Mg inputs to our soil system. Basalts have measured δ^{26}Mg values that average -0.25±0.06‰ over both sites, and precipitation is estimated to have the isotopic composition of seawater (-0.89‰ average BCR-403 value from Bolou Bi et al. (2009)). Figure 3.3 displays the δ^{26}Mg values for all analyzed samples broken into categories by sample type, including the Mg isotopic compositions of our basaltic parent materials and the seawater estimate for precipitation. Our basalt values fall within the range of literature values for oceanic island basalts (Figure 3.3).

3.3.3. Soil Carbonates

Data for the chemistry of the individual carbonate dissolutions are presented in Tables 2.9 and 2.10 of Chapter 2 (2.4.4. Individual Carbonate Extraction). Mg isotopic values for our pedogenic carbonates are shown in Figure 3.3 and fall within literature values for carbonate. Pedogenic carbonates from both soils are similar in δ^{26}Mg to oceanic carbonates at their lightest values (-2.31±0.22‰), displaying a fractionation of ~2‰ from an estimate of the δ^{26}Mg of mixing of basalt (-0.3‰) and precipitation (-0.89‰). Experimental studies show that the Mg isotopic composition of carbonates is controlled by calcite growth processes and that the equilibrium $\Delta^{26}Mg_{calcite\text{-}fluid}$ is probably near -3.5±0.2‰, but that high precipitation rate or vital effects can result in smaller fractionations (Chang et al. 2003; Chang et al. 2004; Rose Koga et

al. 2010; Saulnier et al. 2012; Mavromatis et al. 2013). Our carbonate magnesium isotopic values occupy a large range from -1.05‰ to -2.31‰.

3.3.4. Vegetation

Chemistry values for the vegetation dissolutions are presented in Tables 2.11 and 2.12 in Chapter 2 (2.4.5. Vegetation). Included in this dataset are two additional samples from a nearby study site "Mauna Kea" for comparison. Isotopically the δ^{26}Mg values for vegetation samples range from 0.10±0.32‰ to -0.22±0.24‰ (Figure 3.3), with an average value of -0.07±0.26‰.

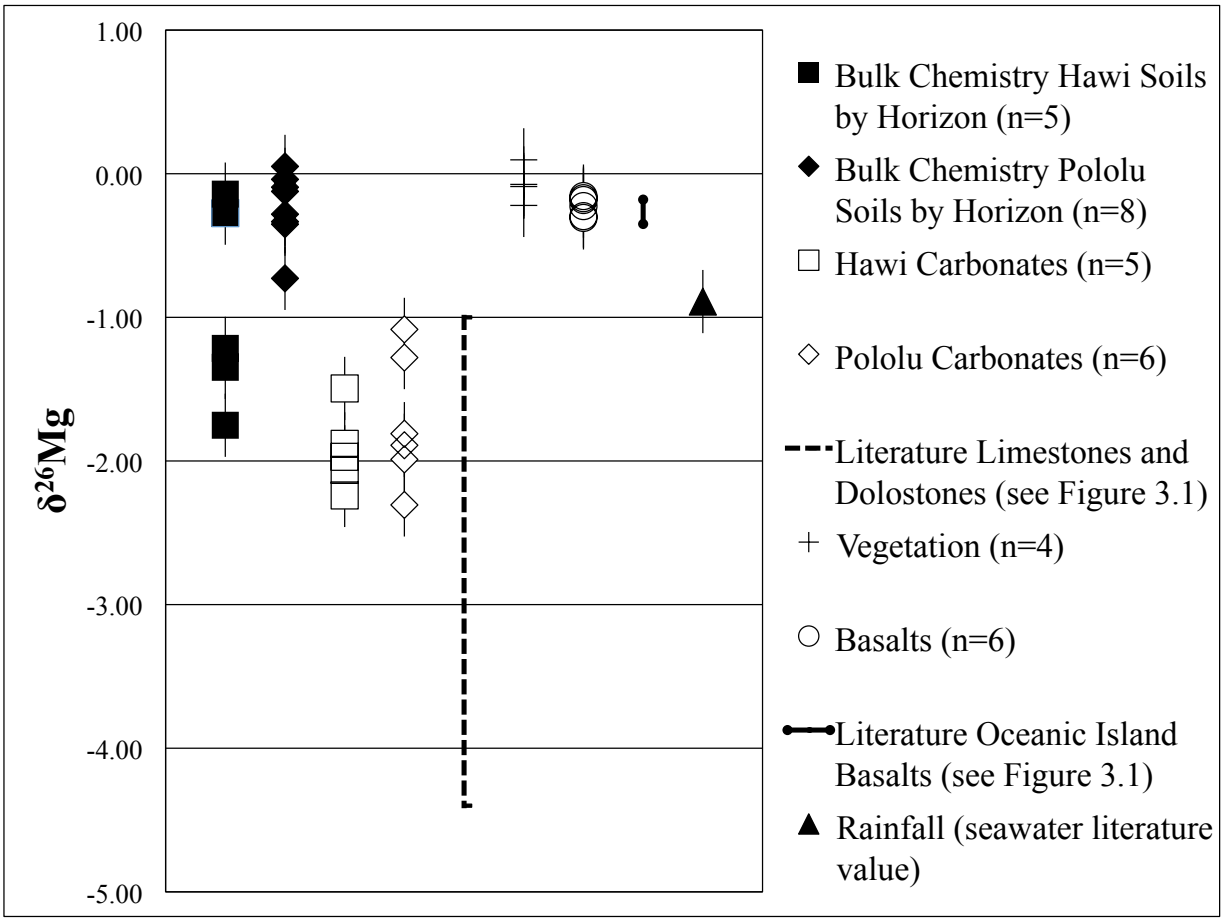

Figure 3.3: Overview of Mg isotope data for bulk soils, carbonates, vegetation, basaltic parent materials, and estimated rainfall along with literature comparisons. Errors shown are 2σ.

3.3.5. Bulk Soil Samples

Data for the chemistry of the bulk soil samples are shown in Tables 2.5, 2.6, 2.7, and 2.8 in Chapter 2 (2.4.3. Bulk Soil Samples). Tables 2.5 and 2.6 show values for the <2-mm portion of each horizon, and Tables 2.7 and 2.8 show the arithmetically weighted average chemistry values for each horizon, given the proportions of the <2-mm and >2-mm fractions. These tables are similar in layout to Tables 3.2 and 3.3. Table 3.2 shows the δ^{26}Mg values for the <2-mm fractions of each horizon along with carbonates, vegetation and parent material. Table 3.3 shows the weighted average δ^{26}Mg values for the combined <2-mm and >2-mm fractions along with carbonates, vegetation and parent material.

δ^{26}Mg values for the <2-mm fractions of the bulk soil samples and the >2-mm saprolite fraction range between -0.14±0.22‰ and -1.75±0.22‰ for the Hawi soil horizons, and between 0.05±0.22‰ and -0.73±0.22‰ for the Pololu soil horizons (Figure 3.3, Table 3.2). Bulk isotopic values for the Pololu soil tend to be heavier than those of the Hawi soil (Pololu mean value -0.24‰ vs. Hawi mean value -0.95‰). Calculating arithmetically weighted average Mg isotope values for each horizon composed of <2-mm fractions and >2-mm fractions changes the ranges slightly (Table 3.3); the Hawi values range from -0.21±0.31‰ to -1.75±0.22‰ and the Pololu values range from -0.01±0.31‰ to -0.21±0.31‰.

Table 3.2: Magnesium isotopic compositions of bulk soils, carbonates, vegetation, and basalts. Bulk soil isotopic compositions are for the <2-mm soil fraction if present in the horizon, with "Saprolite" representing the combined >2-mm soil fractions for a soil. If the horizon is indurated, the isotopic value represents the bulk horizon, since there is no <2-mm soil fraction. Uncertainties are 1σ from the analysis of that particular sample.

Soil Horizon	Depth to Horizon (cm)	Bulk Soil	Carbonate	Vegetation	Basalt
Pololu (350 ka)		**δ^{26}Mg**			
Surface				-0.22±0.12	
A	0-25	-0.33			
Bw1	25-41	-0.12			
Bw2	41-57	0.05±0.14			
	57 (transition)	-0.73±0.07			
C1	57-106	-0.35±0.10	-1.89±0.01		
	57-106 (subset)	-0.28±0.14	-1.99±0.04		
C2	106-143	-0.09	-1.08±0.04		
Saprolite	Throughout profile	-0.04			
Parent Material	143+				-0.31±0.14
Hawi (170 ka)		**δ^{26}Mg**			
Surface				0.10±0.16	
A	0-12	-0.14±0.02			
	12-13	-1.35	-2.06±0.01		
Bk	13-38	-1.75±0.02	-1.88±0.02		
C1	38-75	-1.22	-1.97±0.01		
Saprolite	Throughout profile	-0.27±0.03			
Parent Material	143+				-0.20±0.07

Table 3.3: Magnesium isotopic compositions of bulk soils, carbonates, vegetation, and basalts. Bulk soil isotopic compositions are for the proportionally combined <2-mm and >2-mm soil fractions. If the horizon is indurated, the value is the same as in Table 3.2. Uncertainties are 1σ values using our inter-run uncertainty from sample HI-06-45, as described in the text.

Soil Horizon	Depth to Horizon (cm)	Bulk Soil	Carbonate	Vegetation	Basalt
Pololu (350 ka)		**δ^{26}Mg**			
Surface				-0.22±0.11	
A	0-25	-0.21±0.16			
Bw1	25-41	-0.11±0.16			
Bw2	41-57	-0.01±0.16			
C1	57-106	-0.13±0.16	-1.89±0.11		
C1	57-106 (subset)	-0.11±0.16	-1.99±0.11		
C2	106-143	-0.09±0.11	-1.08±0.11		
Parent Material	143+				-0.31±0.11
Hawi (170 ka)		**δ^{26}Mg**			
Surface				0.10±0.11	
A	0-12	-0.21±0.16			
	12-13	-0.43±0.16	-2.06±0.11		
Bk	13-38	-1.75±0.11	-1.88±0.11		
C1	38-75	-1.22±0.11	-1.97±0.11		
Parent Material	143+				-0.20±0.11

Figure 3.4 illustrates the Mg bulk soil chemistry and Mg isotopic data with depth for the Hawi soil. The first 12 cm of the Hawi soil are more weathered than the rest and free of carbonates based on the tau plots, XRD analyses, sequential extraction, and field observations of Chapter 2 (Figures 2.11, 2.12, 2.18 and Tables 2.1, 2.2). This weathering has removed magnesium from the upper soil preferentially, and Mg concentrations enrich downward. Isotopically, the soil is dominated by the signature of carbonates at depth, but the surface horizon has a bulk δ^{26}Mg near the isotopic composition of parent material. Knowing the bulk soil isotopic composition, the carbonate isotopic composition, and the amount of Mg in both, we can calculate a theoretical isotopic composition for the Mg not associated with carbonate in the soil, which is also plotted in Figure 3.4. Excluded from this plot is the thin layer of carbonate from 12-13 cm in soil depth.

Figure 3.5 illustrates the total horizon bulk dissolution data for the Pololu soil, and shows that the trends seen in the younger Hawi soil continue with further development. The first three horizons of the Pololu soil are similar to the first horizon of the Hawi soil; they are more weathered than the rest of the profile, similar mineralogically, and have preferentially lost Mg as seen in soil depletion index plots, XRD analyses, and sequential extraction fractions from Chapter 2 (Figures 2.11, 2.12, 2.18 and Tables 2.1, 2.2). These three horizons have isotopic compositions heavier than mixing between parent material and precipitation should permit, similar to the first horizon of the Hawi soil. As in the Hawi soil, we can calculate theoretical isotopic compositions for Mg not associated with carbonate in the soil for the C1 and C2 horizons of the Pololu soil. Unfortunately, the mixing methodology used for calculating the total amount of Mg from the <2-mm and >2-mm fractions is biased for the C1 horizon of the Pololu soil. This calculation uses the average >2-mm saprolite for the soil and therefore does not

adequately account for Mg from carbonate in the >2-mm fraction for this horizon, since carbonate is preferentially partitioned to the >2-mm portion of the soil (i.e. the saprolite in this horizon is different from the average soil saprolite). This means that the amount of Mg in the bulk soil for horizon C1 should be slightly higher than shown, and the bulk soil isotopic composition should also be slightly lighter. These factors account for the significantly heavier calculated non-carbonate δ^{26}Mg value shown for this horizon. These issues do not influence the Bk or C horizon of the Hawi soil, or C2 horizon of the Pololu soil, as these horizons were completely indurated; as such there is no <2-mm soil fraction.

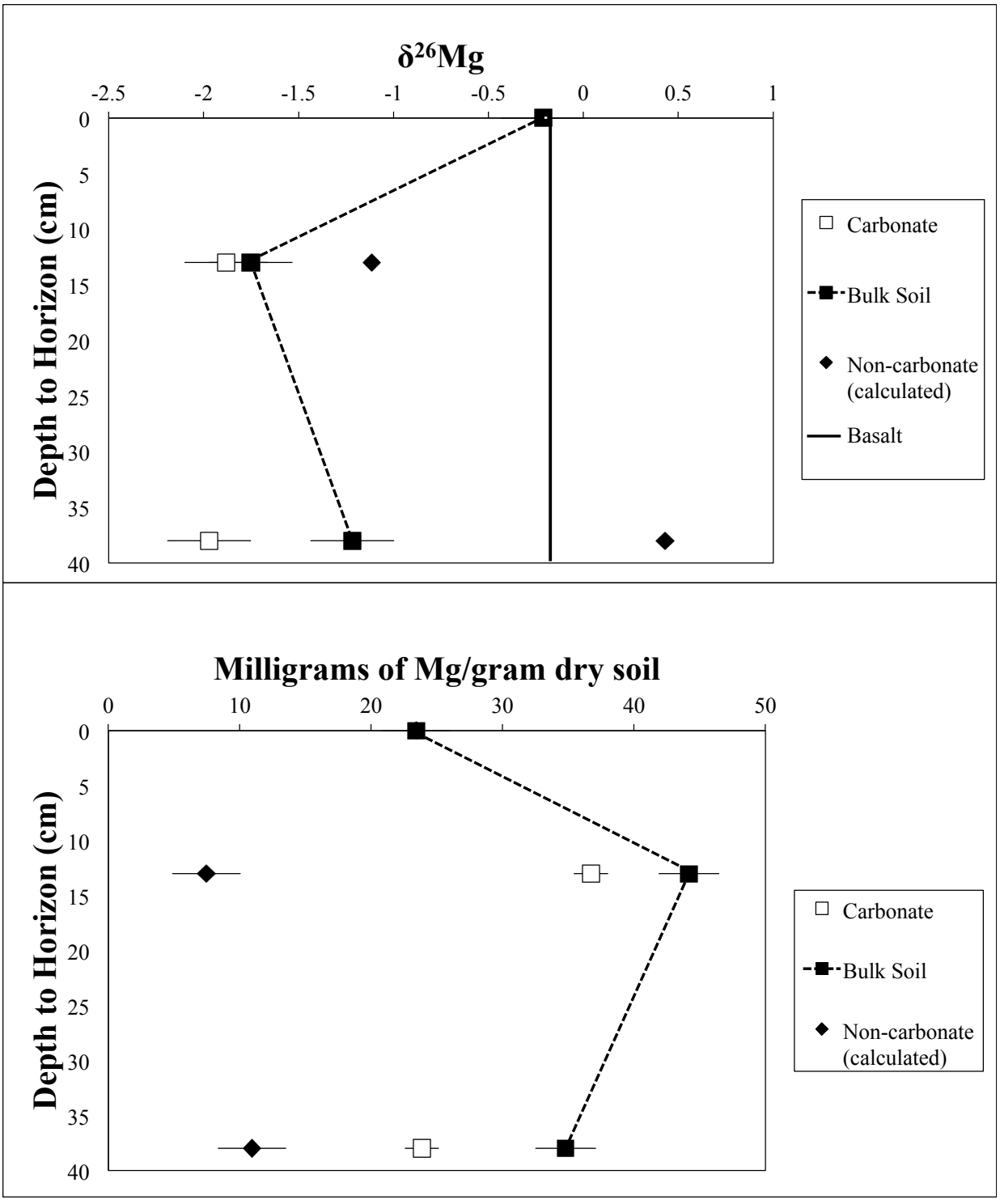

Figure 3.4: δ^{26}Mg values of the carbonate and bulk soil with depth in the Hawi soil profile and amount of Mg in each. Excluded from this plot is the thin layer of carbonate from 12-13 cm in depth, for clarity. δ^{26}Mg values for non-carbonate phases were calculated by mass and isotopic balance for those horizons with both carbonate and non-carbonate phases. Uncertainties shown are 2σ, except for our calculated non-carbonate δ^{26}Mg values, which have large 2σ values (±2‰ and ±1‰).

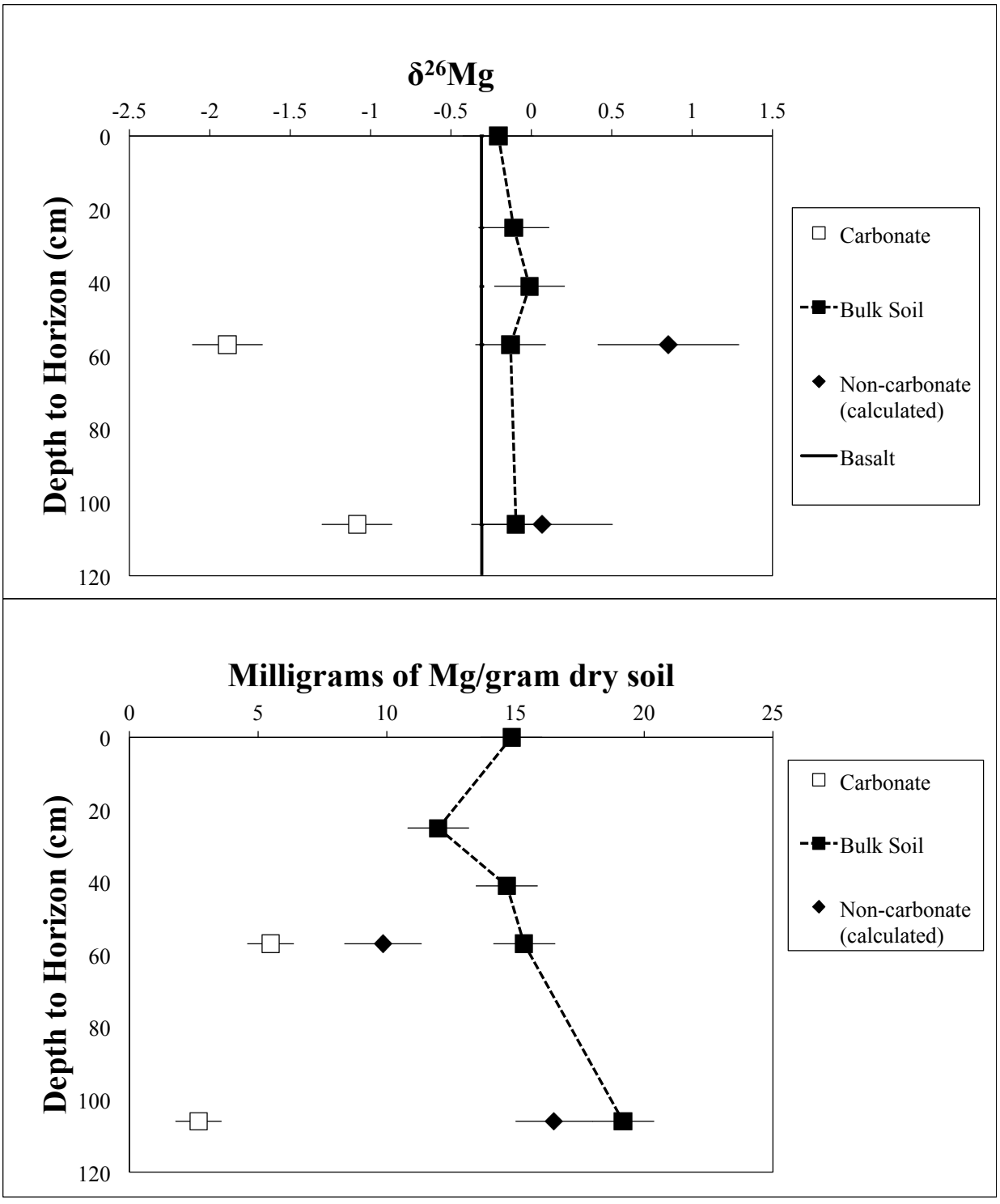

Figure 3.5: δ^{26}Mg values of the carbonate and bulk soil with depth in the Pololu soil profile and amount of Mg in each. δ^{26}Mg values for non-carbonate phases were calculated by mass and isotopic balance for those horizons with both carbonate and non-carbonate phases. Uncertainties shown are 2σ.

3.4. DISCUSSION

3.4.1. Parent Material and Precipitation

Simple mixing between the two dominant sources of soil magnesium, magnesium derived from basalt weathering and magnesium derived from rainfall, cannot explain the variation in magnesium isotopic compositions analyzed. Figure 3.3 shows that most of the bulk soil and carbonate isotopic data fall outside the range that mixing can account for (-0.25±0.13‰ to -0.89±0.1‰). Other potential inputs, such as Asiatic dust, should be insignificant in this system for Mg, given the limited range of δ^{26}Mg values for most silicate minerals and the small amount of Mg that these phases (quartz, illite, feldspar, kaolinite) should contain (Blank et al. 1985; Leinen et al. 1994). Also, dust input to our arid leeward sites is limited compared to wetter and older windward Long Substrate Age Gradient sites where dust input is important (Jackson et al. 1971; Kurtz et al. 2001). Without other significant inputs to the soil system our data suggest that magnesium isotopic fractionation is occurring. In order to understand the extent and cause of these fractionations, an estimate of the relative amount of input of Mg from basalt weathering and rainfall is needed.

3.4.2. Estimating Inputs to the Soil System

The amount of Mg derived from basalt weathering in these soils can be estimated using mass balance constraints provided by Zr, which is an immobile index element in these arid soils (Chadwick et al. 2003). The total amount of Zr in the Hawi and Pololu soils can be used to estimate the amount of Mg released to the soil system via basalt weathering, given that the Zr and Mg concentrations in the parent basalt are known and the amount of Zr in the soil is

accurately determined. The column-integrated Zr mass in a soil composed of *n* depth intervals of thickness *z* is:

$$Zr_{\text{int}} = \sum_{1}^{n} \rho_n [Zr]_n z_n$$

where ρ_n is the dry bulk density for a soil interval and $[Zr]_n$ is the concentration of Zr in that interval. If Zr is conservative the ratio

$$\frac{Mg_{\text{int}}^{con}}{Zr_{\text{int}}} = \frac{[Mg_{parent}]}{[Zr_{parent}]}$$

provides Mg_{int}^{con}, which is the amount of Mg that should be present in the soil if Mg behaved conservatively.

For the Hawi soil Zr_{int} = 19900±900 μg/cm^2, implying 35±2 kg/m^2 of Mg (Mg_{int}^{con}) has been derived from rock weathering given our $[Mg_{parent}]/[Zr_{parent}]$ ratio from basalt sampled beneath our soil profile. Variations in this $[Mg_{parent}]/[Zr_{parent}]$ ratio due to basalt heterogeneity may complicate this simple analysis, particularly for the more differentiated Hawi a'a lava flows. An analysis of another Hawi basalt near our soil study site (Table 2.4) shows significantly higher Mg/Zr ratios, which would translate to larger amounts of Mg derived from rock weathering, if the Hawi soil has been derived from basaltic materials with similar Mg/Zr ratios.

Using modern rainfall rates of 28.0±0.5 cm MAP and rainfall chemistry from Carrillo et al. (2002) extended over 170 ka of soil development, we calculate that 3±3 kg/m^2 of Mg have been added to the Hawi soil system via precipitation. The total amount of Mg input to the Hawi soil system is therefore 38±4 kg/m^2.

Similarly, the total amount of Zr in the Pololu soil (Zr_{int}) is 37800±200 μg/cm^2, yielding an estimate that 141±11 kg/m^2 of Mg (Mg_{int}^{con}) has been released to the soil system via rock weathering. Rainfall Mg input calculations (35.0±0.5 cm MAP for the Pololu site) yield 7±7

kg/m^2 of Mg added. The Pololu soil system therefore has had a total of 148±13 kg/m^2 added to it over the course of 350 ka of development.

With assumptions that the initial liberation of magnesium from minerals does not involve an isotopic fractionation (Ryu et al. 2011), and that rainfall rates have not varied greatly through time, a homogeneous soil derived from basalt and rainfall mixing should approach a $\delta^{26}Mg$ of -0.24±0.22‰ for the Hawi soil system and -0.33±0.22‰ for the Pololu soil system, statistically indistinguishable from basalt isotopic values (Figure 3.6). This illustrates the dominance of the rock weathering input of magnesium in these soils, and this dominance is supported in other studies by looking at cation provenance using Sr isotopes in carbonates (Whipkey et al. 2002). Climate variations through time associated with glacial-interglacial cycles complicate this picture, but even with enhanced rainfall during the glacial cycles (estimated to be up to 3x as high (Ziegler et al. 2003)), rock weathering will still be the dominant source of Mg to our systems.

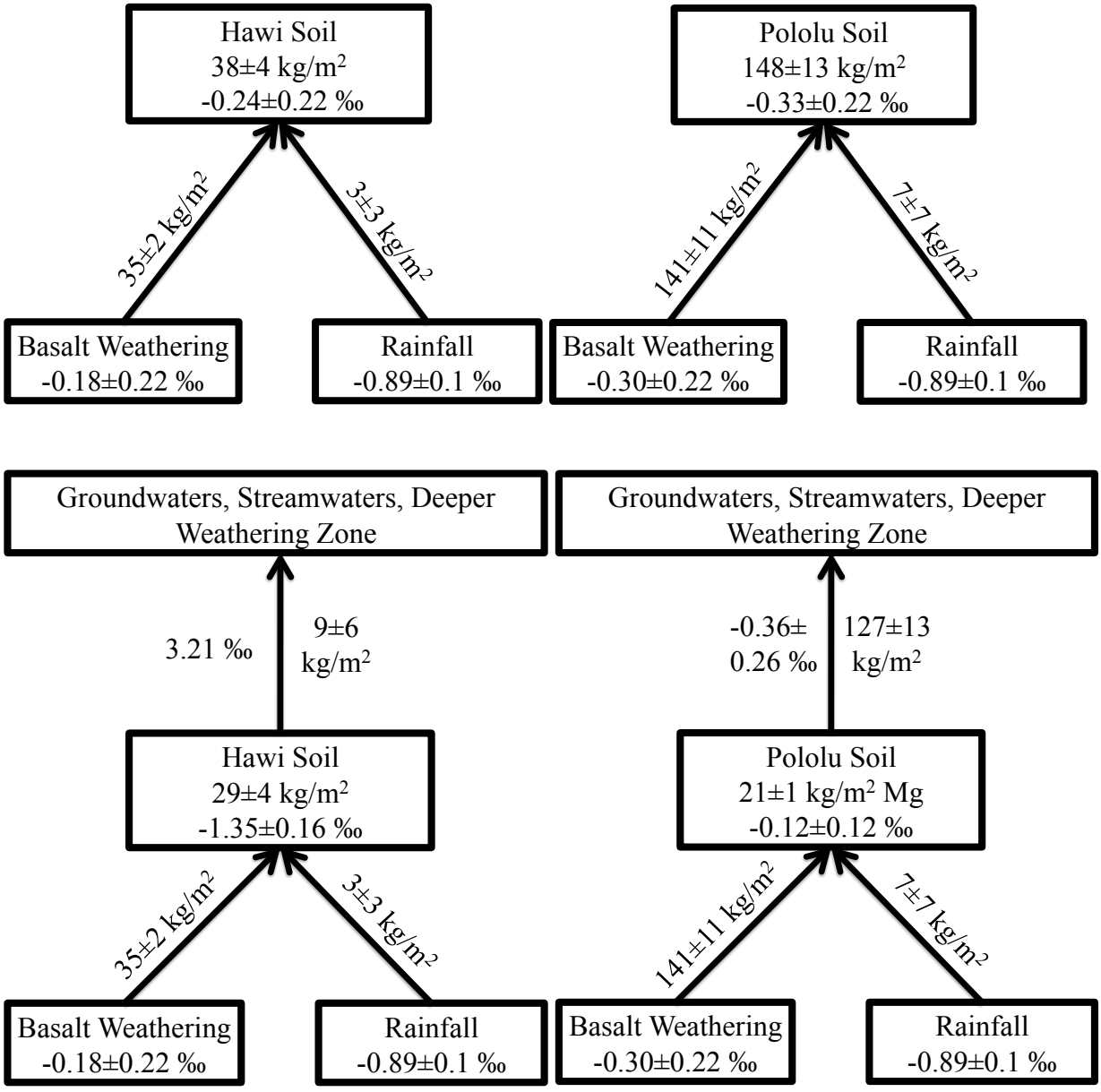

Figure 3.6: Soil Mg inputs and isotopic compositions from basalt weathering and rainfall in the Hawi and Pololu soil systems integrated over soil development (upper diagram). Combination of soil Mg inputs and isotopic compositions with actual measured soil Mg concentrations and isotopic compositions to determine fluxes from the soil systems integrated over soil development (lower diagram). The uncertainty associated with the isotopic export from the Hawi soil is large due to the small amount of Mg exported from the system, but the mean value is shown. Other uncertainties are 2σ.

3.4.3. Integrating the Hawi Soil

Derived in the same way as Zr_{int}, Mg_{int} describes the total amount of Mg present in our soils.

$$Mg_{\text{int}} = \sum_{1}^{n} \rho_n \left[Mg\right]_n z_n$$

By comparing these values to Mg_{int}^{con} we can estimate the amount of Mg that must have been exported from our soil systems. Mg_{int} and $\delta^{26}Mg$ values integrated through the entire Hawi soil profile for the bulk soil samples reveal 29±4 kg/m^2 of magnesium within the soil, with a $\delta^{26}Mg$ of -1.35±0.16‰. When these numbers are combined with our estimates of Mg input to and resulting isotopic composition of the Hawi soil system (38±4 kg/m^2, -0.24±0.22‰), we can calculate the mass and isotopic composition of the export flux of Mg from the Hawi soil system (Figure 3.6). We obtain an export flux of 9±6 kg/m^2, with a mean isotopic composition of 3.21‰. The uncertainty associated with the mean isotopic composition of the export flux is large due to the relatively small amount of Mg exported and large relative uncertainty of that flux, but it is conservative to say that the soil has exported isotopically heavy Mg during its 170 ka of development in order to get to its present state. These uncertainties were calculated using a Monte Carlo approach. Also, variability in parent material Mg/Zr ratios for the Hawi soil may play a role in adjusting these calculations as described in Section 3.4.2 Estimating Inputs to the Soil Systems. Higher Mg/Zr ratios in parental basalts would lead to larger calculated amounts of Mg derived from basalt weathering and larger calculated amounts of Mg exported from the soil system, thereby altering the extremely heavy Mg isotopic flux from the Hawi soil to lighter values.

3.4.4. Integrating the Pololu Soil

Similar calculations for the Pololu soil allow us to compare and contrast it with the Hawi soil. Integrating Mg concentrations and δ^{26}Mg values for the Pololu soil shows that even though the soil is thicker (143 cm vs. 75cm), there is less Mg within the soil system, around 21±1 kg/m^2 Mg with an overall δ^{26}Mg of -0.12±0.12‰. Combining these data with our estimates of Mg input and resulting isotopic composition (148±13 kg/m^2, -0.33±0.22‰) yields an export flux of Mg from the Pololu soil of 127±13 kg/m^2 with δ^{26}Mg = -0.36±0.26‰ (Figure 3.6). Integrated over its development, the Pololu soil has exported Mg with a mean isotopic composition similar to basalt, unlike the Hawi soil.

3.4.5. Chronosequence

The Mg export and isotopic calculations from the Hawi and Pololu soils have interesting implications when the soils are considered as a chronosequence. There are three data points for Mg isotopic and Mg mass evolution through time: t = 0, t = 170 ka, and t = 350 ka (Figure 3.7). At t = 0 soil formation is initiated, and the soil evolves over the course of 170 ka until it reaches the state currently shown by the Hawi site, an isotopically light soil still rich in Mg that has exported isotopically heavy Mg during the course of its development. From that point forward to get to the state of the Pololu soil, isotopically light Mg would need to be exported as the Pololu soil has less negative δ^{26}Mg and is more depleted in Mg. To derive the Pololu soil from the Hawi soil requires Mg export of 118±14 kg/m^2 with mean δ^{26}Mg = -0.62±0.22‰. The mineralogy and morphology of these soils can explain these trends.

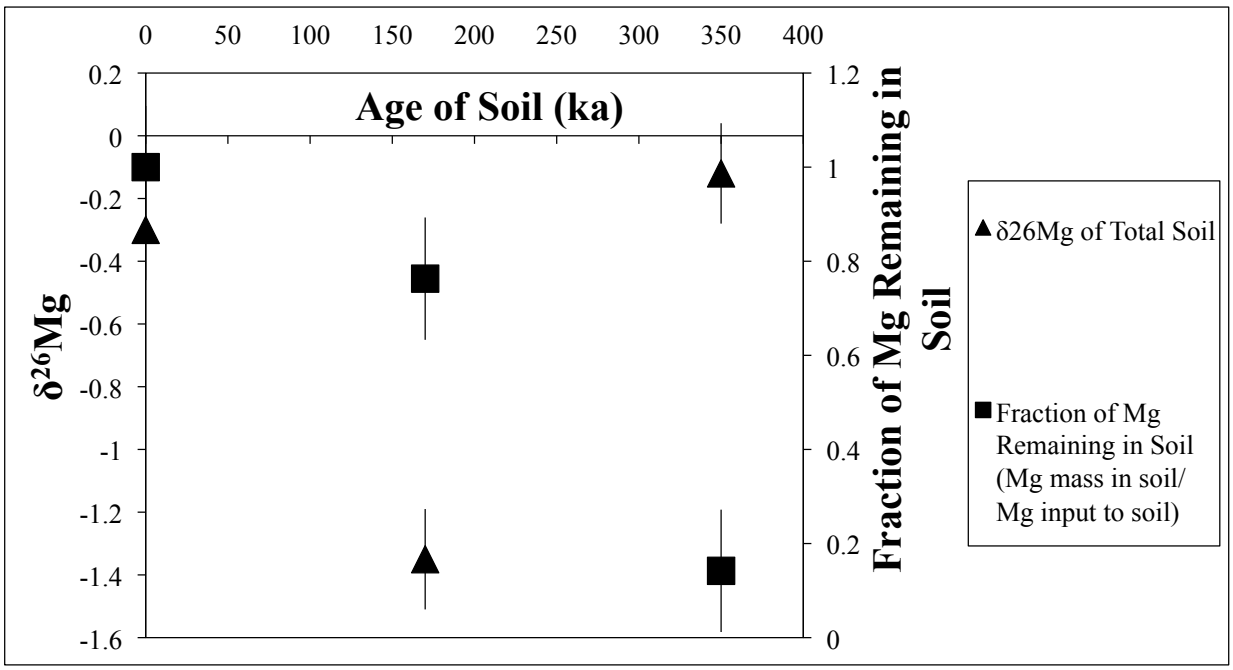

Figure 3.7: Evolution of Hawaiian soils in Mg isotopic composition and the fraction of Mg remaining within soils with time. Errors are 2σ.

3.4.6. Pedogenic Carbonates

The differences between the integrated Hawi and Pololu soils can be explained in part by the relative abundance of pedogenic carbonates in each. Pedogenic carbonates in both soils serve as an important reservoir of magnesium, influencing the magnesium budget and isotopic composition in those horizons in which they appear (Figures 3.4 and 3.5). The carbonates in the Hawi and Pololu soil, account for 69±11% and 16±2% of the total magnesium integrated over the soil profiles, respectively. As the carbonates are an isotopically light reservoir of Mg (Figure 3.3), they drive the bulk Hawi soil to isotopically light values. In the Hawi soil, the carbonates are present at a very shallow depth and dominate the Mg budget in those horizons in which they appear (Figure 3.4). In the Pololu soil, the carbonates are found only at greater depth and are less important in the budgets of Mg for the horizons in which they appear (Figure 3.5). The pedogenic carbonates play an important role in setting the overall soil isotopic composition (Figure 3.8).

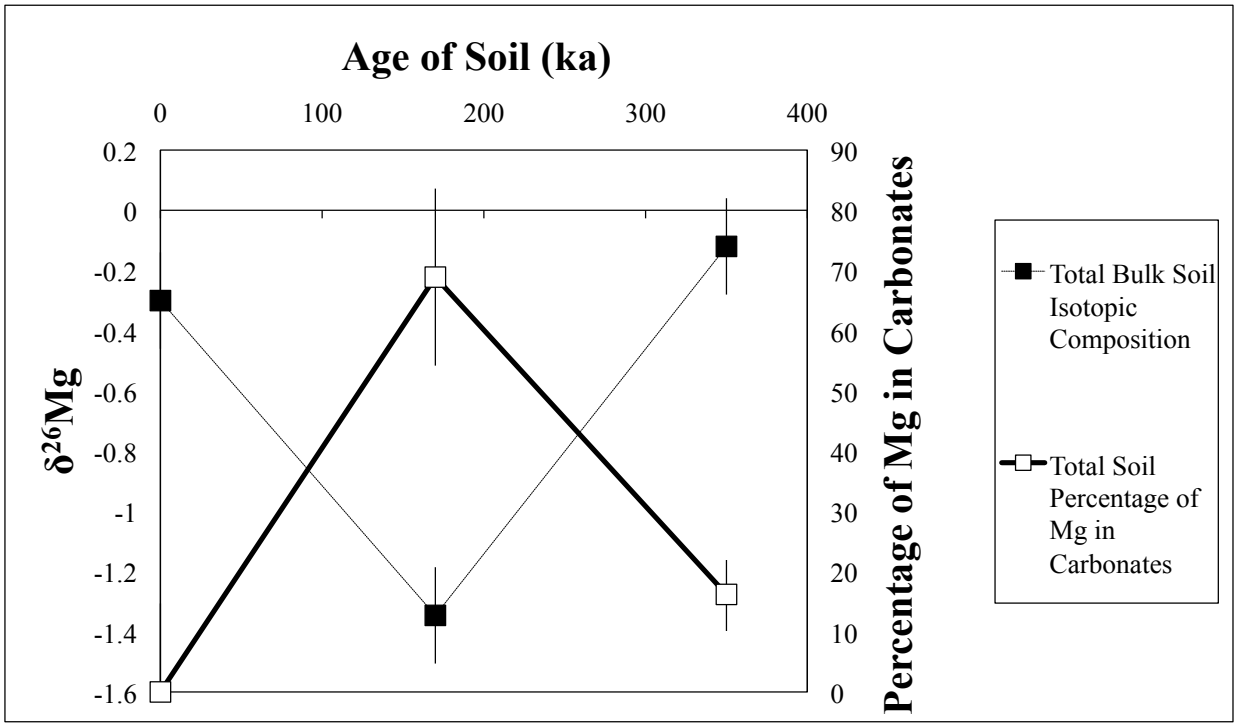

Figure 3.8: Age of soil and trends in carbonate importance in overall Mg budget and isotopic composition. Errors are 2σ.

3.4.7. Forming Pedogenic Carbonates

How carbonates are formed in these soils allows us to determine why they are of differing importance between the Hawi and Pololu soils and what this means for Mg isotopic systematics through time. The range in δ^{26}Mg of our carbonates (-1.05‰ to -2.31‰) suggests a complicated system, as do the high Mg and Sr concentrations (Tables 2.9 and 2.10 in Chapter 2). Additionally, the inability of our carbonate dissolution technique to discriminate between various generations of carbonate averages out detail that sampling on a smaller scale could provide.

Rainfall in these regions is sporadic, and carbonates form during the slow evaporation of soil porewater, as supported by stable isotope studies from Whipkey et al. (2002). This process should result in Rayleigh fractionation of Mg isotopes (Figure 3.9) and fractional crystallization for trace element chemistry. Rate of carbonate formation is important and will determine the $\Delta_{calcite\text{-}water}$ in our Rayleigh fractionation equation (Mavromatis et al. 2013). Within this system, the initial carbonates precipitated would have the lightest Mg isotopic compositions, but over time if all of the magnesium present ends up in the carbonate, no overall isotopic fractionation can actually occur for the carbonate as a whole. Using the equilibrium $\Delta_{calcite\text{-}water}$ of -3.5‰ from Mavromatis et al. (2013) and an estimate of initial soil solution δ^{26}Mg of -0.35‰, we can estimate the average amount of Mg that ends up in carbonates based on our carbonate Mg isotopic compositions if we assume the initial carbonates precipitated remain in our system. These estimates suggest that ~ 60 to 90% of the Mg in solution at the initiation of carbonate precipitation is ultimately incorporated into carbonate and that the remaining fraction of isotopically heavy fluid is exported or partitioned to another phase. At the most rapid rates (2.5 x 10^{-7} mol/m^2-s) of carbonate precipitation in experimental studies by Mavromatis et al. (2013),

and a corresponding $\Delta_{calcite\text{-}water}$ of -2‰, the range broadens to 3 to 80% of the Mg being incorporated into carbonate.

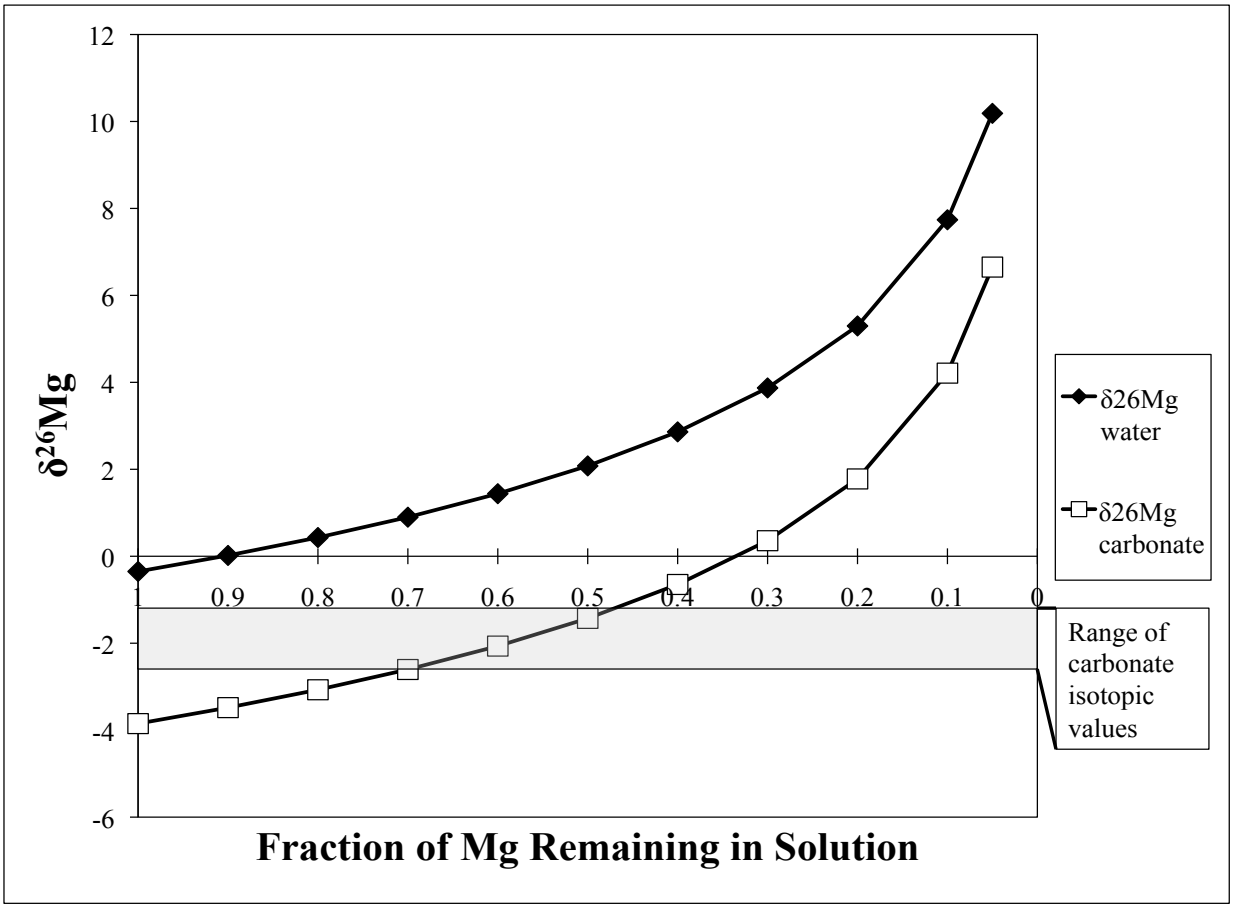

Figure 3.9: Model of Rayleigh fractionation assuming an initial solution δ^{26}Mg of -0.35‰ and calcite-water Δ of -3.5‰.

The removal Mg by subsequent rainfall events and leaching, uptake by vegetation, or the contemporaneous formation of another secondary soil mineral to act as a sink for isotopically heavy Mg, allow fractionations of δ^{26}Mg in the carbonate system to manifest. As such the variations in carbonate δ^{26}Mg can be explained as differences in flushing through the soils or availability of other secondary minerals or vegetation for Mg sinks. This hypothesis may be tested by sampling at the scale of individual carbonate generations, rather than by bulk dissolutions that average out the details of the Rayleigh fractionation occurring. Flushing through the soil system can occur because the high permeability of the basalts allows water to escape from the soil if a rainfall event overwhelms the water-holding capacity of the soil (Stearns and MacDonald 1946; Takasaki 1978).

Further convoluting this picture is evidence that the carbonates are recycled within the soil through time, often becoming more magnesian with age, even forming dolomite (Whipkey et al. 2002). However, neither depth, nor mineralogy, age, or overall carbonate content in the soil show distinctive trends with Mg isotopic composition. One interesting correlation is the high Mg:Ca ratio (1.192±0.004) in the C2 horizon of the Pololu soil along with a heavy δ^{26}Mg value (-1.08±0.08‰), which most likely results from the presence of dolomite. Even the formation of dolomite, however, is linked to the amount of flushing through the soil system, with dolomite formation only occurring when soil water is maintained in the soil for extended periods of time (Whipkey et al. 2002). Overall this suggests that the variation in carbonate δ^{26}Mg among our samples appears to be dominated by the amount of flushing through the soil system or the availability of another Mg sink within the soils to sequester isotopically heavier Mg while the carbonates are forming.

Trace element chemistry further supports that fractional crystallization, and hence Rayleigh fractionation of Mg isotopes, is taking place during the formation of carbonates in these soils. Partition coefficients for both Sr and Mg into calcite are significantly less than 1, and yet these cations make up a significant portion of the bulk carbonate (Tables 2.9 and 2.10 in Chapter 2). This can be explained using a fractional crystallization model. Partition coefficients for these elements are precipitation rate dependent, similar to $\Delta_{calcite\text{-}water}$ for Mg isotopes during Rayleigh fractionation. As we do not know precipitation rates in these systems but expect them to be rapid, we utilized the fastest experimental rates (2.5×10^{-7} mol/m^2-s) from Mavromatis et al. (2013) to determine an appropriate value for D_{Mg}, where:

$$D_{Mg} = \frac{\left(Mg/Ca\right)_{(solid)}}{\left(Mg/Ca\right)_{(fluid)}}$$

This rate gives us a partition coefficient for Mg incorporation into calcite of 0.027. Sr partition coefficients can also be found in the literature over similar precipitation rates in Tang et al. (2008), who provide a D_{Sr} value of 0.092, where D_{Sr} is analgous to D_{Mg}. Using initial solution compositions that mirror Ca:Mg and Sr:Mg ratios in basalts from the Pololu soil, we generate the model of fractional crystallization shown in Figure 3.10.

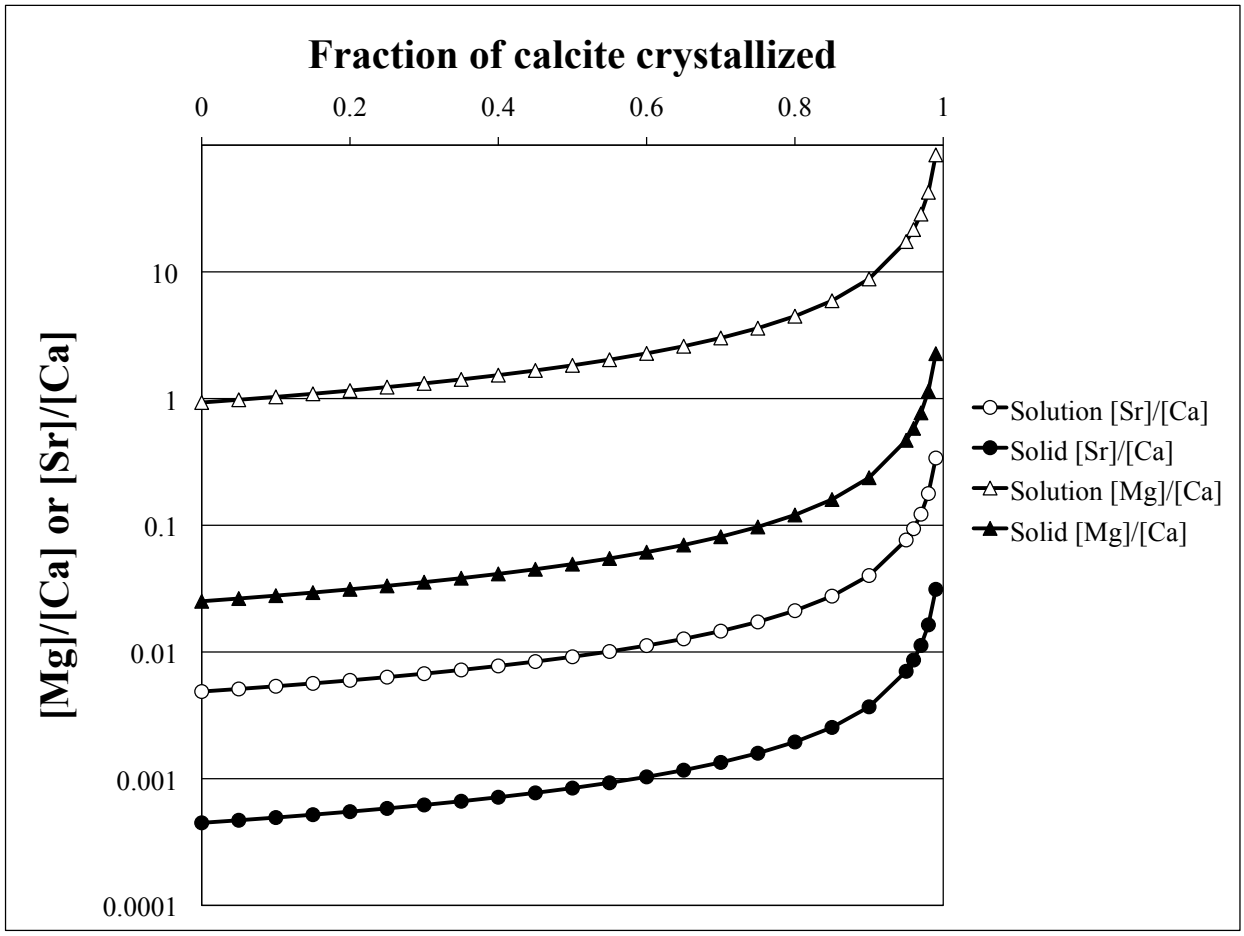

Figure 3.10: Model of fractional crystallization assuming initial solution Mg/Ca ratios and Sr/Ca ratios of Pololu basalt and rate of precipitation 2.5 x 10^{-7} mol/m^2-s.

Given these conditions for our model of fractional crystallization, Mg and Sr contents within bulk carbonate only make sense if almost all of the Mg and Sr in the initial solutions end up within calcite, and the model suggests that the final fraction of "calcite" precipitating should have a Mg:Ca ratio greater than 3. As such bulk carbonate values cannot be reproduced without the export of the initial low Mg/Ca and Sr/Ca carbonates precipitated or the addition of the precipitation of dolomite and perhaps magnesite. Although the addition of dolomite to our system makes sense given the phase has been identified in these soils, issues with our simple model may also be resolved by acknowledging a variety of flaws. The first issue is that our initial solution Mg/Ca and Sr/Ca ratios are unknown and could be highly variable given basalt-derived cations mixing with rainfall, the recycling of earlier carbonate phases, and the preferential removal of Sr and Mg with respect to Ca by secondary phases. The second issue is that rate is not well-constrained in our system, and increases in rate would serve to increase partition coefficients to higher values, making it easier to reach bulk carbonate Sr and Mg values without invoking dolomite precipitation. Associated with this issue is that the partition coefficients used for Mg and Sr into calcite are dependent upon the solution composition in the particular precipitation study, and it is highly unlikely that our soil solution happens to mirror the conditions found in Mavromatis et al. (2013) and Tang et al. (2008). The third issue is that there are difficulties with Mg incorporation into calcite and non-trace element behavior, as significant Mg incorporation alters the structure of calcite, which in turn influences partition coefficients, particularly of Sr, increasing the amount of Sr that may be incorporated into the calcite lattice (Ichikuni 1973; Carpenter and Lohmann 1992; Rimstidt et al. 1998). Given the caveats cited above, the use of Sr and Mg trace element chemistry is woefully underconstrained in trying to model fractional crystallization in these systems. However, even with these flaws in our model,

the high Mg:Ca and Sr:Ca ratios present in our bulk carbonates suggest that at some point solutions with extremely high Mg:Ca and Sr:Ca ratios must have existed in this system. The creation of these high Mg:Ca and Sr:Ca solutions given our evaporative model of carbonate formation is best explained through fractional crystallization.

3.4.8. Differences in the Soil Functioning of the Hawi and Pololu Soils

Carbonates may dominate the Hawi study site, but they take on a secondary role in the Pololu site (Figure 3.8). This difference is the result of mineralogical and morphologic changes in the soil system through time. The Hawi soil has a relatively thin surface horizon free of carbonate, dominated by kaolinite, noncrystalline silicate phases, hematite, and gibbsite (Figures 2.11, 2.12, 2.18 and Tables 2.1, 2.2 in Chapter 2). Over an additional 180 ka of development, the Pololu soil has developed thicker surficial horizons free of carbonate and dominated by the same phases as in the upper Hawi soil horizon (Figures 2.11, 2.12, 2.18 and Tables 2.1, 2.2 in Chapter 2). These thicker horizons in turn increase the water-holding capacity of the soil system, preventing flushing through the system from happening as easily and increasing the amount of time that soil water is maintained in the soil. These factors limit carbonate production while promoting formation of other secondary soil phases, such as halloysite (Zeigler et al 2003). As such, the Pololu soil has evolved to a point where the Mg budget is dominated by phases other than carbonate.

3.4.9. Other Secondary Soil Minerals

In order to understand Mg isotopic fractionation in the Pololu soil, we must understand the influence that other secondary soil minerals have on Mg budgets and isotopic fractionations. The uppermost horizons of the Hawi and Pololu soils are free of carbonates and have bulk soil

δ^{26}Mg values that reflect this. These values range from -0.01±0.31‰ to -0.21±0.31‰, suggesting that kaolinite, short-range-order phases, hematite, and gibbsite as a whole may be associated with the incorporation of isotopically heavy Mg, as these values are heavier than mixing between basalt weathering and precipitation would allow. This observation suggests that the weathering products of these upper horizons follow previously reported ideas of how Mg isotopic fractionation during weathering works, with isotopically heavier Mg sequestered into weathering products and isotopically lighter Mg released to solution. Because each individual soil horizon is somewhat different in the relative abundance of each of the weathering products, and yet they are all statistically indistinguishable in isotopic composition, the particular silicate weathering product phase that the Mg is incorporated into may not be too important, and fractionations around the same magnitude may occur for entire groups of phases. The surficial horizons are strongly depleted in Mg overall, as can be seen in the soil depletion index plots for the soils (Figures 2.11 and 2.12 in Chapter 2). It is only after a sufficiently thick layer of these horizons forms, as in the Pololu soil, that the non-carbonate minerals dominate the soil Mg budget. Further evidence for these minerals as a sink for isotopically heavy Mg can be seen in the mass and isotopic balances for individual horizons in the Hawi and Pololu soils (Figures 3.4 and 3.5). In those horizons where carbonates occur, the bulk soil is often isotopically heavier than carbonate values, implying that a significant isotopically heavy reservoir of non-carbonate secondary soil minerals must exist. For example, balancing the C2 horizon in the Pololu soil requires the presence of a non-carbonate soil reservoir with a δ^{26}Mg of -0.07±0.28‰ (Figure 3.5).

3.4.10. Vegetation

Vegetation can play an important role in the translocation of elements throughout the soil profile, enriching surface horizons in biologically essential elements and depleting those elements at depth. We see this enrichment effect with K in both the Hawi and Pololu soils (Table 2.6 in Chapter 2). Recent studies show that the export of elements such as Ca, Sr, and Ba and resulting elemental isotopic compositions are influenced by biological uptake into plants combined with aeolian erosion at the Hawi study site (Vitousek and Chadwick 2013; Bullen and Chadwick, in press). Uptake of Mg by biota and subsequent aeolian removal should result in the preferential enrichment in isotopically light Mg, as Mg in vegetation removed at these sites is isotopically heavy. However, if this phenomenon were dominating Mg export at our study sites through time, the Pololu soil should be isotopically lighter than the Hawi soil. This mechanism does not appear to be a major influence on the Mg system, as more Mg is retained in the soil over time than either Ca or Sr (Figure 2.12 in Chapter 2), causing secondary mineral formation and export via leaching to dominate Mg isotopic fractionation over biotic uptake and aeolian removal.

3.5. CONCLUSIONS

The Hawi and Pololu soils illustrate how Mg isotopes are fractionated during arid basalt weathering overall and how Mg isotopes can be used within soil systems. The prevailing view of weathering and Mg isotopic fractionation appears to be validated, in that isotopically light Mg is exported to streamwaters and isotopically heavy Mg is sequestered in soils, if the weathering products exclude carbonates. The formation of pedogenic carbonates, which, like their oceanic counterparts, are associated with incorporation of isotopically light Mg, complicates this picture

greatly. The carbonates themselves have a wide range of isotopic compositions, which appears to be influenced by the ability of a soil to have a sink or export mechanism for isotopically heavy Mg left in solution after carbonates begin to precipitate. We have also shown that the influence of these carbonates varies over the lifetime of the soils, from being the dominant influence on the export of Mg to being a secondary pool that influences individual horizons. This variation is the result of the mineralogic and morphologic development of the soil through time, which in turn influences soil characteristics such as water-holding capacity and rates of secondary mineral formation and recrystallization. Importantly, as soil systems evolve through time, so can the isotopic composition of the Mg exported.

WORKS CITED

Bizzarro, M., Paton, C., Larsen, K., Schiller, M., Trinquier, A., Ulfbeck, D., 2011. High-precision Mg-isotope measurements of terrestrial and extraterrestrial material by HRMCICPMS – implications for the relative and absolute Mg-isotope composition of the bulk silicate Earth. Journal of Analytical Atomic Spectrometry, 26: 565-577.

Black, J.R., Epstein, E., Rains, W.D., Yin, Q.Z. and Casey, W.H., 2008. Magnesium-isotope Fractionation During Plant Growth. Environmental Science & Technology, 42(21): 7831-7836.

Blank, M., Leinen, M., Prospero, J.M., 1985. Major Asian eolian dust inputs indicated by the mineralogy of aerosols and sediments in the western North Pacific. Nature 314: 84-86.

Bolou Bi, E.B., Poszwa, A., Leyval, C., Vigier, N., 2010. Experimental determination of magnesium isotope fractionation during higher plant growth. Geochimica et Cosmochimica Acta, 74: 2523-2573.

Bolou Bi, E.B., Vigier, N., Brenot, A. and Poszwa, A., 2009. Magnesium isotope compositions of natural reference materials. Geostandards and Geoanalytical Research, 33(1): 95-109.

Bolou Bi, E.B., Vigier, N., Poszwa, A., Boudot, J.P., Dambrine, E., 2012. Effects of biogeochemical processes on magnesium isotope variations in a forested catchment in the Vosges Mountains (France). Geochimica et Cosmochimica Acta, 87: 341-355.

Brenot, A., Cloquet, C., Vigier, N., Carignan, J. and France-Lanord, C., 2008. Magnesium isotope systematics of the lithologically varied Moselle river basin, France. Geochimica et Cosmochimica Acta, 72(20): 5070-5089.

Bullen, T., and Chadwick, O., in press. Ca-Sr-Ba stable isotope systematics of a soil climosequence: a new window onto leaching and biotic uplift as pedogenic processes. Geology.

Carpenter S. J. and Lohmann K. C. (1992) Sr/Mg ratios of modern marine calcite: Empirical indicators of ocean chemistry and precipitation rate. Geochim. Cosmochim. Acta 56, 1837–1849.

Carrillo, J.H., Hastings, M.G., Sigman, D.M. and Huebert, B.J., 2002. Atmospheric deposition of inorganic and organic nitrogen and base cations in Hawaii. Global Biogeochemical Cycles, 16(4): 1076 doi:10.1029/2002GB001892.

Chang, V.T.C., Makishima, A., Belshaw, N.S. and O'Nions, R.K., 2003. Purification of Mg from low-Mg biogenic carbonates for isotope ratio determination using multiple collector ICPMS. Journal of Analytical Atomic Spectrometry, 18(4): 296-301.

Chang, V.T.C., Williams, R.J.P., Makishima, A., Belshawl, N.S. and O'Nions, R.K., 2004. Mg and Ca isotope fractionation during CaCO3 biomineralisation. Biochemical and Biophysical Research Communications, 323(1): 79-85.

Chadwick, O. A., Gavenda, R. T., Kelly, E. F., Ziegler, K., Olson C. G., Elliot, W. C., Hendricks D. M. (2003) The impact of climate on the biogeochemical functioning of volcanic soils. Chemical Geology, 202: 195-223.

Galy, A., Belshaw, N.S., Halicz, L. and O'Nions, R.K., 2001. High-precision measurement of magnesium isotopes by multiple-collector inductively coupled plasma mass spectrometry. International Journal of Mass Spectrometry, 208(1-3): 89-98.

Huang, K.J., Teng, F.Z., Wei, G.J., Ma, J.L., Bao, Z.Y., 2012. Adsorption- and desorption-controlled magnesium isotope fractionation during extreme weathering of basalt in Hainan Island, China. Earth and Planetary Science Letters 359-360: 73-83.

Ichikuni M. (1973) Partition of strontium between calcite and solution: Effect of substitution by manganese. Chem. Geol. 11: 315–319.

Jackson, M.L., Levelt, T.W.M., Syers, J.K., Rex, R.W., Clayton, R.N., Sherman, G.D., Uehara, G., 1971. Geomorphological relationships of tropospherically derived quartz in the soils of the Hawaiian Islands. Soil Science Society of America Proceedings 35: 515-525.

Kurtz, A.C., Derry, L.A. and Chadwick, O.A., 2001. Accretion of Asian dust to Hawaiian soils: Isotopic, elemental, and mineral mass balance. Geochimica et Cosmochica Acta, 65: 1971– 1983.

Leinen, M., Prospero, J.M., Arnold E., and Blank M., 1994. Mineralogy of aeolian dust reaching the North Pacific Ocean. 1. Sampling and analysis. Journal of Geophysical Research 94D: 8584-8598.

Mavromatis, V., Gautier, Q., Bosc, O., Schott, J., 2013. Kinetics of Mg partition and Mg stable isotope fractionation during its incorporation in calcite. Geochimica et Cosmochimica Acta, 114: 188-203.

Opfergelt, S., Georg, R.B., Delvaux, B., Cabidoche, Y.-M., Burton, K.W., Halliday, A.N., 2012. Mechanisms of magnesium isotope fractionation in volcanic soil weathering sequences, Guadeloupe. Earth and Planetary Science Letters, 341- 344: 176-185.

Opfergelt, S., Burton, K.W., Georg R.B., West, A.J., Guicharnaud, R.A., Sigfusson, B., Siebert, C., Gislason, S.R., Halliday, A.N., 2014. Magnesium retention on the soil exchange complex controlling Mg isotope variations in soils, soil solutions and vegetation in volcanic soils, Iceland. Geochimica et Cosmochimica Acta, 125: 110-130.

Pogge von Strandmann, P.A.E. et al., 2008. The influence of weathering processes on riverine magnesium isotopes in a basaltic terrain. Earth and Planetary Science Letters, 276: 187–197.

Rimstidt, J.D., Balog, A., Webb, J., 1998. Distribution of trace elements between carbonate minerals and aqueous solutions. Geochimica et Cosmochimica Acta, 62(11): 1851-1863.

Rose-Koga, E.F. and Albarede, F., 2010. A data brief on magnesium isotope compositions of marine calcareous sediments and ferromanganese nodules. Geochemistry, Geophysics, Geosystems, 11(3): 1-12.

Ryu, J.S., Jacobson, A.D., Holmden, C., Lundstrom C., Zhang, Z., 2011. The major ion, $\delta^{44/40}$Ca, $\delta^{44/42}$Ca, and $\delta^{26/24}$Mg geochemistry of granite weathering at pH = 1 and T = 25 _C: power-law processes and the relative reactivity of minerals. Geochimica et Cosmochimica Acta, 75: 6004-6026.

Saulnier, S., Rollion Bard, C., Vigier, N., Chaussidon, M., 2012. Mg isotope fractionation during calcite precipitation: An experimental study. Geochimica et Cosmochimica Acta, 91: 75-91.

Stearns, H.T. and Macdonald, G.A., 1946. Geology and Ground-water Resources of the Island of Hawaii. Bulletin of the Division of Hydrography, 9.

Takasaki, K.J., 1978. Summary appraisals of the nation's groundwater resources – Hawaii Region. Geological Survey Professional Paper, 813-M.

Tang, J., Kohler, S.J., Dietzel, M., 2008, Sr^{2+}/Ca^{2+} and $^{44}Ca/^{40}Ca$ fractionation during inorganic calcite formation: I. Sr incorporation. Geochimica et Cosmochimica Acta 72: 3718-3732.

Teng, F-Z., Li, W-Y., Ke, S., Marty, B., Dauphas, N., Huang, S., Wu, F-Y., Pourmand, A., 2010. Magnesium isotopic composition of the Earth and chondrites. Geochimica et Cosmochimica Acta, 74: 4150-4166.

Tipper, E.T., Galy, A. and Bickle, M.J., 2006. Riverine evidence for a fractionated reservoir of Ca and Mg on the continents: Implications for the oceanic Ca cycle. Earth and Planetary Science Letters, 247(3-4): 267-279.

Tipper, E.T., Gaillardet, J., Louvat, P., Capmas, F., White, A.F., 2010. Mg isotope constraints on soil pore-fluid chemistry: Evidence from Santa Cruz, California. Geochimica et Cosmochimica Acta, 74: 3883-3896.

Vitousek P.M., and Chadwick, O.A., 2013. Pedogenic thresholds and soil process domains in basalt-derived soils. Ecosystems. DOI: 10.1007/s10021-013-9690-z.

Wimpenny, J., Gislason, S.R., James, R.H., Gannoun, A., Pogge von Strandmann, P.A.E, Burton, K.W., 2010. The behavior of Li and Mg isotopes during primary phase dissolution and secondary mineral formation in basalt. Geochimica et Cosmochimica Acta, 74: 5259-5279.

Wimpenny, J., Colla, C.A., Yin, Q.Z., Rustad, J.R., Casey, W.H., 2014. Investigating the behaviour of Mg isotopes during the formation of clay minerals. Geochimica et Cosmochimica Acta, 128: 178-194.

Whipkey, C.E., Capo, R.C., Hsieh, J.C.C. and Chadwick, O.A., 2002. Development of magnesian carbonates in Quaternary soils on the island of Hawaii. Journal of Sedimentary Research,72(1): 158-165.

White, W., in press. Isotope Geochemistry. *Chapter 11 Unconventional Isotopes and Approaches*. Wiley-Blackwell.

Young, E.D. and Galy, A., 2004. The isotope geochemistry and cosmochemistry of magnesium. In: C.M. Johnson, B.L. Beard and F. Albarede (Editors), Geochemistry of Non-Traditional Stable Isotopes. Reviews in Mineralogy & Geochemistry: 197-230.

Ziegler, K., Hsieh J.C.C., Chadwick, O.A., Kelly E.F., Hendricks, D.M., Savin, S.M., 2003. Halloysite as a kinetically controlled end product of arid-zone basalt weathering. Chemical Geology, 202: 461-478.

CHAPTER 4

MAGNESIUM ISOTOPIC COMPOSITIONS OF SEQUENTIAL EXTRACTION FRACTIONS FROM TWO ARID HAWAIIAN (USA) SOILS

Abstract

This study uses a sequential extraction technique to investigate the Mg isotopic compositions of soil phases in an arid soil chronosequence on the Island of Hawaii. This procedure breaks soils into seven fractions: adsorbed cations, SOM, carbonates, short-range-order phases, sesquioxides, kaolin group minerals, and residuum. The most interesting sequential extraction fractions in the <2-mm portions of these soils are the adsorbed cations, short-range-order phases, and residuum phases.

Adsorbed cations have an average δ^{26}Mg value of -1.05±0.06‰ when looking at soil horizons not influenced by carbonate. The adsorbed cations are isotopically lighter than precipitation and the only reservoir of isotopically light Mg in soil horizons lacking carbonate. The ephemeral nature of this fraction also suggests that both soils are exporting isotopically light Mg. The short-range-order phases in both soils are near the Mg isotopic composition of basalt (Hawi soil average δ^{26}Mg -0.30±0.12‰) or isotopically heavier than basalts (Pololu soil average δ^{26}Mg 0.00±0.08‰), suggesting preferential incorporation of heavy Mg during the formation of short-range-order phases. This fraction also dominates the distribution of Mg in these <2-mm soil fractions. The residuum phases contained significant amounts of Mg and were one of the most variable sequential extraction fractions, displaying isotopic differences with depth and between soils. This variability suggests complex behavior that may be associated with the complex variety of phases that make up this fraction. Looking at all the sequential extraction fractions shows that only the adsorbed cations and carbonates are isotopically lighter than

precipitation in our soil systems, with all other fractions isotopically similar to or isotopically heavier than basalts. This shows that the formation of secondary silicate and oxide weathering phases is associated with the incorporation of isotopically heavy Mg, leading to the export of isotopically light Mg from the <2-mm portions these systems.

4.1. INTRODUCTION

As described in Chapter 3 (3.1. Introduction), Mg isotopes can be a useful tool in understanding ecosystem-scale Mg cycling and may eventually be useful in understanding large-scale continental weathering. However, previous work with Mg isotopes has focused on larger-scale issues with analyses of bulk soils or sediments, waters and rocks. Over time studies have incorporated finer detail analyses focusing on clay fractions and exchangeable cations (Opfergelt et al. 2012; Wimpenny et al. 2014; Opfergelt et al. 2014), but no study has yet attempted to understand the distribution of Mg and partitioning of Mg isotopes throughout a soil profile by a detailed sequential extraction technique. This study characterizes the magnesium isotopic compositions of soil mineralogical fractions from the sequential extraction technique described in Chapter 2 (2.3.6. Soil Sequential Extractions). This method allows us to understand the roles that mineralogy and secondary mineral formation play in magnesium isotope fractionation in unprecedented detail.

The prevailing understanding of how Mg isotopes are fractionated during weathering suggests that isotopically light Mg is released to streamwaters during the weathering of parent materials, and the remaining pool of isotopically heavy Mg is stored in soils or plants (Tipper et al. 2006; Brenot et al. 2008). We have shown in Chapter 3 that this is not necessarily the case in all weathering environments and that in our arid Hawaiian soil system, the evolution of the

functioning of the soil and soil mineralogy can lead to changes in the isotopic composition of the Mg exported over time. This observation highlights the importance of analyzing individual reservoirs of Mg within soil, to determine under which suites of secondary soil phases the "isotopically light Mg to water, isotopically heavy Mg to soil and plants" gestalt of Mg isotope fractionation should hold. Further, by looking at soil phase Mg contents and δ^{26}Mg values, the level of detail in ecosystem-scale Mg cycling is enriched.

4.1.1 Study Sites

The Kohala chronosequence (Hawi and Pololu) soil study sites are reviewed in Chapter 2 (2.1.3. Soil Sites).

4.2. METHODS

4.2.1. Soil Sampling

The methods behind soil and rock sampling, bulk soil and rock dissolutions, individual carbonate dissolutions, vegetation dissolutions, and sequential extractions may all be found in Chapter 2 (2.3. Methods).

4.2.2. Isotopic Analysis

Descriptions of the isotopic analysis of samples may be found in Chapter 3 (3.2.2. Isotopic Analysis). One additional ion exchange chemistry step was used for the treatment of the sesquioxide sequential extraction fractions prior to isotopic analysis. Due to the high concentrations of Na in the extraction supernatant, an additional pretreatment ion exchange column was used to separate Na from the sample. This ion exchange column consisted of 25 ml of Dowex AG 50W X12 cation exchange resin (10x the exchange capacity of the columns used

in Bolou Bi et al. (2009)). Samples were introduced in 10 ml of 0.5 M HCl and eluted from the columns with 70 ml of 6 N HCl, after 300 ml of 0.5 M HCl was used to separate Na.

4.3. RESULTS

4.3.1. Isotope Overview, Standards, and Blanks

All magnesium isotope data are presented in Table 4.1 as δ^{26}Mg and δ^{25}Mg relative to DSM3. Figure 4.1 illustrates a three-isotope plot with all of our collected data, but only δ^{26}Mg values are shown in subsequent figures as all samples fall near the terrestrial equilibrium mass fractionation line (our slope=0.517; terrestrial equilibrium mass fractionation line slope=0.521 from Young and Galy (2004)). Although standard deviations were calculated for each magnesium isotopic value, one sample (HI-06-45) was run every time (n=21) isotopic analyses were conducted, to monitor long-term instrumental variability. The data in Figure 4.1 are all plotted with 2σ error values for this sample, which is 0.22‰ for δ^{26}Mg and 0.12‰ for δ^{25}Mg. Basalt standards BHVO-2 and BE-N yielded mean δ^{26}Mg values of -0.21±0.14‰ (-0.19±0.05‰, Bizzaro et al. 2011) and -0.33±0.22‰ (-0.28±0.08‰, Bolou Bi et al. 2009), respectively over this period of time. These standards were processed with each new batch of samples to ensure adequate ion exchange chemistry. Procedural blanks were processed with each batch of ion exchange chemistry and varied from 3 ng to 52 ng of Mg, which is insignificant compared to the 50 μg of Mg passed through the exchange columns during purification.

Table 4.1: Overview of Mg isotope data. SE is the standard error of the mean.

Sample or Standard	$\delta^{26}Mg$	$\delta^{25}Mg$	n	SE on $\delta^{26}Mg$
Soil Bulk Dissolutions				
Hawi				
KT 9-1 B	-0.14	-0.07	2	0.01
KT 9-2 B	-1.35	-0.70	1	
Pololu				
KT 7-1 B	-0.33	-0.18	1	
KT 7-2 B	-0.12	-0.07	1	
KT 7-3 B	0.05	0.04	2	0.10
KT 7-5 B	-0.35	-0.16	2	0.07
KT 7-6 B	-0.28	-0.14	3	0.08
Individual Carbonates				
Hawi				
KT 8-6 C	-1.05	-0.56	4	0.08
KT 9-2 C	-1.50	-0.77	6	0.05
KT 9-2 PCD	-2.06	-1.07	2	0.01
Pololu				
KT 7-5 C	-1.81	-0.95	5	0.04
KT 7-6 C	-2.31	-1.20	5	0.04
KT 7-5 PCD	-1.89	-0.99	2	0.01
KT 7-6 PCD	-1.99	-1.05	3	0.02
Basalts				
Hawi				
KT 8-7 R	-0.18	-0.08	2	0.06
KT 9-5 R	-0.21	-0.11	2	0.02
Pololu				
KT 7-8 R	-0.30	-0.15	1	
KT 7-9 R	-0.31	-0.16	2	0.10
Other Hawaiian basalts				
KT 1 R	-0.23	-0.14	6	0.04
KT 4 R	-0.17	-0.11	2	0.06
KT 11-11 R	-0.16	-0.07	1	
Exchangeable Cations				
Hawi				
KT 9-1 A	-1.17	-0.62	6	0.03
KT 9-2 A	-1.15	-0.61	3	0.10
Pololu				
KT 7-1 A	-1.02	-0.55	5	0.06
KT 7-2 A	-1.04	-0.58	4	0.06
KT 7-3 A	-1.00	-0.54	4	0.09
KT 7-5 A	-1.27	-0.66	5	0.04
KT 7-6 A	-1.24	-0.67	4	0.07

Table 4.1 (Continued)

Sample or Standard	$\delta^{26}Mg$	$\delta^{25}Mg$	n	SE on $\delta^{26}Mg$
Soil Organic Matter (SOM)				
Hawi				
KT 9-1 SOM	0.41	0.20	1	
KT 9-2 SOM	-1.66	-0.86	2	0.05
Pololu				
KT 7-1 SOM	-0.12	-0.06	1	
KT 7-2 SOM	0.04	0.02	1	
KT 7-3 SOM	-0.08	-0.04	1	
KT 7-5 SOM	-1.32	-0.70	1	
KT 7-6 SOM	-1.55	-0.79	1	
Short-Range-Order Phases (SRO)				
Hawi				
KT 9-1 SRO	-0.21	-0.12	3	0.07
KT 9-2 SRO	-0.38	-0.22	2	0.01
Pololu				
KT 7-1 SRO	-0.06	-0.05	2	0.03
KT 7-2 SRO	-0.06	-0.03	2	0.07
KT 7-3 SRO	0.14	0.06	2	0.01
KT 7-5 SRO	-0.02	-0.02	3	0.03
KT 7-6 SRO	0.02	-0.01	3	0.01
Sesquioxides				
Hawi				
KT 9-1 Ox	-0.39	-0.21	3	0.11
KT 9-2 Ox	-0.45	-0.24	5	0.11
Pololu				
KT 7-1 Ox	-0.29	-0.17	3	0.04
KT 7-2 Ox	-0.02	-0.03	4	0.08
KT 7-3 Ox	-0.21	-0.13	6	0.06
KT 7-5 Ox	-0.39	-0.20	5	0.02
KT 7-6 Ox	-0.32	-0.18	4	0.14
Residuum				
Hawi				
KT 9-1 F	-0.13	-0.09	5	0.04
KT 9-2 F	-0.15	-0.08	6	0.11
Pololu				
KT 7-1 F	0.05	0.04	6	0.09
KT 7-2 F	0.12	0.05	6	0.06
KT 7-3 F	0.74	0.36	5	0.09
KT 7-5 F	0.62	0.31	6	0.05
KT 7-6 F	0.57	0.28	5	0.08

Table 4.1 (Continued)

Sample or Standard	$\delta^{26}Mg$	$\delta^{25}Mg$	n	SE on $\delta^{26}Mg$
Vegetation				
Hawi				
B1	0.10	0.05	8	0.06
Pololu				
P2	-0.22	-0.11	12	0.04
Other Hawaiian vegetation				
AUW1	-0.07	-0.04	12	0.04
AUW2	-0.09	-0.03	10	0.02
Standards				
Instrumental Reproducibility Sample				
HI-06-45	-0.46	-0.24	21	0.02
Reference Materials				
CRPG SRM980	-4.00	-2.06	8	0.04
CRPG SRM980b	-4.08	-2.08	4	0.08
Column Processed Rock Standards				
BHVO-2	-0.21	-0.12	15	0.02
BEN	-0.33	-0.16	9	0.02
BEN	-0.31	-0.18	5	0.08

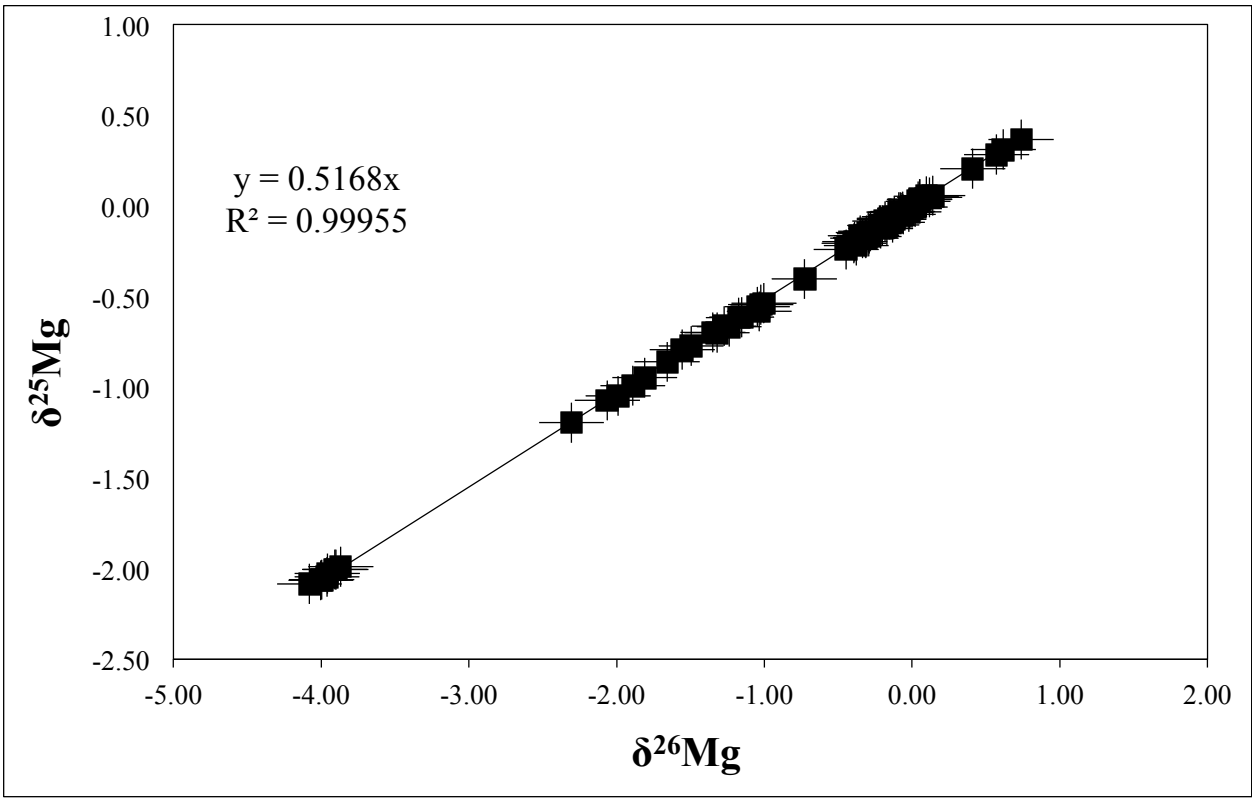

Figure 4.1: Three-isotope plot of all Mg data. All data fall on the terrestrial mass fractionation line.

4.3.2. Parent Material and Precipitation

Data for the bulk chemistry of basalt dissolutions are presented in Tables 2.3 and 2.4 from Chapter 2 (2.4.2. Parent Material and Precipitation). Chapter 3 (3.3.2. Parent Material and Precipitation) describes the Mg isotopic compositions of basalts and rainfall. These δ^{26}Mg values are also shown in Figure 4.2, which displays the δ^{26}Mg values for all analyzed samples broken into categories by sample type.

4.3.3. Individual Carbonate Extraction

Data for the chemistry of the individual carbonate dissolutions are presented in Tables 2.9 and 2.10 of Chapter 2 (2.4.4. Individual Carbonate Extraction). The δ^{26}Mg values of these carbonates are discussed in Chapter 3 (3.3.3. Soil Carbonates), and Mg isotopic values relevant to this study are displayed in Figure 4.2.

4.3.4. Vegetation

Chemistry values for the vegetation dissolutions are presented in Tables 2.11 and 2.12 in Chapter 2 (2.4.5. Vegetation). The δ^{26}Mg values of these dissolutions are discussed in Chapter 3 (3.3.4. Vegetation) and presented again in Figure 4.2.

4.3.5. Bulk Soil Samples

Data for the chemistry of the <2-mm bulk soil samples are shown in Tables 2.5 and 2.6 in Chapter 2 (2.4.3. Bulk Soil Samples). Data for the Mg isotopic composition of the <2-mm soil fractions may be found in Table 3.2 in Chapter 3 (3.3.5. Bulk Soil Samples). These δ^{26}Mg values are presented in Figure 4.2.

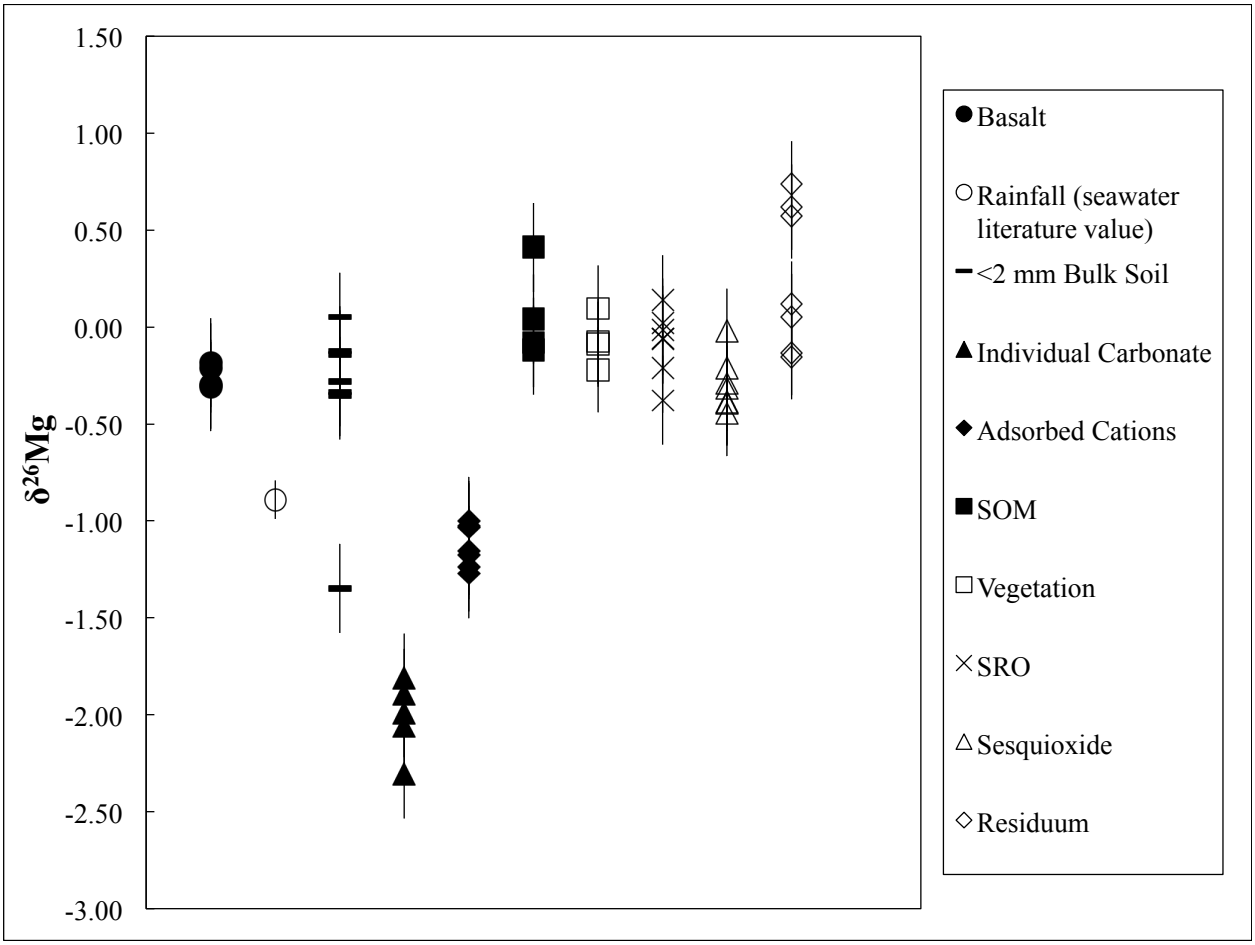

Figure 4.2: Overview of Mg isotope data for <2-mm bulk soils, carbonates, sequential extraction fractions, vegetation, basaltic parent materials, and estimated rainfall. SOM δ^{26}Mg values exclude fractions contaminated by carbonate. Errors shown are 2σ.

4.3.6. Sequential Extraction

4.3.6.1. Adsorbed Cations

Data for the chemistry of the adsorbed cations by soil horizon are described in Chapter 2 (2.4.6.1. Adsorbed Cations). Mg isotopic data for this sequential extraction fraction by soil horizon is presented in Table 4.2. Mg/Ca and Sr/Ca ratios of this sequential extraction fraction suggest that the extraction inadvertently dissolved some carbonate in those horizons that contain carbonate. Looking at the δ^{26}Mg values of the adsorbed cations in the lowest horizon of the Pololu soil further supports the idea that reactive calcite was dissolved, as these values are the isotopically lightest δ^{26}Mg values for the adsorbed Pololu cations. Even with this carbonate influence in the lowest portions of both soils, the δ^{26}Mg of all the adsorbed cation fractions is consistent with depth and between soils, only ranging from -1.00±0.17‰ to -1.27±0.09‰. Excluding horizons with carbonate influence from both soils, the unweighted average Mg isotopic composition of adsorbed Mg is -1.05±0.06‰.

Table 4.2: The Mg isotopic compositions of sequential extraction fractions and the <2-mm bulk soil by horizon in the Hawi (170 ka) and Pololu (350 ka) soils. Kaolin fractions were not measured for δ^{26}Mg due to low Mg contents, and carbonate δ^{26}Mg values are shown as the bulk individual carbonate dissolutions. Errors shown are 1 standard error.

Soil Horizon	Depth to Horizon (cm)	<2-mm Bulk Soil	Adsorbed Cations	SOM	Carbonate	SRO	Sesquioxide	Residuum
Pololu (350 ka)		**δ^{26}Mg**						
A	0-25	-0.33	-1.02±0.06	-0.12	--	-0.06±0.03	-0.29±0.04	0.05±0.09
Bw1	25-41	-0.12	-1.04±0.06	0.04	--	-0.06±0.07	-0.02±0.08	0.12±0.06
Bw2	41-57	0.05±0.10	-1.00±0.09	-0.08	--	0.14±0.01	-0.21±0.06	0.74±0.09
C1	57-106	-0.35±0.07	-1.27±0.04	-1.32	-1.89±0.01	-0.02±0.03	-0.39±0.02	0.62±0.05
	57-106 (subset)	-0.28±0.08	-1.24±0.07	-1.55	-1.99±0.02	0.02±0.01	-0.32±0.14	0.57±0.08
Hawi (170 ka)		**δ^{26}Mg**						
A	0-12	-0.14±0.01	-1.17±0.03	0.41	--	-0.21±0.07	-0.39±0.11	-0.13±0.04
	12-13	-1.35	-1.15±0.10	-1.66±0.05	-2.06±0.01	-0.38±0.01	-0.45±0.11	-0.15±0.11

4.3.6.2. SOM

The chemistry data of the SOM fractions by soil horizon are presented in Chapter 2 (2.4.6.2. SOM). Mg isotopic data for this sequential extraction fraction by soil horizon are shown in Table 4.2. The δ^{26}Mg values of the SOM fractions appear to be isotopically homogeneous with depth, until reaching soil horizons with carbonate, where the δ^{26}Mg values shift toward lighter values. As with the adsorbed cation sequential extraction fraction, Mg/Ca and Sr/Ca ratios, along with this shift in Mg isotopic composition, suggest contamination of the SOM sequential extraction fraction with carbonate in those soil horizons that contain carbonate. Uncontaminated isotopic values for the SOM fractions have an unweighted average δ^{26}Mg of -0.05±0.08‰ for the Pololu soil with a range of 0.04‰ to -0.12‰. The only uncontaminated value for the Hawi soil comes from the uppermost horizon and is 0.41‰.

4.3.6.3. Sequential Carbonates

The chemical analyses of the sequential carbonate dissolution are presented in Chapter 2 (2.4.6.3. Sequential Carbonates). Isotopic analyses were not conducted on these carbonate extractions, as the removal of carbonate during earlier adsorbed cation and SOM extractions could bias δ^{26}Mg values for carbonates by preferentially removing more reactive carbonate. As such the individual bulk soil carbonate dissolutions are a better representation of carbonate Mg isotopic values in these systems. Furthermore, analyses of adsorbed cation fractions and SOM extraction fractions contaminated by carbonates illustrate that the carbonate removed during those steps was isotopically light, similar to carbonate δ^{26}Mg values of the individual carbonate extraction.

4.3.6.4. SRO Phases

The chemistry data for the short-range-order phase extraction are in Chapter 2 (2.4.6.4. SRO Phases). Mg isotopic data for this sequential extraction fraction by soil horizon are presented in Table 4.2. Isotopically, the SRO phases are homogenous with depth, but there is a slight difference between the Hawi and Pololu soils. The Pololu fractions range from 0.14±0.01‰ to -0.06±0.09‰, with an unweighted average value of 0.00±0.08‰. The Hawi values range from -0.21±0.11‰ to -0.38±0.01‰ with an unweighted average value of -0.30±0.12‰.

4.3.6.5. Sesquioxides

Sesquioxide fraction chemistry data are in Chapter 2 (2.4.6.5. Sesquioxides). Mg isotopic data for this sequential extraction fraction by soil horizon are shown in Table 4.2. In terms of isotopic composition the extraction is consistent with depth and between soils, only ranging between -0.02±0.15‰ and -0.45±0.25‰. Unfortunately, these samples were less reproducible than others due to their complicated chemistry. An unweighted average isotopic composition for this extraction is -0.30±0.14‰.

4.3.6.6. Kaolin Group Minerals

Chapter 2 (2.4.6.6. Kaolin Group Minerals) shows the chemical analysis of the kaolin group mineral sequential extraction. The large amount of Na used in the sequential extraction technique, as well as the small amount of Mg liberated from these phases, prevented analyzing this fraction for δ^{26}Mg.

4.3.6.7. Residuum

The chemistry data of the residuum fractions are presented in Chapter 2 (2.4.6.7. Residuum). Mg isotopic data for this sequential extraction fraction by soil horizon are shown in Table 4.2. The δ^{26}Mg values for this extraction show variability with depth and between the Hawi and Pololu soils. Unfortunately these samples were less reproducible than others due to their complicated chemistry, and so they have larger 1σ uncertainties. The Pololu soil ranges from 0.05±0.22‰ to 0.74±0.20‰ with isotopically heavier values deeper within the soil. The Hawi soil has lighter isotopic values for both horizons, averaging -0.14±0.02‰.

4.3.6.8. Sequential Extraction Totals

Chapter 2 (2.4.6.8. Sequential Extraction Totals) shows total sequential extraction chemistry values for analyzed elements by summing the concentrations of each element over all sequential extraction fractions. We can do this summation with Mg concentrations and δ^{26}Mg values to create a weighted total δ^{26}Mg value. This calculation allows us to see if the weighted δ^{26}Mg value of the sequential extractions approaches the δ^{26}Mg value of our <2-mm bulk horizon dissolution, as a check on the efficacy of the sequential extraction's isotopic results. Figure 4.3 shows these calculations by horizon for the Hawi soil, and Figure 4.4 shows these results by horizon for the Pololu soil. These values agree well with one another given the caveats associated with this analysis. It should be noted that kaolin group minerals are excluded from this analysis and that the sequential carbonates were not analyzed for Mg isotopic values and instead individual carbonate δ^{26}Mg values are used in their place. Further, the sequential extraction and <2-mm bulk horizon dissolutions were not performed on exactly the same sample split, adding some additional uncertainty due to sample heterogeneity. The greatest differences

in Mg isotopic composition occur in the horizons that contain carbonate, suggesting heterogeneity in the carbonate phase.

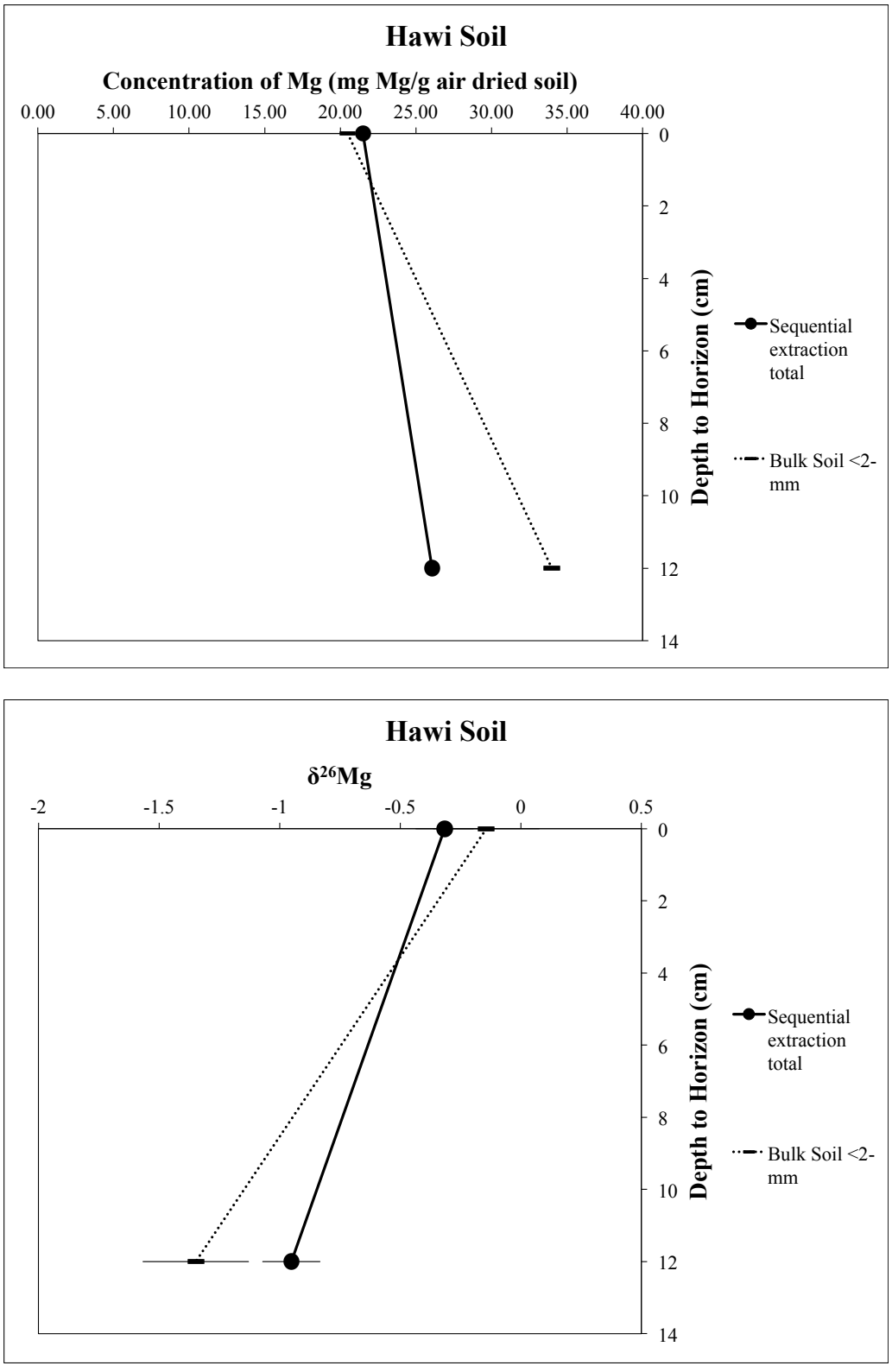

Figure 4.3: Comparison of Mg concentration and δ^{26}Mg of the Hawi soil with depth by summation of sequential extraction fractions and actual bulk soil Mg concentrations and δ^{26}Mg. Uncertainties shown are 2σ for isotope data.

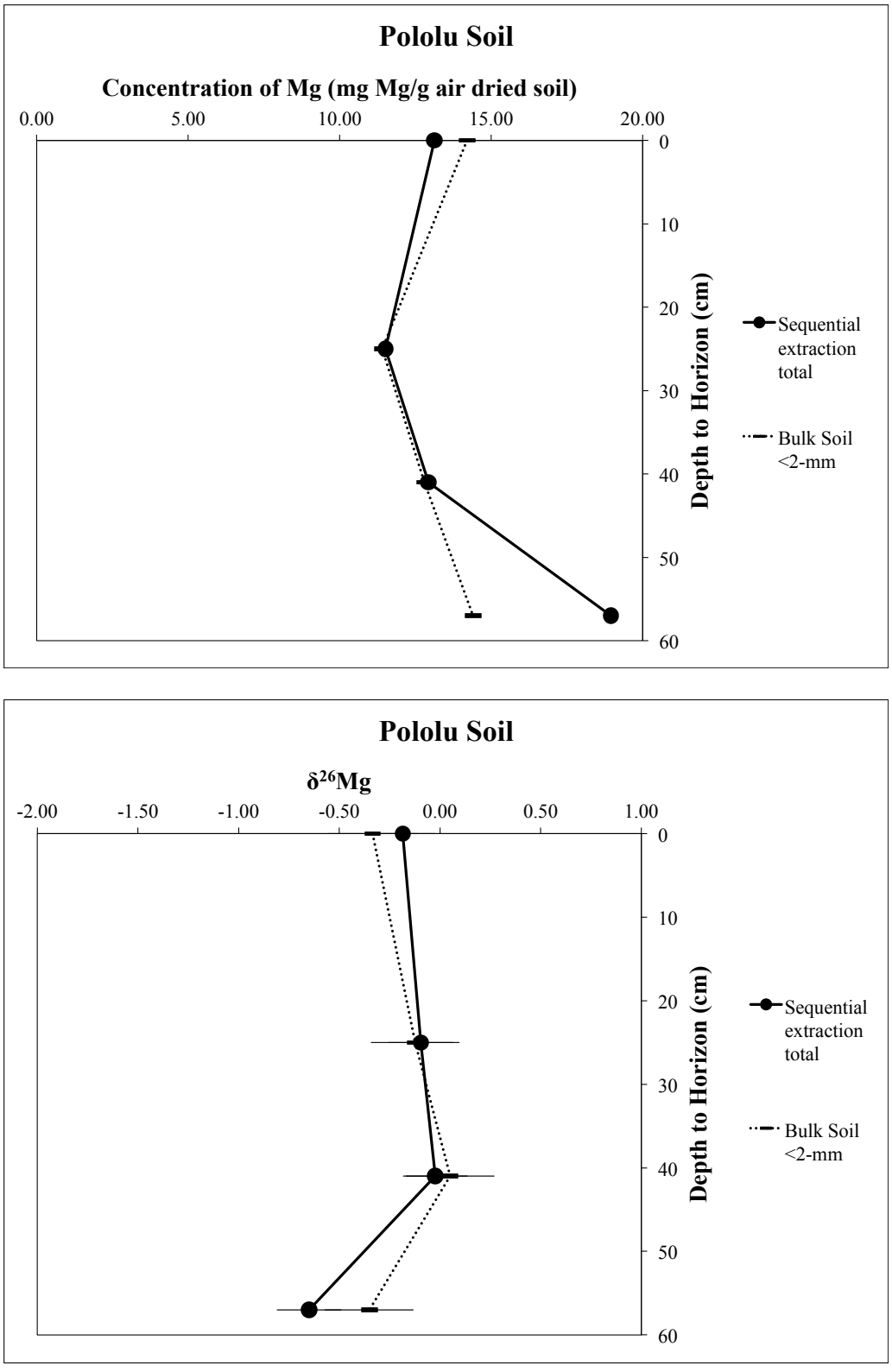

Figure 4.4: Comparison of Mg concentration and δ^{26}Mg of the Pololu soil with depth by summation of sequential extraction fractions and actual bulk soil Mg concentrations and δ^{26}Mg. Uncertainties shown are 2σ for isotope data.

4.4. DISCUSSION

4.4.1. Parent Material and Precipitation

Most measured sequential extraction fractions (Figure 4.2) fall outside the isotopic values that mixing between parent material and rainfall allows (0.25±0.13‰ to -0.89±0.1‰). Estimates from Chapter 3 (3.4.2. Estimating Inputs to the Soil System) suggest that a homogeneous soil derived from mixing of input endmembers would approach -0.27±0.24‰ for the Hawi system and -0.33±0.24‰ for the Pololu soil system. This gives us a baseline to assess fractionation in the soil environment.

4.4.2. Sequential Extractions

In order to interpret the meaning of the differences in Mg isotopic composition and Mg content of our sequential extraction fractions, we must think of each of the sequential extractions in their proper pedological framework, as described in Chapter 2 (2.5. Discussion). It is important to bear in mind that these analyses are conducted on the >2-mm soil fractions, preferentially excluding soil phases more prevalent in the >2-mm soil fraction. Sequential extraction δ^{26}Mg values and Mg contents with depth are presented in Figures 4.5 and 4.6 for the Hawi and Pololu soils, respectively.

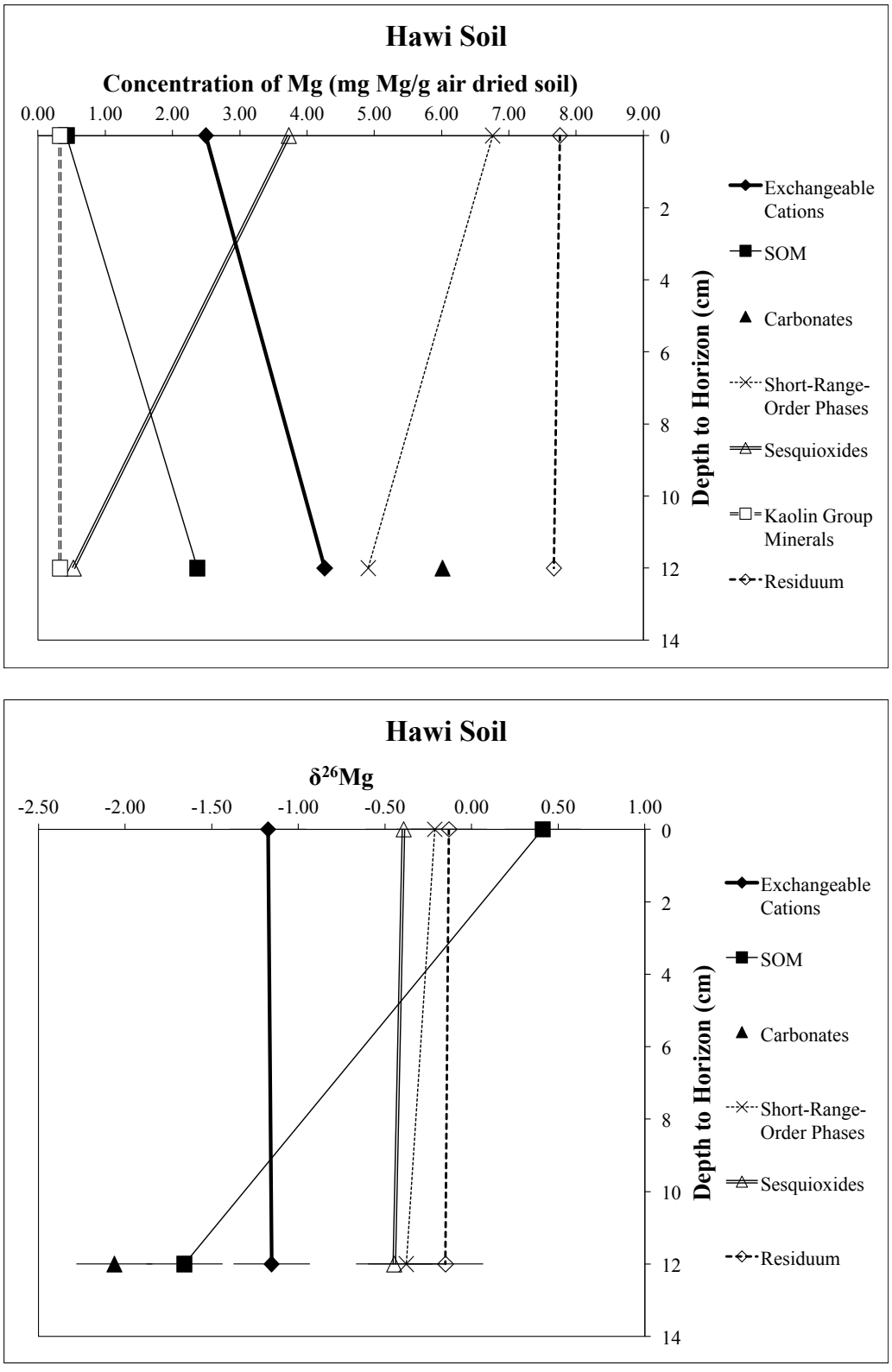

Figure 4.5: Mg concentrations and δ^{26}Mg values of the Hawi soil sequential extraction fractions by depth. Uncertainties shown are 2σ for isotope data.

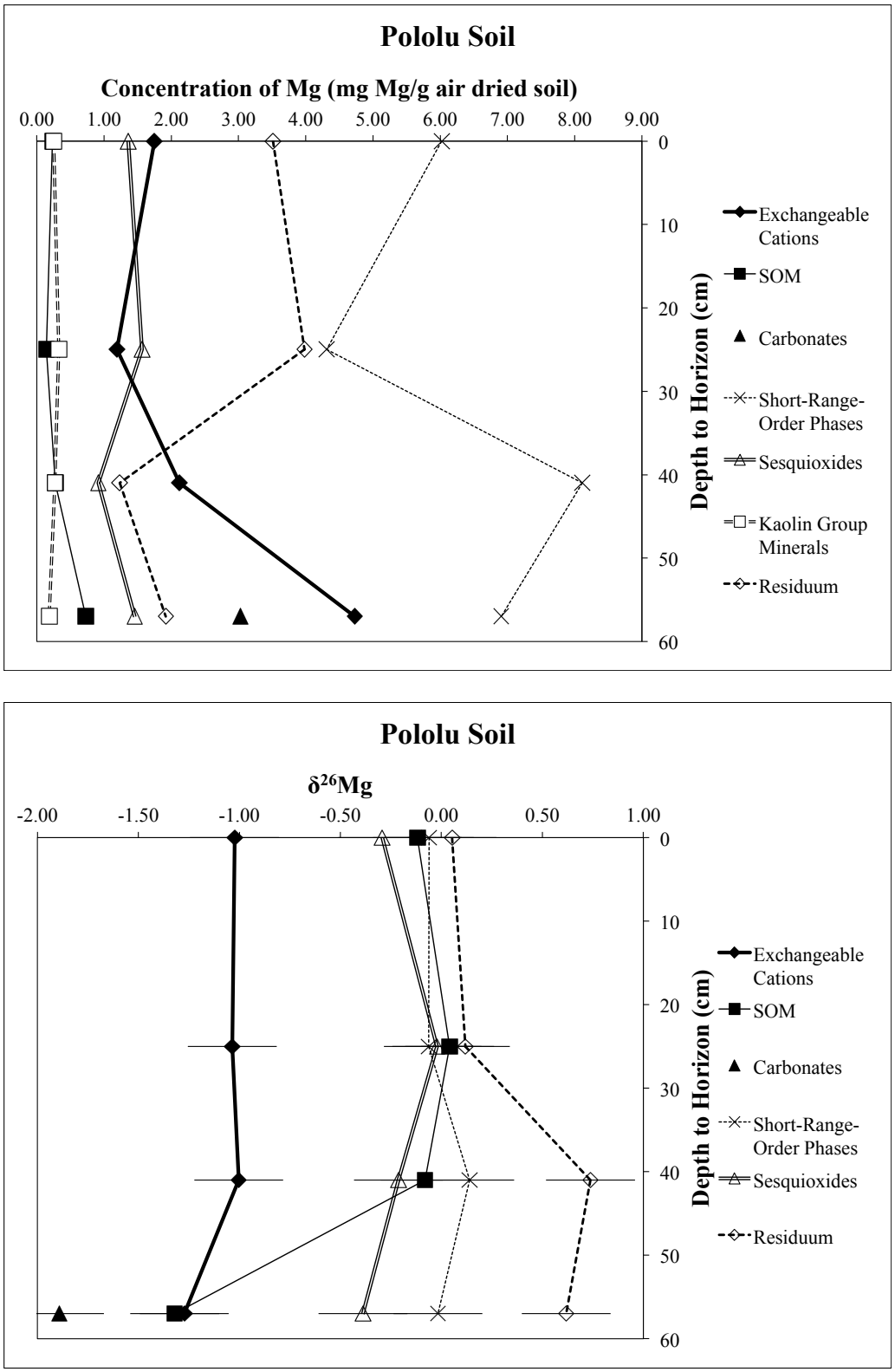

Figure 4.6: Mg concentrations and δ^{26}Mg values of the Pololu soil sequential extraction fractions by depth. Uncertainties shown are 2σ for isotope data.

4.4.2.1. Adsorbed Cations

The adsorbed cations in both the Hawi and Pololu soils are a significant reservoir of Mg (Figures 4.5 and 4.6), containing between 9% and 25% of the Mg in the <2-mm fractions of each soil horizon. We have shown that the higher values in this range are inflated by accidental carbonate dissolution in the soil horizons that contain carbonate and that the adsorbed cation fractions for these horizons also have Mg isotopic compositions skewed to lighter values for the same reason. Isotopically, adsorbed fractions uncontaminated by carbonate are lighter than what mixing between precipitation and basalt weathering should allow, averaging -1.05±0.06‰ between both soils. This observation adds to the significance of the adsorbed cations, as they are the only sequential extraction fractions isotopically lighter than precipitation in soil horizons without carbonate (Figures 4.5 and 4.6). Understanding why this sequential extraction fraction is isotopically light requires understanding the evolution of soil porewaters in the Hawi and Pololu soil systems.

The adsorbed cations are the most ephemeral of the sequential extraction fractions and the fraction most responsive in the soil system on short timescales. As such, their Mg isotopic compositions are not indicative of long-term soil formation trends, but instead are dominated by the evolution of soil porewaters following recent rainfall events in our soil systems. In Chapters 2 and 3 we explored how the sporadic nature of rainfall in these environments is one of the most important influences on these soils, leading to the development of carbonates within the soil and causing strong wet-dry cycles which modify mineralogy over time (Ziegler et al. 2003). This sporadic nature of rainfall ultimately plays an important role in the Mg isotopic composition of adsorbed cations in our soil systems.

A rainfall event will mobilize a portion of the adsorbed cations in the soils and provide the water necessary to weather primary and secondary phases. Rainfall also translocates these cations and anions in the soil system, potentially exporting ions if the magnitude of the rainfall event is greater than the water-holding capacity of the soil. The remaining soil porewater then gradually evaporates away, with secondary phase precipitation, uptake by vegetation, and adsorption/desorption modifying the soil porewater in a closed system until the next rainfall event. As such, the elemental and isotopic compositions of our soil porewaters are likely complicated and vary through time and space. In this conceptual model, the adsorbed cations we measured probably reflect the final stages of this complicated system, as our samples were collected after a long period of minimal rainfall at these study sites.

Studies have suggested that adsorbed Mg fractions reflect the Mg isotopic composition of natural waters with little or no fractionation (Wimpenny et al. 2014). If this is the case, then the isotopic compositions of the analyzed adsorbed cations should be equivalent to the isotopic composition of soil porewater after the porewater has undergone the complicated modification through time described above. As such, the isotopic compositions of the adsorbed cations should be a recorder of the net processes influencing soil porewater isotopic evolution. As all the adsorbed cations fractions have isotopic compositions consistently lighter than what mixing between rainfall and basalt weathering should allow (Figure 4.2), this evidence suggests that at both study sites the net processes influencing Mg isotopes in soil porewater yields the removal of isotopically heavy Mg from porewater. The simplest way to accomplish this result is to have isotopically heavy Mg preferentially incorporated into secondary mineral phases, a process that the Mg isotopic compositions of our other sequential extraction fractions support. Futhermore, as the adsorbed cations are a relatively mobile Mg fraction, the next time a significant rainstorm

comes through the area, isotopically light Mg will most likely be removed from adsorption sites and exported from each soil.

This idea may seem anathema to the conclusions drawn in Chapter 3 about the Hawi soil being a net exporter of isotopically heavy Mg (3.4.3. Integrating the Hawi Soil), but the adsorbed cations are simply describing the export of Mg over short timescales, whereas the analysis conducted in Chapter 3 is based on the net export of Mg from this soil system throughout the soil's entire development. Taken at face value, this observation would imply that the Hawi soil has begun to export isotopically light Mg, which will eventually allow it to progress to the state of the modern Pololu soil, while still currently remaining a net exporter of isotopically heavy Mg when looking at the integrated state of the soil over time. However, issues arise with this straightforward analysis. As we do not know the duration or intensity of the last rainfall event at these systems, we cannot definitively determine which processes led to the adsorbed Mg that was analyzed.

The homogeneity of δ^{26}Mg values of the adsorbed cations between soils and with depth is also of interest because the Hawi and Pololu soils vary with respect to mineralogy and SOM content, both with depth and between soils (Chapter 2, Figure 2.18). This homogeneity supports the findings of Wimpenny et al. (2014) that no significant fractionation occurs during this adsorption, or at least that the fractionation is uniform no matter the substrate in our soils.

The homogeneity of the δ^{26}Mg values is also of interest because of recent work by Bullen and Chadwick (in press) at the Hawi study site. This work is described briefly in Chapter 3 (3.4.10. Vegetation) but is described in greater detail here. Their work suggests that biolifting processes result in variations in the isotopic composition of exchangeable Ca, Sr, and Ba with depth in soils, which is consistent with preferential partitioning of isotopically light Ca, Sr, and

Ba into plants and the subsequent removal of that plant material from the soil system by erosive forces. For Mg this process should result in isotopically light Mg remaining in the adsorbed Mg fraction of soil surface horizons, as isotopically heavy Mg is preferentially partitioned to plants (Black et al. 2008; Bolou Bi et al. 2010; Bolou Bi et al. 2012). Although all the adsorbed Mg fractions are lighter than mixing estimates for both soils, there is no surficial enrichment that would suggest preferential removal by vegetation and erosion. Furthermore, if we look at the bulk <2-mm and >2-mm combined soils described in Chapter 3, we would expect this process to enrich the bulk soil in isotopically light Mg over time, which is not seen when comparing the Hawi and Pololu soils (Chapter 3, Figure 3.7). There are two potential reasons for this discrepancy between Mg and Ca, Sr, and Ba. The first is that enough Mg is left in these soils that biolifting is not a dominant process in the evolution of the isotopic composition of Mg. Mg τ values are less negative than Ca τ values (Chapter 2, Figure 2.11), and Mg/Ca ratios in the initial basalts are near unity, suggesting that biolifting would have to be a larger influence on Mg in order to result in significant variations in Mg isotopes. The second reason is simply that the different roles of Mg and Ca (and also Ca mimics Sr and Ba) in biology allow Mg to be returned to the soil system easily after plant death, prior to preferential removal by erosive forces. Mg in vegetation is usually in intracellular spaces, whereas Ca, Sr, and Ba are usually in extracellular spaces acting as glue between plant cell walls (Fraústo da Silva and Williams 1991). When a plant dies it is much easier for Mg to be leached away prior to erosive transport compared to Ca, Sr, and Ba. For either or both of these reasons biolifiting might not be important when looking at Mg isotopes in these soils.

4.4.2.2. Soil Organic Matter and Vegetation

SOM contains a relatively small portion of Mg within our soils (Figures 4.5 and 4.6), holding between 1% and 5% of the Mg in the <2-mm fractions of each soil horizon. We have shown that the higher values in this range are inflated by accidental carbonate dissolution in the soil horizons that have carbonate and that the SOM fractions for these horizons also have Mg isotopic compositions skewed to lighter values for the same reason. Isotopically, fractions uncontaminated by carbonate are heavier than our estimates of mixing between precipitation and basalt weathering should allow, averaging -0.05±0.08‰ for the Pololu soil and 0.41‰ for the Hawi soil (Figures 4.5 and 4.6). Vegetation, meanwhile, ranges in isotopic composition from 0.10±0.32‰ to -0.22±0.24‰ (Chapter 3, Figure 3.3), with an average value of -0.07±0.26‰. This overlap suggests that the transformation of vegetation to SOM results in little Mg isotopic fractionation in these systems, but the nature of SOM is complicated in any soil, and caveats exist with this simple analysis.

Debates over the formation, nature, and residence time of SOM in soils continue to the present day. However, SOM is a longer-lived reservoir than adsorbed cations or vegetation in our soil systems and can interact in synergistic ways with short-range-order phases to create stabilized aggregates that increase the residence time of both SOM and short-range order phases (Parfitt 2009). As such, when comparing the overall Mg isotopic composition of the SOM pool to that of vegetation, we must acknowledge that the isotopic composition of SOM is the integrated result of soil processes operating over decades or centuries, whereas the vegetation δ^{26}Mg values are the product of processes operating over a much shorter timescale. It may therefore be coincidence that our vegetation values and SOM values match in Mg isotopic composition. The δ^{26}Mg of SOM in other study sites has not yet been characterized in the

literature, and so further work must be conducted to determine the exact relationship between these two reservoirs of Mg in ecosystems.

Our vegetation $\delta^{26}Mg$ values support previous work (Black et al. 2008; Bolou Bi et al. 2010; Bolou Bi et al. 2012) that shows that isotopically heavy Mg is preferentially incorporated into vegetation (Chapter 3, Section 3.3.4. Vegetation). If we assume that the soil porewater that Mg is being withdrawn from by vegetation has an isotopic composition near our mixing estimates for the Hawi and Pololu inputs (Chapter 3, Figure 3.6), we calculate a $\Delta^{26}Mg_{vegetation\text{-}porewater}$ of ~ 0.2‰, smaller than most fractionations found in the aforementioned studies. As described previously in the section on adsorbed cations, the isotopic composition of soil porewater varies through time and space in these soils. If we use the isotopic composition of the adsorbed cations as an estimate of soil porewater $\delta^{26}Mg$ values, the calculation of the fractionation factor would yield a $\Delta^{26}Mg_{vegetation\text{-}porewater}$ of ~ 1‰. The range of $\Delta^{26}Mg_{vegetation\text{-}porewater}$ values from ~ 0.2‰ to ~ 1‰ seems reasonable, but the true fractionation factor is somewhere in the middle of these $\Delta^{26}Mg_{vegetation\text{-}porewater}$ values, as plants are simultaneously removing Mg from these soil porewaters as the soil porewaters evolve to the light Mg isotopic compositions displayed by the adsorbed cations.

4.4.2.3. Carbonates

As the sequential extraction is looking specifically at the <2-mm fractions of the Hawi and Pololu soils, the importance of carbonate in our analyses is underplayed since soil particles cemented together by carbonates are excluded by the sieving process. Even so in these <2-mm fractions carbonates can be important reservoirs of Mg in the soil horizons in which they appear, accounting for 16% of the Mg in the lowest horizon of the Pololu soil and 60% of the Mg in the lowest portion of the Hawi soil (Figures 4.5 and 4.6). Also these two percentages of Mg derived

from carbonate should be even higher, as both the adsorbed cation extraction and SOM extraction have dissolved some portion of the carbonates present. Carbonates in these soils are a longer-lived reservoir of Mg than adsorbed cations, SOM or vegetation, but their formation is still heavily influenced by the sporadic nature of rainfall in these regions as described in detail in Chapter 3 (3.4.7. Forming Pedogenic Carbonates).

The sequential carbonates were not analyzed for δ^{26}Mg due to concerns with preferential dissolution of reactive carbonate during the adsorbed cation and SOM sequential extractions. Instead, Mg isotopic values from the bulk individual carbonate dissolution are used to represent these fractions in our calculations (Chapter 3, 3.3.3. Soil Carbonates). We can also directly estimate the Mg isotopic composition of the carbonates contaminating the SOM fraction if we assume that the actual contribution from SOM to the amount of Mg in the horizon is the same as the horizon above in the soil, and that the Mg in excess is derived from carbonate. This simple calculation yields contamination by carbonate with a δ^{26}Mg of -2.08‰, a completely reasonable value given the δ^{26}Mg values of the measured bulk carbonates in these horizons (Chapter 3, Figure 3.3). This result suggests that the carbonate removed by the adsorbed cation and SOM sequential extractions is not significantly different from the individual bulk carbonate.

4.4.2.4. Short-Range-Order Phases

The short-range-order phases dominate the Mg budget in the Pololu soil and are a substantial reservoir of Mg in the Hawi soil, containing between 19% and 63% of the Mg in the <2-mm portion of every soil horizon (Figures 4.5 and 4.6). The Pololu soil SRO fractions are isotopically heavier than estimates from Chapter 3 of mixing between basalt weathering and rainfall (average Pololu SRO δ^{26}Mg of 0.00±0.08‰ vs. mixing estimate of -0.33±0.22‰). The Hawi soil SRO fractions are near our estimates of mixing between basalt weathering and rainfall

(average Hawi SRO δ^{26}Mg of -0.30±0.12‰ vs. mixing estimate of -0.24±0.22‰). However, calculating Δ^{26}Mg values for the formation of these phases is complicated due to their extended existence within the soils, as well as the mechanism of the formation of these phases.

The SRO phases are maintained in the soil environment over thousands of years, gradually recrystallizing to the more stable phases sampled by our sesquioxide, kaolin group mineral, and residuum sequential extractions. The longevity of these phases in the soils means that the δ^{26}Mg values of the SRO fractions analyzed are the integrated results of SRO formation and modification over thousands of years. On shorter timescales, individual generations of SRO phases may have variable δ^{26}Mg depending on the conditions of their formation. As such, when looking over long timescales, mixing estimates between basalt weathering and rainfall are probably better to assess Mg isotopic fractionation caused by the formation of the SRO phases, rather than estimates of porewater isotopic values determined from our adsorbed cations described above.

A further complication to this analysis is that SRO phases may not precipitate directly from solution. This complexity is seen in Figures 2.7, 2.8, and 2.9 of Chapter 2 where these phases appear to be direct alteration products of primary minerals. Within soil, heterogeneity is important, and the simplifying assumption of direct precipitation from a homogeneous solution does not hold.

Conservatively put given the caveats outlined above, SRO phases appear to preferentially incorporate isotopically heavy Mg with a relatively small fractionation in the Pololu soil system (~0.3‰). The Hawi system does not appear to have this fractionation given our current mixing estimates between basalt weathering and rainfall. The difference between the Mg isotopic compositions of SRO phases in the two soils is currently not understood, but differences in the

proportions of ferrihydrite, allophane, and imogolite between the soils might play a role. The Hawi soil has lower Fe:Al ratios in the SRO fractions (Chapter 2, Table 2.20), suggesting less ferrihydrite in these soils, which is supported by soil color as well. Attempts to characterize the δ^{26}Mg values of the individual SRO phases may solve this problem.

These analyses are the first Mg isotopic analyses of the short-range-order phases in soils, and given their importance in the Mg budget of these soils, as well as the ubiquitous nature of ferrihydrite in the environment, these phases should play a large role in determining the fractionation of Mg isotopes in soils around the globe. This discussion also sets the stage for subsequent mineralogy fractions, many of which are derived from the recrystallization of the short-range-order phases.

4.4.2.5. Sesquioxides

Sesquioxide phases account for 2% to 17% of the Mg budget in the <2-mm soil fractions of the Pololu and Hawi soils (Figures 4.5 and 4.6). These phases display an average Mg isotopic composition of -0.30±0.14‰, near mixing estimates between basalt weathering and rainfall inputs for both soils. The δ^{26}Mg values are also not significantly different between the Hawi and Pololu soil systems at our level of analytical uncertainty. Once again the timescale over which these phases form and are modified is important in understanding the meaning behind the δ^{26}Mg reported. The sesquioxide phase hematite is stable in this soil system over an extended period of time, representing one of the final products of weathering in these systems (Chapter 2, Figure 2.5). As such the Mg isotopic composition of this sequential extraction fraction should be the integrated product of hematite formation and modification over nearly the entire age range of our soils.

The δ^{26}Mg values of the sesquioxide phases should be compared to the Mg isotopic composition of ferrihydrite, which is the precursor of hematite in these soils. Hematite forms at the expense of ferrihydrite due to aggregation, dehydration and internal structural rearrangements (Schwertmann and Taylor 1989). These transitions do not involve dissolution and reprecipitation from solution, which suggests that the initial Mg isotopic composition of ferrihydrite plays a role in determining the Mg isotopic composition of the final hematite produced. However, we must again note timescale differences between the residence time of the ferrihydrite and hematite fractions in these soils, as ferrihydrite cycles more rapidly in these systems than hematite. As such the Mg isotopic composition of the modern ferrihydrite in the Hawi and Pololu soils does not necessarily represent the Mg isotopic composition of the average ferrihydrite that has transformed over time to form hematite.

Unfortunately we were unable to deconvolute the complicated relationship of Mg distribution among ferrihydrite, allophane, and imogolite, or of Mg isotopic composition among ferrihydrite, allophane, and imogolite. This prevents us from understanding exactly where Mg is in the short-range-order phases and whether or not the Mg isotopic composition varies among ferrihydrite, allophane, and imogolite. If we assume that ferrihydrite has the δ^{26}Mg value we have analyzed for the Pololu short-range-order phases (0.00±0.08‰), we find that the transition from ferrihydrite to hematite appears to be associated with the preferential expulsion of isotopically heavy Mg. If instead we assume that ferrihydrite has the δ^{26}Mg value we have analyzed for the Hawi short-range-order phases (-0.30±0.12‰), it appears that no fractionation occurs with this reorganization of the ferrihydrite into hematite. Only further work will resolve this issue.

One concept briefly discussed in Chapter 2 (2.5.4 A Horizons) is the idea that the transformation from ferrihydrite to hematite most likely results in the expulsion of Mg from hematite. This process may be important in providing a Mg flux within these soils as they age. Comparisons of Figures 2.17 and 2.18 in Chapter 2 clearly show that short-range-order phases are a small portion of the mineralogy, but a large Mg reservoir. Sesquioxide phases and kaolin group minerals on the other hand are large portions of the mineralogy of these soils, but relatively small Mg reservoirs. This difference in mineralogical abundance and Mg distribution suggests that the transformation of short-range-order phases to more stable sesquioxides and kaolin group minerals results in the release of Mg to the weathering environment. Unfortunately, as we were unable to determine the Mg distribution amongst the SRO phases, it was impossible to determine if the transition from ferrihydrite to hematite, or allophane and imogolite to kaolin group phases, was ultimately responsible for most of the difference in Mg distribution between these soil reservoirs.

4.4.2.6. Kaolin Group Minerals

The kaolin group minerals account for 1% to 3% of the Mg budget in the <2-mm soil fractions of the Pololu and Hawi soils (Figure 4.5 and 4.6). Their low Mg contents, coupled with the technique used for their extraction, prevented the analysis of δ^{26}Mg values for these fractions. However, their limited Mg contents suggest that these phases do not play an important role in the overall Mg isotopic composition of the soils at either study site. The kaolin group minerals are stable in these soils over extended periods of time, similar to hematite, but may eventually alter to gibbsite after extreme desilication (Hsu 1989).

As discussed above in the section on sesquioxides, the kaolin group minerals can form at the expense of allophane and imogolite over time, and this transformation may result in a

significant expulsion of Mg as allophane and imogolite transform into these more stable phases. Kaolin group minerals can also precipitate directly from solution, however, adding further complexity to understanding the Mg contents of these phases.

4.4.2.7. Residuum

Residuum phases play a large role in the Mg budget of the <2-mm soil fractions of the Pololu and Hawi soils providing 10% to 36% of the Mg in each soil horizon (Figure 4.5 and 4.6). These phases also have variable Mg isotopic compositions that change with depth in the soils, and change between the Hawi and Pololu soils (Figure 4.5 and 4.6). However all δ^{26}Mg values for these fractions are heavier than mixing estimates between basalt weathering and rainfall inputs for both soils. Understanding the complexity of this dissolution is important in interpreting the variation in Mg isotopic composition between soils and with depth in the Pololu soil.

The mineralogy of our residuum sequential extraction is diverse. This fraction removed any remaining primary basalt phases, along with the weathering product gibbsite and the weathering products of spinels. Elemental ratios and trends help us to decipher exactly what this dissolution has extracted.

Gibbsite is one of the most stable products of weathering in these environments and most likely provides a significant portion of the Al that we find in this sequential extraction fraction (Chapter 2, Table 2.25). However, gibbsite probably contains very little Mg, as the kaolin group minerals from which gibbsite can form have very little Mg. Gibbsite can also form from short-range-order phases and directly from solution in some cases; it remains to be seen if such formation mechanisms are associated incorporation of Mg.

Other Mg reservoirs in the residuum sequential extraction are primary basalt phases like plagioclase feldspar, orthopyroxene, and olivine. These phases would be associated with higher concentrations of Na, Mg, Ca, Fe, and Al in the chemistry data for the residuum sequential extraction. Fe and Al however, are also derived from other sources, so enriched Na, Mg, and Ca numbers are a better indication of the dissolution of these phases. Broadly speaking, these elements are enriched in the Hawi soil residuum sequential extraction fractions compared to the Pololu soil residuum sequential extraction fractions (Chapter 2, Table 2.25).

Another primary phase from basalt that exists in these soils are spinel group minerals, which are resilient to weathering. Chemical evidence for the existence of these phases, or of their weathering products pedogenically produced over time, may be found in the horizons of the Pololu soils. These horizons show significant amounts of Fe and Ti in approximately a 2:1 molar ratio, along with Mn concentrations positively correlated with Fe (Chapter 2, Figure 2.14). Spinels are of particular interest because these oxide phases are an isotopically heavy reservoir of Mg within basalt. Experimentally-derived $\Delta^{26}Mg_{spinel\text{-}forsterite}$ values vary with temperature but are on the order of 1‰ at 700°C (Macris et al. 2013). Depending on the equilibration temperature of the spinel and olivine phases in our basalts, spinel could be quite isotopically heavy compared to the bulk basalt Mg isotopic compositions described (average $\delta^{26}Mg$ - 0.25±0.06‰).

We currently do not have a satisfactory explanation of the Mg isotopic variations in the residuum sequential extraction fraction, but believe that further characterization work on the soil phases represented by this dissolution will help to elucidate our results.

4.4.2.8. Sequential Extraction Totals

Chapter 2 provides the weighted average of Mg in the sequential extraction fractions of the <2-mm portions of the Hawi and Pololu soils (Chapter 2, Figure 2.19).

In a similar fashion we can also calculate the average Mg isotopic composition of each sequential extraction fraction for all horizons in both soils (Figure 4.7). These two figures give us a view of which soil phases dominate the Mg budget along with the Mg isotopic compositions of the entire <2-mm soil fraction throughout the Hawi and Pololu soils. SRO and residuum phases are isotopically heavy and significant reservoirs of Mg, but the enrichment in heavy Mg is small enough that these fractions can be offset by the light isotopic compositions of adsorbed cations and carbonates, which are smaller reservoirs of Mg in the total soils. This results in the overall <2-mm fractions of our soils ending up with Mg isotopic compositions near our input mixing estimates from Chapter 3 (-0.24±0.22‰ for the Hawi, -0.33±0.22‰ for the Pololu).

As many sequential extractions did not vary in Mg isotopic composition with depth in the soils, the average values presented in the results section are similar to the total weighted average Mg isotopic compositions throughout the soils in Figure 4.7. It should be noted that Figure 4.7 includes data from carbonate-contaminated adsorbed cation fractions skewing the weighted averages of these sequential extractions to slightly isotopically lighter values. Of note is the weighted average Mg isotopic composition of the residuum fraction for the Pololu soil, which is significantly enriched in isotopically heavy Mg.

Figure 4.7 illustrates the consistency in Mg isotopic compositions in many of the sequential extractions between the Hawi and Pololu soils, suggesting that the soil-forming processes influencing the Mg isotopic compositions of the sequential extraction fractions are operating similarly in both soils over these long (100 ka) timescales. This finding is important

and suggests the trends in Mg isotopic composition we see are maintained through time, and not the result of stochastic variations in these systems. The largest differences between soils observed occur in the residuum phases and SOM fractions, which is probably a result of the complicated nature of the residuum dissolution dissolution, and singular SOM analysis from the Hawi soil.

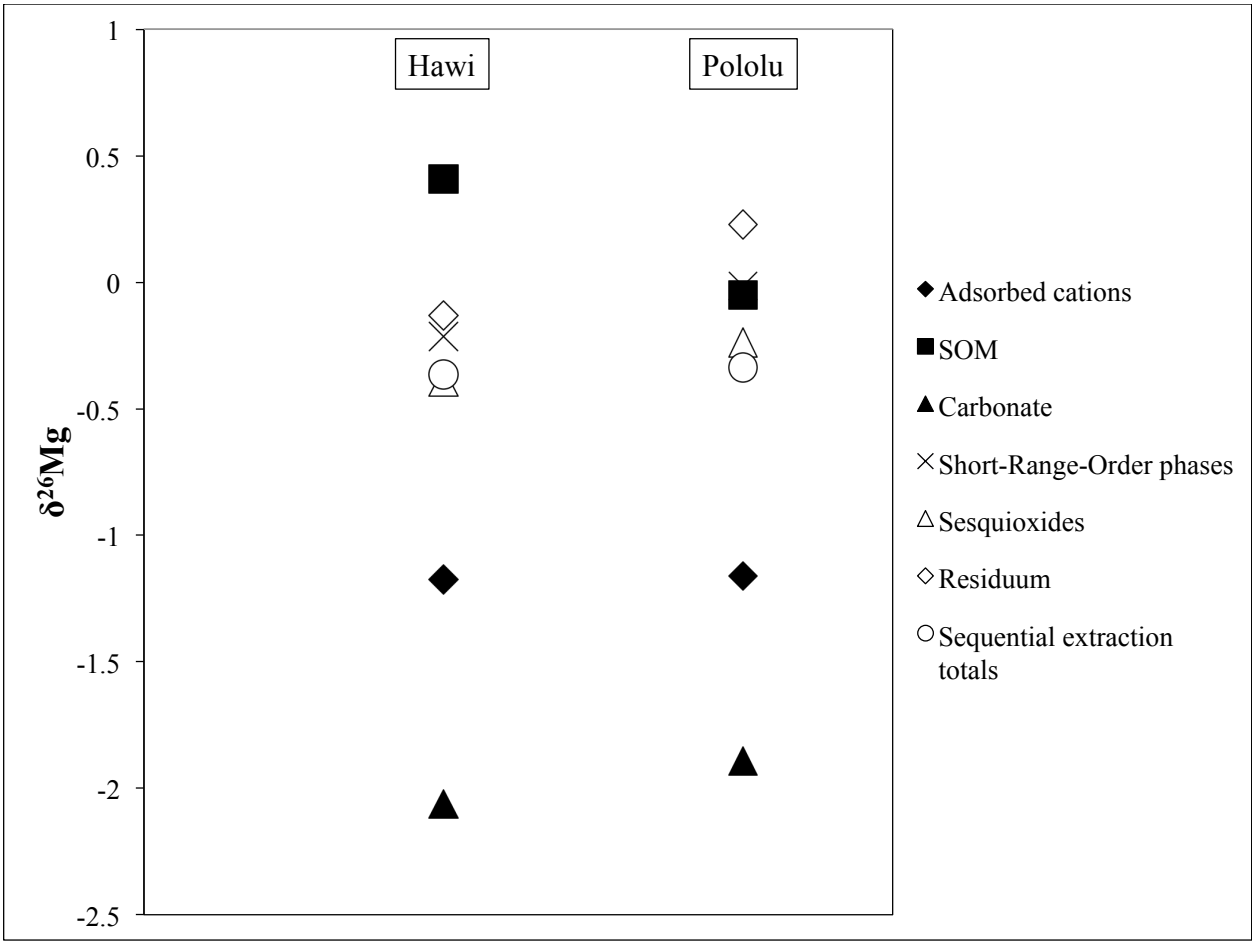

Figure 4.7: Weighted average δ^{26}Mg values of each sequential extraction fraction by soil. SOM fractions contaminated by carbonate are excluded from this calculation. Uncertainties are not shown for clarity.

4.5. CONCLUSIONS

This study is the first of its kind to deconstruct a soil into its constituent parts and measure the Mg isotopic compositions of those parts. We show that simple mixing between Mg inputs to our soil systems can explain few of the variations in Mg isotopic compositions observed in the <2-mm portions of these soil horizons.

Adsorbed cations in these soil systems are isotopically lighter than mixing can account for, and are the only store of isotopically light Mg in soil horizons without carbonate. The nature of the adsorbed cation fraction suggests that isotopically light Mg is being exported from both the Hawi and Pololu soils, and that biolifting is not a dominant influence on Mg at these study sites. SOM is isotopically heavy compared to mixing inputs, but is such a small fraction of Mg that it plays little role in bulk soil Mg isotopic composition. Carbonate sequential extraction fractions are important at depth in these soils and can be a large reservoir of isotopically light Mg. The importance of carbonate in the <2-mm soil fractions, however, is limited compared to the role these phases play in the <2-mm and >2-mm bulk soil described in Chapter 3, due to the role of carbonate as a cementing agent in these systems. Short-range-order phases dominate the Mg budget in the <2-mm fractions of these soils. The short-range-order fractions are isotopically near basalt values in the Hawi soil and isotopically heavier than basalt values in the Pololu soil, suggesting preferential incorporation of isotopically heavy Mg during the formation of these phases. The short-range-order phases are of additional interest because of their metastability, transforming into the sesquioxide phases and kaolin group minerals over time. The sequioxide fractions contain less Mg than the short-range-order mineral phases and are isotopically similar to basalts. Without knowing the Mg content and Mg isotopic composition of the ferrihydrite portion of the short-range-order minerals, however, it is impossible to say anything definitively

about the transition from ferrihydrite to hematite in terms of Mg explusion or Mg isotopic fractionation. Kaolin group minerals contribute little to the Mg budgets of these soils, so little that we were unable to analyze them for Mg isotopic compositions. The residuum sequential extraction is a complex mixture of basalt-derived primary phases, gibbsite, and the weathering products of spinels, making understanding the nature of this fraction difficult. This fraction displays variations with depth and between soils, suggesting complex behavior that requires further investigation.

These soil systems are complex, and understanding the functioning of all of the sequential extraction fractions in the soil system and how they relate to one another as they operate on different timescales is challenging. By using the chronosequence approach and comparing the Hawi and Pololu soils, we can be reasonably certain that the Mg isotopic compositions of many of our sequential extractions are meaningful and not the product of chance fluctuations in the soils systems. Coupled with the results of Chapter 3, this work strongly supports that the formation of most silicate and oxide weathering products results in preferential uptake of isotopically heavy Mg, and expulsion of light Mg into soil solution.

Acknowledgements: Thanks to Gregg McElwee, Aimeryc Schumacher, Eva Golos, and Delphine Yeghicheyan for all of their technical support and efforts. This work is supported by the National Science Foundation Grant 0922070. This work made use of the Cornell Center for Materials Research Shared Facilities, which are supported through the NSF MRSEC program (DMR-1120296).

WORKS CITED

Black, J.R., Epstein, E., Rains, W.D., Yin, Q.Z. and Casey, W.H., 2008. Magnesium-isotope Fractionation During Plant Growth. Environmental Science &Technology, 42(21): 7831-7836.

Bizzarro, M., Paton, C., Larsen, K., Schiller, M., Trinquier, A., Ulfbeck, D., 2011. High-precision Mg-isotope measurements of terrestrial and extraterrestrial material by HRMCICPMS – implications for the relative and absolute Mg-isotope composition of the bulk silicate Earth. Journal of Analytical Atomic Spectrometry, 26: 565-577.

Bolou Bi, E.B., Poszwa, A., Leyval, C., Vigier, N., 2010. Experimental determination of magnesium isotope fractionation during higher plant growth. Geochimica et Cosmochimica Acta, 74: 2523-2573.

Bolou Bi, E.B., Vigier, N., Brenot, A. and Poszwa, A., 2009. Magnesium isotope compositions of natural reference materials. Geostandards and Geoanalytical Research, 33(1): 95-109.

Bolou Bi, E.B., Vigier, N., Poszwa, A., Boudot, J.P., Dambrine, E., 2012. Effects of biogeochemical processes on magnesium isotope variations in a forested catchment in the Vosges Mountains (France). Geochimica et Cosmochimica Acta, 87: 341-355.

Brenot, A., Cloquet, C., Vigier, N., Carignan, J. and France-Lanord, C., 2008. Magnesium isotope systematics of the lithologically varied Moselle river basin, France. Geochimica et Cosmochimica Acta, 72(20): 5070-5089.

Bullen, T., and Chadwick, O., in press. Ca-Sr-Ba stable isotope systematics of a soil climosequence: a new window onto leaching and biotic uplift as pedogenic processes. Geology.

Fraústo da Silva, J. J. R., and Williams R. J. P., 1991. The biological chemistry of the elements: The inorganic chemistry of life. Clarendon Press, Oxford. 1991.

Hsu, P.H., 1989. Aluminum Hydroxides and Oxyhydroxides. In: Dixon, J.B., and Weed, S.B., (Eds.) Minerals in Soil Environments. 2nd ed., Soil Science Society of America Book Series 1.

Macris C.A., Young, E.D., Manning, C.E., 2013, Experimental determination of equilibrium magnesium isotope fractionation between spinel, forsterite, and magnesite from 600 to 800 °C. Geochimica et Cosmochimica Acta, 118: 18-32.

Opfergelt, S., Georg, R.B., Delvaux, B., Cabidoche, Y.-M., Burton, K.W., Halliday, A.N., 2012. Mechanisms of magnesium isotope fractionation in volcanic soil weathering sequences, Guadeloupe. Earth and Planetary Science Letters, 341-344: 176-185.

Opfergelt, S., Burton, K.W., Georg, R.B., West, A.J., Guicharnaud, R.A., Sigfusson, B., Siebert, C., Gislason, S.R., Halliday, A.N., 2014. Magnesium retention on the soil exchange complex controlling Mg isotope variations in soils, soil solutions and vegetation in volcanic soils, Iceland. Geochimica et Cosmochimica Acta 125: 110-130.

Parfitt, R.L., 2009. Allophane and imogolite: role in soil biogeochemical processes. Clay Minerals 44: 135-155.

Schwertmann, U., and Taylor, R.M., 1989. Iron oxides. In: Dixon, J.B., and Weed, S.B., (Eds.) Minerals in Soil Environments. 2nd ed., Soil Science Society of America Book Series 1.

Tipper, E.T., Galy, A. and Bickle, M.J., 2006. Riverine evidence for a fractionated reservoir of Ca and Mg on the continents: Implications for the oceanic Ca cycle. Earth and Planetary Science Letters, 247(3-4): 267-279.

Wimpenny, J., Colla, C.A., Yin, Q.Z., Rustad, J.R., Casey, W.H., 2014. Investigating the behaviour of Mg isotopes during the formation of clay minerals. Geochimica et Cosmochimica Acta, 128: 178-194.

Young, E.D. and Galy, A., 2004. The isotope geochemistry and cosmochemistry of magnesium. In: C.M. Johnson, B.L. Beard and F. Albarede (Editors), Geochemistry of Non-Traditional Stable Isotopes. Reviews in Mineralogy & Geochemistry: 197-230.

Ziegler, K., Hsieh J.C.C., Chadwick, O.A., Kelly E.F., Hendricks, D.M., Savin, S.M., 2003. Halloysite as a kinetically controlled end product of arid-zone basalt weathering. Chemical Geology, 202: 461-478.